Synthetic strategies for denatured cytochrome-c analogues towards analytical reporting of NOx species

By

Al Cerillio Farao

MSc Nano Science

Submitted in fulfillment of the requirements for the degree

Doctor of Philosophy

in the

Department of Chemistry

Faculty of Science

University of the Western Cape

August 2019

Supervisor: Prof. Priscilla Baker

Dr. Fanelwa Ajayi

Keywords

Denatured cytochrome-c analogue

Conductive polymers

Cyclic voltammetry

Diffusion coefficient

Electrochemistry

Imine

Metalloproteins

Nitric oxide donor

Nitrites

Nitrates

Redox activity

Sensor strategy

Synthetic urine

Schiff base

Standard error

Summary

Nitric oxide (NO) plays a key role as biological messenger in the biological system, however detection and quantification thereof has always posed significant problems. NO_x is a principal constituent of air pollutants. There are seven oxides of nitrogen of which N_2O, NO and NO_2 are most important. NO is a free radical and reacts extremely fast with oxygen, peroxides and superoxides. It's these reactions which are responsible for NO's fleeting existence.

The specific detection and quantification of NO still remains challenging. Most techniques rely on the measurements of secondary nitrite and nitrate species. Electrochemical techniques using ultra micro-electrode systems presented the possibility of direct detection of NO, offering a range of favourable characteristics; good selectivity towards NO, good sensitivity, fast response, long-term stability and ease of handling.

Electrochemical detection of NO relies on the modification of electrode surfaces and exploiting the redox properties of NO. NO can either be oxidized or reduced electrochemically depending on the nature of the solution. Under cathodic current NO is reduced to nitrosyl, a highly unstable derivative of NO. These nitrosyls are subject to a serious of chemical reactions to eventually form nitrous oxide. Due to the interferences presented by the electrochemical reduction of NO, the electro oxidation of NO is therefore the methodology of choice for NO detection. The electrochemical oxidation of NO occurs at positive potentials around 800 mV vs. Ag/AgCl. However this potential range is not only favourable to NO oxidation but can lead to the oxidation of several other biological species. These interfering species are biologically present at concentrations higher than NO therefore selectivity is of the highest order when designing these electrode systems. Some nitric oxide sensors are limited in their sensitivity, stability and reproducibility.

Direct electron transfer between redox proteins and conductive membrane layers has been scrutinized for years in an attempt to reproduce the mechanistic charge transfer processes for sensor application. However, literature reports have presented many arguments on the complexities associated with depositing these enzymes on electrode surfaces for the purpose of reproducing direct electron transfer at metalloprotein centres.

The study sets out to design a material which could mimic the electrochemistry of

denatured cytochrome-c. To achieve this it was imperative to design a polymer which could reproduce the electrochemistry of the ligands coordinated to the metal centre of the metalloprotein. A novel Schiff base was synthesized by cross-linking naphthalene to pyrrole to produce the monomer, N,N-bis((1H-pyrrol-2-yl)methylene)naphthalene-2,3-diamine). The monomer was electrodeposited on a screen print carbon electrode (SPCE) vs. Ag/AgCl and served as a supporting layer for denatured cytochrome-c. Cytochrome-c is classified as a metalloprotein. These metalloproteins possess metal centres which when denatured unfolds and allows access to the metal centre. Cytochrome-c was subjected to thermal denaturation which opened up the iron centre. The denatured metalloprotein was cross-linked to the ligand to reconstruct the heme centre environment. This was believed to facilitate the electrochemical activity of the system and allow for electrochemical analysis of these metalloproteins for sensor application. The redox behaviour of the sensors were modelled in phosphate buffer solution (PBS) with cyclic voltammetry. Electrochemical analysis reported the sensors to possess reversible electrochemistry with diffusion control characteristics. The sensor recorded a redox system in the negative potentials range. Following the establishment of the electrochemical profile of the sensor an attempt was made to produce a synthetic analogue of denatured cytochrome-c. Iron (II) was chelated to the monomer N,N-bis((1H-pyrrol-2-yl)methylene)naphthalene-2,3-diamine) to form an iron ligand complex. The complex was subjected to a series of characterization techniques which confirmed coordination to the metal centre. The iron ligand complex was electrodeposited on a SPCE over the potential window of -1 V and 1 V to model the electrochemical behaviour of the sensor. The material was found to be electroactive. Subsequent electrochemical analysis revealed the system to have electrochemical properties, analogous to that of the denatured cytochrome-c system. The sensor was applied in NO and NO_2 studies and displayed an affinity towards NO. Based on extrapolated values it was postulated that the lower limit range for NO detection was in the range of 30 to 40 nM. The potentials recorded were lower than the reported oxidation potentials for nitric oxide. The sensor displayed stability and selectivity towards nitric oxide within a complex matrix. The complex matrix employed in this study was synthetic urine that was synthesised in the lab. The sensor displayed the capacity for linear range of NO detection with very low error margins.

Declaration

I hereby declare that "*Synthetic strategies for denatured cytochrome-c analogues towards analytical reporting of NOx species"* is my own work, that has not been submitted for any degree or examination in any other university, and that all sources I have used or quoted have been indicated and acknowledged by complete references.

Al Cerillio Farao

Signature: ……

Date: ……

Acknowledgements

This work is dedicated to everyone whom has supported me throughout this journey, who whispered words of encouragement in times of uncertainty, and who cracked a few jokes when I was too serious. This has been a testing journey, one worth taking, for the beauty lies not in the reward but in that which unveils itself along the way.

To the Moodley family, thank you for all the support throughout the years and for accepting me as one of your own. I appreciate everything that you do for me. Your hard work and commitment to excellence is admirable and inspires me daily to be the best version of myself.

To my supervisor Professor Baker thank you for allowing me the opportunity to be a part of your team. Your support and guidance throughout the years has been crucial to my development. I value all the words of encouragement, the tough love, it is greatly appreciated. To Dr Ajayi for all your support, from my undergraduate years to the present, you were always ready and willing to offer a helping hand, thank you. To Professor Iwuoha and the Sensor Lab team thank you for your commitment and dedication it creates an inspiring environment.

I would also like to thank Ms Jackson, you a "rock star". A special thank you to the Chemistry Department for your all support it is appreciated. Thank you to the NRF, your financial support made this project possible. To Campus France thank you for affording me the opportunity of a life-time. My experience at Chimie ParisTech is unforgettable. To Professor Fethi, Professor Anne, Professor Sophie and the CNRS team, thank you for your warm reception and taking me under your wing.

Most importantly, I would like to express my gratitude to my wife Kim you have been with me from the start. You have carried me through tough times, shared in my laughter and joys. We made it my love! To my parents, you are my moral compass and I am humbled by your unconditional love and support. Thank you for patience and understanding and for allowing me the opportunity to explore what life has to offer.

Through suffering comes liberation that is only possible through God

Table of Contents

List of figures

List of tables

"Per aspera ad astra ad infinitum"

Chapter 1

1. Research proposal

The following section discusses the life cycle of nitric oxide (NO) in the ecosystem. It describes the presence of NO in the atmosphere and the impact thereof on climate change. Presented here is a brief overview of the regulation of NO which is followed by an extensive discussion on biological synthesis thereof, sources, health complications associated with NO and possible applications of NO markers.

1.1 Nitric oxide in the atmosphere

The earth's atmosphere is made up of a collection of gasses that represent the gaseous phase of biogeochemical cycle nitrogen, oxygen and carbon dioxide. The atmosphere is made up of a collective of segmented altitudes. The troposphere which is closest to the earth. This region is made up of the air we breathe, and where weather systems occur. The air pressure increases with altitude exponentially, 90% of the atmospheric's mass is in the troposphere[1]. Gases released from the earth tend to mix throughout the troposphere, the region is identified by slow vertical transport. Above the troposphere the temperature begins to increase with altitude as result of absorption of light energy by ozone. The top boundary of the troposphere, the tropopause, is identified by the altitude with the lowest temperature[2]. The area above this is called the stratosphere where the temperature is higher resulting in the slow vertical mixing. The chemical makeup of the stratosphere is different to that of the troposphere. The water concentration is much lower, very little water vapour makes it through the cold trap as water condenses into clouds in the troposphere. Methane oxidation is another source

of stratospheric vapour but very little water vapour is present in this region accounting for low cloud formation[3]. The clouds in the troposphere play a crucial role in ozone regulation, very little ozone reach the stratosphere as they either dissolve in the water or are broken down by chemical reactions in the troposphere. Some of the molecules that reach the stratosphere are nitrous oxide (N_2O), carbonyl sulfide (OCS), methane (CH_4), chlorofluorocarbons (CFCs) and halogenated compounds[3].

The earth's atmosphere consists mainly of N_2, O_2, Ar and H_2O, in addition to these components are a multitude of trace gases. The atmospheric trace gases can be divided into short-lived and long-lived trace gases. Most long-lived trace gases are important contributors to greenhouse gases and the atmospheric radiation budget. The short-lived chemical species make up the reactive species and govern the oxidation capacity of the atmosphere, the ability of the atmosphere to oxidize chemical compounds to water-soluble gases. The upper troposphere and lower stratosphere are dynamically and chemically distinct regions. The upper troposphere is characterised by fast migration of trace gas initiated by weather systems and convection.

The presence of NO in the troposphere is both natural and anthropogenic and is represented by eq (1.1 and 1.2)[4]. There are seven oxides of nitrogen of which N_2O, NO and NO_2 are most important that makes up the collective NO_x. NO_x is a principal constituent of air pollutants[5]. The dissociation products of NO_2, NO and O, are involved in the photochemical production of O_3. In the troposphere O radicals required for oxygen formation cannot be produced due to the lack of UV radiation blocked by the stratospheric ozone layer. On the other hand the role of NO_x in the troposphere is to catalyse the production of ozone as illustrated in the following equations[6].

$$NO + HO_2 \rightarrow NO_2 + OH \quad (1.1)$$

$$NO_2 + h\nu_{(\lambda<400nm)} \rightarrow NO + O(^3P) \quad (1.2)$$

$$O(^3P) + O_2 + M \rightarrow O_3 + M \quad (1.3)$$

Eq (1.1) depicts the production of oxygen (O_2) and nitrogen dioxide (NO_2) through the reaction of NO with perhydroxyl radical (HO_2). The photodissociation of NO_2 into NO and ground state oxygen atoms ($O(^3P)$) at wavelengths less than 400 nm[7] is depicted in eq (2). The rate of O_3 production depends on NOx concentration in the atmosphere. Photodissociation of ozone in the upper troposphere is associated with hydroxyl radical production which is the main oxidizing specie in the upper

troposphere[7].

A 2012 analysis from the WMO Global Atmosphere Watch programme showed the global average of CO_2, CH_4 and N_2O reached new highs. Compared to levels preceding the industrial age the levels have increased by 141%, 260% and 120% respectively. The atmospheric increase of CO_2 from 2011 to 2012 was higher than the average growth rate over the past 10 years. N_2O growth rate for the same period is a bit smaller compared to 2010 to 2011 but was still higher than the average growth rate. The report showed atmospheric levels of CH_4 increasing at a consistent rate. Radiative forcing by long-lived greenhouse gasses has by increased 32% with CO_2 accounting for 80% of this increase. In 2014 the average atmospheric increases of CO_2 from 2013 to 2014 was close to the average over the past 10 years. For NO_2 and CH_4, increases for the same period was larger than observed for 2012 to 2013 and greater than the mean rates over the past 10 years. The radiative forcing for the period of 1990 to 2014 increased by 36% with CO_2 making up 80% thereof. This poses a major problem because it directly impacts the earth's climate system[7].

1.2 Sources of nitric oxide

Africa is the only continent which has significant land mass in both hemispheres. Africa's total emissions are made of three region types. The first is windblown dust due to large arid regions, the next is densely vegetated forests and biomass burning. The third type is anthropogenic, which are generally clustered, of which industrialized South Africa makes up the largest component[8].

Vehicle emissions are major contributor to air quality deterioration. In urban areas vehicle emissions have been reported to be responsible for 90 to 95% of CO and 60 to 70% of nitrogen oxides within the atmosphere[9]. Emissions levels which require management locally and regionally are sulphur dioxide, nitric oxides, carbon dioxide, volatile organic carbons, persistent organic pollutants and particulate matter. Some of these compounds undergo chemical transformation which results in secondary pollution. Pollutant transport by wind, can result in these secondary pollutants causing problems in distant areas and even trans-boundary pollution[10]. Air quality is a direct threat to human health. Through inhalation these pollutants have direct access to our bodies and result in respiratory illnesses. Environmentally, these pollutants can cause

acid rain which results in secondary pollution such as acidification of soils and water bodies. Eutrophication is a condition where nitrogen stimulates the production of blue algae that causes the death of fish[11]. Sources of air pollution can be divided into natural and anthropogenic sources. Anthropogenic sources of air pollution comes from fossil fuel burning, electricity generation, vehicle and aircraft emissions and waste incineration. Secondary particulate emission concentrations are dependent on point source concentration, temperature humidity and time. The most common secondary pollutants are sulphates (SO_4^{2-}) and nitrates (NO_3^-) which emanates from sulphur dioxide and NO_x respectively. Nitric oxide is a product of high temperature combustion which is then photochemically converted to NO_2[12]. In Cape Town vehicle emissions have been assigned the major contributor to brown smog. A study by Walton (2005) identified five major sources to the brown haze problem. The sources that were identified were CBD, Cape Town international airport, Caltex Oil Refinery, Consol Glass and urban areas Khayelitsha and Mitchell's Plain. Based on the CALPUFF modelling system which tracked the spatial and temporal distribution of NO_x and SO_2 and PM10 (particulate matter with aerodynamic diameter less than 10 µM) found the CBD to be the greatest contributor of these pollutants due to the high traffic volumes[12]. According to the "National Environmental Management: Air Quality Act", the objective of the act is to enforce the implementation of the air quality management plans in South Africa to enhance the quality of ambient air. It includes a list of pollutants which require an Atmospheric Emission License that stipulates emissions standards[13].

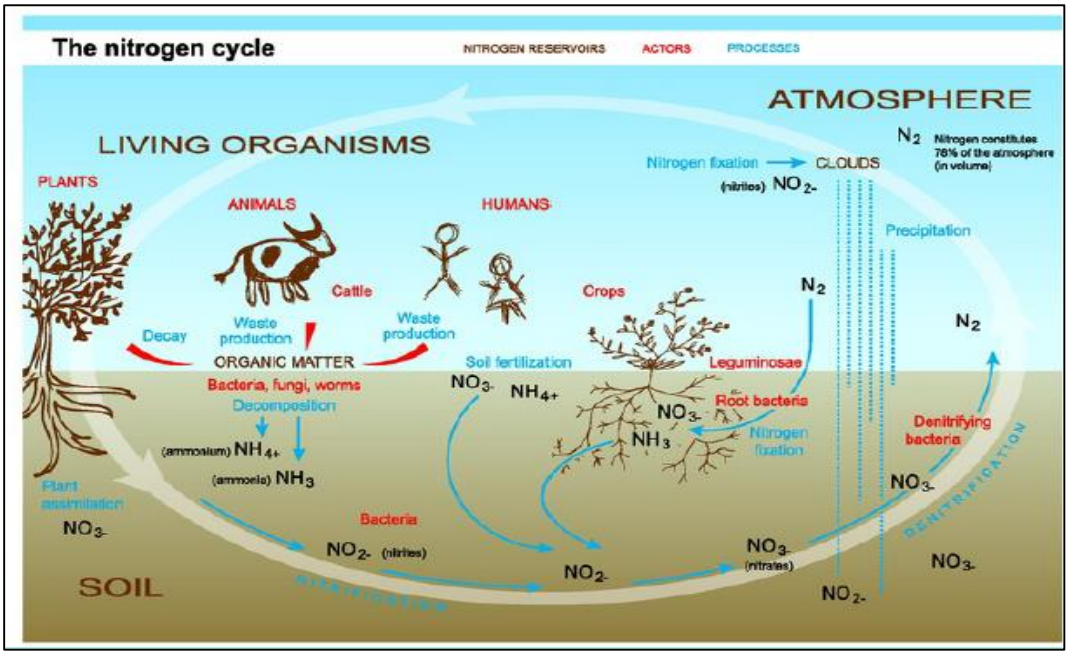

Figure 1: The nitrogen cycle[14]

The diagram in figure 1 illustrates the major nitrogen reservoirs, processes and contributors to the nitrogen cycle. Nitrogen forms part of an import class of biological chemicals. The conversion of nitrogen to bio-available nitrogen is essential to life's processes and can only be performed by biotic processes[15]. Nitrogen fixation can only be carried out under anaerobic conditions to essentially produce NO. NO is a product of biological processes but in recent years the environmental quota has come from anthropogenic intervention.

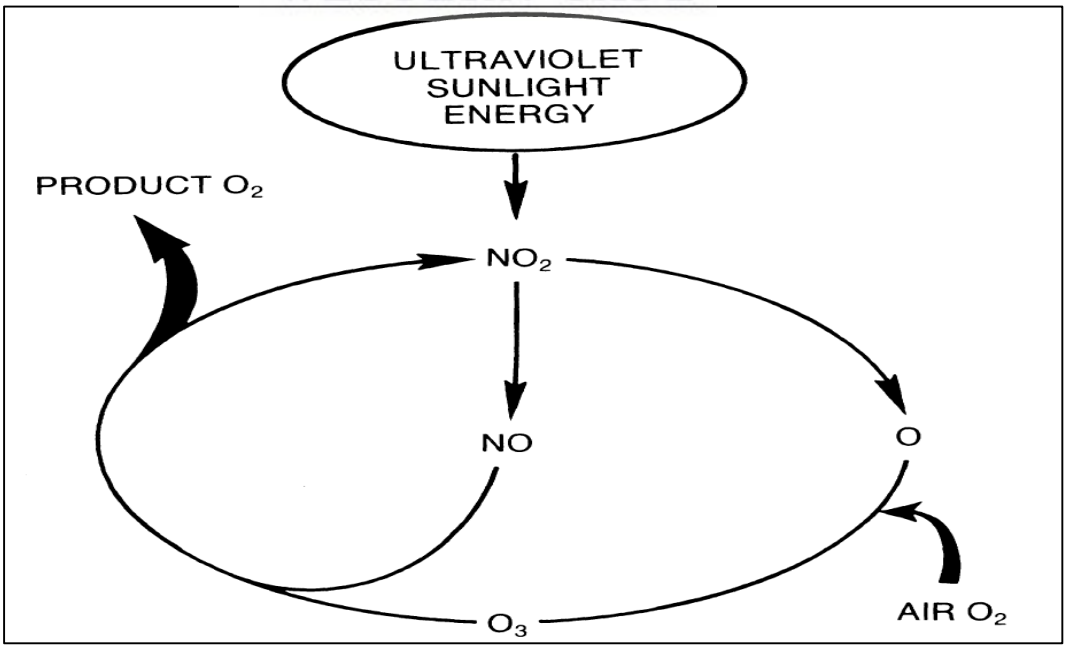

Figure 2: Atmospheric NO_2 photolytic cycle[5]

The nitrogen cycle has a major impact on the ecosystem. NO and N_2O are components of the nitrogen cycle and are powerful greenhouse gases which are directly involved in the production of O_3[16]. In the troposphere the oxidation of volatile organic compounds proceed in the presence of NO_x and sunlight which leads to production of ozone (see figure 2). Maintaining the NO_x balance is important as it has a direct impact on ozone production[17]. NO reacts with O_3 to produce NO_2 and forms the collective NO_x gas. NO has been reported to be directly involved in the production of OH and can have a direct impact on the oxidizing capacity of the atmosphere[18].

Portman, Daniel and Ravishankara (2012) reported on the chemical effects of source gases on stratospheric ozone. Their research built on existing knowledge and found all greenhouse gases play a role in the future evolution of ozone. The ozone hole was caused by a build-up of halocarbons. This resulted in heterogeneous reactions on aerosol particles to form reactive chlorine reservoirs. However, it's expected for ozone to recover once halocarbons return to natural levels. NO_2 on the other hand has been identified as the largest ozone-destroying gas of anthropogenic origin, and controlling N_2O emissions would make provision for a reduction in future ozone destruction[19].

The understanding of the regulation of trace gases is fundamental in interpreting climate regulation. This has sparked a demand in the quantification of such data which can be used for predictive modelling. The presence of NO in soil has been ascribed by Pilegaard (2013) as products of chemical and microbial activity. NO is mainly produced in soil by processes such as nitrification, denitrification and chemodenitrification (see figure 3). These processes can either be abiotic or biotic. Abiotic processes are only relevant in acidic soils with high NO_2^- concentration[20]. In nitrification NO and N_2O are by-products of ammonium oxidation to nitrate by nitrosobacteria.

$$NH_4^+ \rightarrow NH_2OH \rightarrow HNO \rightarrow NO \rightarrow NO_2^- \rightarrow NO_3^- \qquad (1.4)$$

(Eq) 1.4 outlines the nitrification pathway under oxygenated conditions as proposed by Ludwig et al., (2001). The rate of nitrification is controlled by the availability of NH_4^+ [20]. Under conditions where oxygen is depleted nitrate is reduced to nitrite and then to NO. During denitrification micro-organisms reduce nitrogen oxides to gaseous products[21].

$$NO_3^- \rightarrow NO_2^- \rightarrow NO_{(g)} \rightarrow N_2O_{(g)} \rightarrow N_{2(g)} \quad (1.5)$$

Figure 3 illustrates the production of nitric oxide in soil and the diffusion into the atmosphere[22]. The production and use of NO in soil can be ascribed to microbial activity and chemical activity. Nitrogen emission from soil forms part of the major sources of atmospheric NO. NO produced in soil can be decomposed either chemically or biologically. Emissions of NO from the soil is controlled by soil moisture which controls oxygen transport. Under dry conditions nitrification results in the emission of NO from soil. Under wet conditions denitrification inhibits the emission of NO from the soil[21].

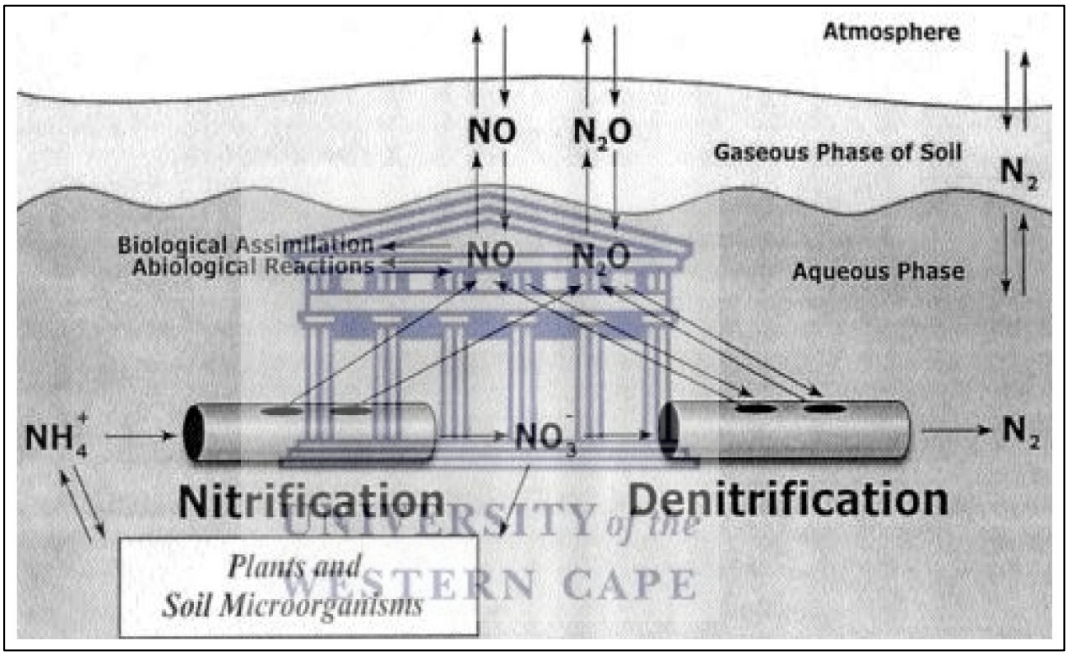

Figure 3: Soil emission of NO and N_2O[23]

Nitrogen oxides are vital to the ecosystem but modern agricultural practices has led to an imbalance in the biogeochemical cycle. The use of NH_3 based fertilizers has a direct impact on the levels of nitrites and nitrates in the water table. Higher levels of NH_3 will impact soil nitrification and denitrification processes, and lead to increased levels of N_2O and NO[24]. NO_x emissions from soil has been reported to be comparable to anthropogenic emitted NO_x to the amount of 20-24 Tg N per year.

Of all the sources of anthropogenically produced NO_x the combustion of fossil fuels contributes the most. NO_x proceeds via four pathways during the combustion process; through the Zeldovich reaction of atmospheric nitrogen and oxygen which occurs at

high temperatures, the oxidation of nitrogen compounds chemically embedded in organic matter, the reaction of hydrocarbon radicals with atmospheric nitrogen and the heterogeneous reactions of solid carbonaceous substances[25].

1.3 The significance of nitric oxide

NO is a free radical and is directly involved in plant physiological processes. NO influences a range of cellular processes in plants and has also been reported as a plant physiological mediator[26]. In bacteria and eukaryotes NO has been reported to play a crucial role in metabolic pathways. In some gram positive bacteria NO is required to regulate some metabolic pathways. Although there's been few reports on the generation of NO in bacteria Sasaki et al., (2016) proposed the pathway Arginine → NO → NO_3^- → NO_2^- where organic nitrogen was mineralised during vegetative cell growth[27]. The primary function of NO in plants is still debated but studies have reported that the production of NO forms part of a myriad of cellular processes. In more recent reports nitrite has been proposed as the substrate for NO synthesis via enzymatic and non-enzymatic routes[26]. The role of NO in plants has been reported to facilitate symbiosis. A common model used to illustrate this is the nitrogen-fixing symbiosis between leguminous plants and nodule producing bacteria. Nodule development occur alongside NO development, any disruption to NO production impairs nodule development[28]. Giudice et al., (2011) investigated the presence of NO and its roles on M trancatula-S. meliloti symbiosis based on the leguminous plants and nodule producing bacteria symbiotic theory. They reported a dependence on NO for optimal symbiosis which was explained on the premise of a link between cytokinin and NO signalling during nodulation[29].

NO functions from metabolic intermediates to defence mechanisms for invading species. In macrophages nitric oxide is generated as a cytotoxic weapon to poison pathogens. NO has also been described as a metabolic intermediate and helps to regulate the concentration of NO in denitrifying bacteria. On a cellular level NO can damage cells by competing with the host for metal acquisition[30]. Autreaux et al (2002) reported on nitric oxide's ability to inhibit ferric uptake regulation activity in E. coli. Ferric uptake regulatory proteins are involved in specific DNA sequences.

NO regulates important functions, one of the primary functions of NO is to regulate the interaction of O_2 with haemoglobin[31]. However, NO has a short life-span and its functions are mostly restricted to areas in close proximity to its production site, before it is oxidized by haemoglobin[32]. A short overview of the biochemistry of nitric oxide by Hill et al. (2010) provided the framework for the biological role of NO. Nitric oxide is largely derived from enzymatic and non-enzymatic pathways. Enzymatically, nitric oxide is produced by a group of enzymes nitric oxide synthase (NOS). The activity of this enzyme is regulated by various factors which include Ca^{2+} and the calcium binding protein and physical forces. NOS is stimulated by L-arginine and converted to L-citrulline and NO (see figure 2). Different isoforms of nitric oxide synthase (NOS) have different physiological functions. NOS1 (nNOS) and NOS3 (eNOS) are involved in microvascular tone while NOS1 is linked to the systemic regulation of blood pressure. These enzymes are mainly expressed in the vascular endothelium but has also been found in neurons, epithelial cells etc. NOS2 also called inducible NOS (iNOS) has the highest capacity to generate NO and is mainly expressed in multiple cells in response to inflammatory stimuli. Large amounts of NO has been associated with inflammatory disease of the gastrointestinal tract[33]. The main role of NO is to interact with metal centres to allow for electrochemical interactions[33].

NO can't be stored in the cells it's produced in. The expression of nitric oxide endogenously is tightly regulated, and is highly specific. Excessive production of NO has been linked to conditions such as cancer[34]. The expression of NOS in the body is targeted at a subcellular level. Strategies that are currently employed as standard practice for the monitoring of cellular nitrogen is through lipid modification and protein-protein interactions. NO is expressed by three isomeric enzymes which targets different cellular levels[35]. NO has been reported to modulate different processes related to cancer. Figure 4 illustrates the enzymatic synthesis process of nitric oxide.

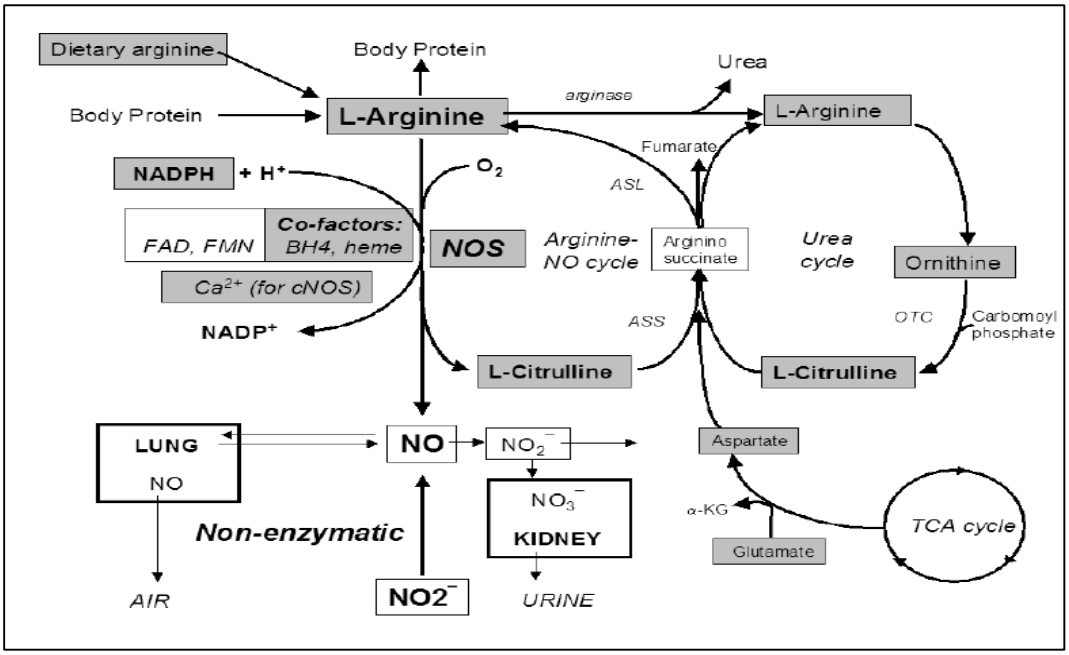

Figure 4: Nitric oxide synthesis pathway[36]

NO synthesis in mammalian cells proceed via the oxidation of L-arginine. The oxidation process is catalysed by the enzyme nitric oxide synthases and occurs in vascular endothelial cells. In order to synthesize nitric oxide from L-arginine the reducing agent NADPH is required. This reaction involves the reduction of arginine to citrulline. In addition to this process the synthesis of NO is regulated by the calcium-calmodulin enzymes and four co-factors NADPH, FAD, FMN and hemes[37]. Hemes and its components are coordination complexes and referred to as components of haemoglobin. These hemes can be described as iron coordinated to porphyrin which acts as a ligand. Flavin adenine dinucleotide (FAD) and flavin mononucleotide (FMN) are biomolecules involved in metabolic processes[38]. It can also be produced endogenously from nitrite. This occurs under acidic and hypoxic conditions where nitrite is reduced to NO by heme proteins. Nitric oxide is a free radical with a very short half reported in the range of 2 ms to 2s. Endogenously nitric oxide reacts with ferrous iron Fe^{2+} and other radicals. The reaction between NO and Fe^{2+} in nitrosylation, where NO coordinates with Fe^{2+}, is responsible for all biological effects of NO. The coordination of NO with the ferrous heme is involved with many biological processes. NO controls a number of actions in the body such as vasodilation and regulation of normal vascular tone. It also inhibits platelet aggregation which prevents thrombus formation to list a few[37]. The interaction of NO with Fe^{2+} is very rapid and can therefore coordinate easily to haemoprotein iron, free iron and iron-

sulphite complexes. The binding process of NO to haemoglobin is also a method by which the body regulates nitric oxide in the body[39]. Interferents such as O_2^- interferes with the nitrosylation process where NO can no longer coordinate with Fe^{2+} [4031].

Nitric oxide synthase can be analysed by a range of methods based on either citrulline or NO formation. NO formation can be measured quantitatively in two ways, the oxidation of haemoglobin and the formation of NO_2^- + NO_3^-. The oxidation of haemoglobin is measured by spectrophotometric assays. NO_2^- is measured by the enzymatic reduction of NO_3^- and performing the Griess test. The other method involves measuring NO_2^- through chemiluminescence or HPLC with UV detectors[38].

Nitric oxide concentrations can serve as a measure of disease. Physiological nitric oxide production is affected by illness. NO production has been reported to be affected in patients with sepsis[36]. Sepsis is the body's response to infection which results in metabolic changes. Arginine is the only substrate that allows for the production of NO through nitric oxide synthase. Metabolic changes induced by infections can have a direct impact on the metabolism of arginine[41]. A study by Luiking, Poeze, Ramsay and Deutz (2009) investigated the production of arginine from citrulline. Ten critically ill patients with septic shock and two other control group patients were used in their study. The study found protein breakdown in patients with sepsis were higher compared to the controlled groups which had a direct impact on citrulline and arginine metabolism. This was characterized by decreased production in citrulline and arginine and nitric oxide[42].

The availability of nitric oxide has been reported to be affected by obesity. Diminishing expressions of NOS3 enzymes has been reported in obese adults and rodents. Studies have shown there to be an interdependency between insulin resistance, obesity and endothelial dysfunction. However, conceptualising this relationship appears challenging. Insulin has been associated with endothelial dysfunction. Georgescu et al., (2011) examined the mechanism and correlates by which obesity affected subcutaneous adipose tissue. The study reported diabetes to alter the structure, function and biochemistry of peri-umbilical adipose tissue. Insulin stimulates the production and release of nitric oxide, however structural modification to arterioles by obesity was found to cause a significant reduction in eNOS expression and NO production[43]. A study by Kraus et al., (2012) investigated the relationship

between inducible nitric oxide synthase (iNOS) based on the rodent model which demonstrated a strong relationship between insulin resistance and iNOS. The study concluded there to be no relationship between insulin resistance and iNOS protein expression[44].

Under pathological conditions, where higher concentrations of induced NOS are recorded the metabolic pathway of NO changes. When this occurs NO can directly regulate the functions of ion channels and interfere with cellular processes. In spite of NO's role in homeostasis NO radicals can cause DNA damage. DNA damage can result in two ways, reaction of NO with molecular oxygen or superoxides. Reactions with molecular oxygen can result in the formation of carcinogenic N-nitrosoamines. Reaction of NO with superoxides can produce peroxynitrite anions that can cause cellular damage[45]. Studies have reported on the involvement of NO in gastrointestinal ulcer formation and inflammation. Patients that tested positive for gram negative bacterial infections in gastrointestinal disease showed higher levels of iNOS mRNA expression[33]. The study by Kaise et al., (2003) examined the expression of iNOS in patients with duodenal and gastric ulcers. iNOS expression in the gastroduodenal mucosa was found to be higher in patients infected with gram negative bacteria associated with gastrointestinal disease, and recorded a decrease on iNOS expression when the bacteria was eradicated[46].

NOS effect in tumour growth has been outlined in a review by Xu et al., (2002) reported on the absence of iNOS in tumorigenic cells which promoted intestinal tumorigenesis in mice. Gal and Wogan (1996) investigated the impact of excess NO in the spleen and lymphatic tissue of mice. They developed an experimental model where they stimulated a specific immune response to induce iNOS expression in macrophages located in the spleen and kidney. NO was found to only induce mutation in the spleen of the mice and not the kidneys[47]. In breast cancer NOS was detected in invasive tumours grade 1 and benign tumours showed no detectable levels of NOS activity. Elevated levels of NO was reported for constitutive and inducible NOS for invasive tumours. The study concluded positive expression for NOS expression in breast tumours but was related to the grade of the tumour[48].

NO has been found to have contrasting effects on tumour growth, it either stimulates or supresses it. Ambs et al., (1998) modified tumour proteins to endogenously express

NOS and found NOS expression in non-mutated tumour proteins had reduced tumour growth. However, where these proteins were mutated to over express NO tumour growth was promoted[49].

1.4 Problem statement

NO plays an important role in biological processes. This makes the development of fast and sensitive detection methods very essential for measuring NO in biological samples and organisms. Although electrochemical techniques allow for good spatial and temporal resolution for long-term NO detection, NO detection for electrochemical sensors still remain challenging. NO has a very short half-life. NO is a free radical and reacts extremely fast with oxides, peroxides and superoxides.

Nitrites are electroactive species which have been reported to readily oxidize at platinum electrodes polarized at +0.9 V. However the high oxidation potential of nitrites introduces the prospect of interferences from other species in complex media[50]. Nitric oxide oxidation proceeds via an electrochemical mechanism. In the first step nitric oxide is oxidized by the solid electrode to form a nitrosonium cation (NO^+) which is a strong Lewis acid which explains the short lifespan of these species. The NO^+ ion is subsequently converted to nitrite. The oxidation potential of nitric oxide and nitrite is between 60 to 80 mV more positive than 800 mV, and forms the basis of nitric oxide detection in solid electrode systems. It is this very characteristic which facilitates the discrimination between oxidation products, nitrites and nitrates, of nitric oxide[51].

Advancements in improving sensitivity and selectivity with these sensors have been established in literacy to evolve around the development of suitable membranes for these electrodes[52]. Badea et al, 2001 designed a sensor that could effectively discriminate against nitrites and nitrates based on nitrite oxidation in acetate buffer using a Pt electrode. The electrode was polarised at +900 mV against AgCl reference. In order to make Pt electrodes selective to nitrite oxidation the electrodes were modified with cellulose acetate membranes. The membranes were applied in the design of an amperometric sensor for the detection of H_2O_2. Although the sensor was never tested for nitrite permeability, in its application the sensor displayed good mechanical stability and selectivity towards nitrite though low. Direct electron

transfer, between redox proteins and conductive membrane layers, has been scrutinized for years in an attempt to reproduce the mechanistic charge transfer processes for sensor application. Research has reported on the complexities associated with depositing these enzymes on electrode surfaces, for the purpose of reproducing direct electron transfer at the protein. One such enzyme is cytochrome-c, class I of the c-type cytochrome family. Cytochrome-c is a protein containing heme moiety. It's linked to specific cysteines via thioether linkages and surrounded by a folded peptide chain[53]. During electron transfer reactions the heme alternates between reduced ferrous (Fe^{2+}) and oxidized ferric (Fe^{3+}) states[54]. Although cytochrome-c adsorbs strongly to metal electrode surfaces such Au, Ag, Pt of Hg it suffers conformational change of the protein which leads to retardation in electron-transfer kinetics[55].

Considering the complexities presented in literature when working with these hybrid systems, is it possible to synthetically emulate biosensors. Will these synthetic sensors be capable of reproducing the functions of its biosensor counterpart when exposed to specific analytes. More importantly will these sensors be stable and will the process be reproducible.

Millar and Day (1996) investigated the biological effects of nitric oxide (NO) on cytochrome oxidase. Previous reports cited NO affects respiration by inhibiting cytochrome oxidase. Therefore, the focus of the research was more on plant mitochondrial electron transport in the mitochondria. NO was found to inhibit oxygen consumption via the cytochrome pathway, however as the concentration of NO reduced the inhibition of respiration via the cytochrome pathway was reversed. In the presence of NO respiratory inhibition was circumvented by alternative oxidase which facilitated electron flow[56].

1.5 Research hypothesis

Specific detection and quantification of NO still remains challenging[52]. Although many analytical techniques have been developed, some of the most common techniques are chemiluminescence, UV-vis spectroscopy, electron paramagnetic resonance and electrochemistry[57]. All these techniques have limited application with respect to sensitivity and specificity. Most techniques rely on the measurements of secondary nitrite and nitrate species. Electrochemical techniques using ultra micro-

electrode systems presented the possibility of direct detection of NO offering a range of favourable characteristics; good selectivity towards NO, good sensitivity, fast response, long-term stability and ease of handling[52].

Electrochemical detection of NO relies on the modification of the electrodes surfaces and exploiting the redox properties of NO. NO can either be oxidized or reduced electrochemically depending on the nature of the solution. Affinity towards NO can be achieved by modifying the electrodes with materials selective towards NO oxidation.

NO in its free form is highly reactive in biological systems and is converted to nitrite and nitrates in water in the presence of oxygen. S-nitrosothiols have been reported to play a key role in transnitrosation reactions. Amino acids such as cysteine play a key role in the production of S-nitrosothiols through the degradation of GSNO (S-nitrosoglutathione) resulting in higher NO concentrations[58]. Palemerini, Arienti and Palombari (2003) exploited this cellular production of NO process to assay the production of NO by cells. The system consisted of a graphite electrode, two $Ni_{1-x}O$ or Ag/Ag_2O reference electrodes and a zirconium phosphate protonic conductor. This was connected to a reaction vessel and a trap containing acidic solutions of MnO_4^- which converted NO to a more stable analogue for detection. With this system they were able to detect NO concentrations as low as 5 to 10 pico molar. The system has been reported effective for the monitoring of the release kinetics of NO donors[59]. Brown and Schoenfisch (2018) presented work that drew comparison between metollophthalocyanine (MPc) analogues. MPc compared to Metalloporphyrins (MP) catalysts presented greater thermal and chemical stability. Iron-phthalocyanine (FePc), cobalt-phthalocyanine, nickel-phthalocyanine and zinc-phthalocyanine were identified in a previous study as the most catalytic MPc complexes. NO selectivity is generally achieved through permeable membranes or electrocatalysts. Permeable electrodes enhance selectivity. Anionic and cationic membranes enhance selectivity by electrostatic repulsion. Although multiple membranes can facilitate selectivity it compromises electrode sensitivity[60]. Electrocatalysts function by enhancing NO signals or reduce the oxidation potential by means of electron transfer kinetics. Signal enhancement is generally restricted to the target analyte. Theoretical and experimental selectivity coefficients were calculated for each complex to tease out any signal interferents. FePc displayed the greatest selectivity for NO[61].

Literature is overwhelmed with publications in measurements and detection methods of nitric oxide. However, detection of nitric oxide still remains challenging. Some nitric oxide sensors are limited in their sensitivity, stability and reproducibility. Sensors selective towards nitric oxide have additional coatings which are vital in the ability of these sensors to minimize interferences[5152]. Sensor performance depends on the electrode material and polymerization conditions that dictates polymer properties. The potential at which NO is detected depends on the substrate, electrochemical properties of the membrane and surface roughness[60]

1.6 Aims and objectives:

Aim 1:

To synthesize a highly conjugated Schiff base compound that will serve as a suitable platform for metalloproteins, specifically cytochrome-c. The metalloprotein has a central heme which lies at the core and forms the basis of its electrochemical properties. The Schiff-base will orientate the metalloprotein in a manner which will retain and promote its innate electron transfer capabilities.

Objectives:

- To synthesize a highly conjugated heterocyclic Schiff base material by means of a standard condensation reaction.
- Physical and electrochemical characterization to confirm successful formation of the hinge type Schiff base. Spectroscopy techniques such as Fourier-transform infrared spectroscopy (FTIR) will give confirmation of the imine linkage. Schiff bases show strong IR absorption bands for O-H (3475 – 3392cm-1), N-H (3386 – 3313cm-1) and C=N (1632 – 1592) respectively. In the case of successful formation of the imine absorption bands at 3375cm^{-1} and 1621cm^{-1} is expected. Ultraviolet-visible spectroscopy (UV-Vis) is extremely useful when studying molecules with conjugated pi systems. It is expected of H-NMR analysis to reveal singlet peaks for N=CH- in the vicinity of 8.5.
- The Schiff base will then be electrodeposited and modified with the metalloprotein cytochrome-c. Electrochemistry will be performed on the denatured enzyme composite to map the redox behaviour of the system, using primarily cyclic voltammetry and square wave voltammetry.

Aim 2:

Metalloproteins however present some limitations one of which is electron transfer retardation. Therefore, a synthetic analogue of cytochrome-c will be synthesized that will mimic its electron transfer process. This process will proceed by synthesizing a Schiff-base macromolecule from the monomer that will replicate the redox properties of the Schiff-base metalloprotein complex.

- The Schiff-base ligands will be used in the design of a FeL_4 type complex to simulate the orientation and structure of denatured cytochrome-c, by chelating the iron with the Schiff base through refluxing the Schiff base in an alcoholic iron salt solution.
- The spectroscopic and electrochemical evaluation of the FeL_4 complex and its ability to mimic the redox properties of the cytochrome-c deposited onto the Schiff base modified electrodes. Spectroscopy techniques such as FTIR will give confirmation of the iron linkage to the Schiff base in the mid infrared region in the vicinity of 500 cm^{-1}. EDS and EELS will give evidence of the presence of elemental iron

Aim 3:

The composite material will then be applied in NOx detection studies. In the design of the composite material the heme structure of cytochrome-c was emulated by using the Schiff-base ligand and complexing it with iron. The electron transfer reactions of the complex was then compared to the Schiff-base modified with denatured cytochrome-c.

- A UV control study will be performed aimed at evaluating time-dependent changes to the concentration of nitric oxide in phosphate buffer at pH 7.
- The response of the sensor systems developed will be evaluated using NO donor, diazeniumdiolates (Z)-1-(N, N-diethylamino)-diazen-1-ium-1,2-diolate (DEA-NONOate). DEANONOate spontaneously decomposes to nitric oxide in neutral pH and will be electrochemically detected. The electrochemical

techniques that will facilitate the experimental research are cyclic voltammetry and square wave voltammetry.

- The sensor systems will be assessed in the application of nitric oxide recovery. Screen printed carbon electrodes modified with the iron ligand material will be applied in experimental studies to recover nitric oxide from synthetic urine.

Chapter 2

2. Literature review

The following review discusses the prospects of Schiff base ligands and their applications as suitable biosensor platforms for NOx detection. NO oxide plays a key role as biological messenger in the biological system, however detection and quantification of NO have always posed significant problems. NO is a free radical and react extremely fast with oxygen, peroxides and superoxides. It's these reactions which are responsible for NO's fleeting existence. And this is why the specific detection and quantification of NO still remains challenging[52].

2.1 Background

Presently there are many techniques available for measuring gases for quantitative or qualitative analysis. Many of the techniques however are sophisticated and technical with instrumentation requiring serious capital investment. Therefore the past few years there has been extensive efforts devoted to the development of gas sensor technologies. Gas sensors are chemical sensors that translates chemical states into electric signals. In these sensors a sensitive layer is in contact with the analyte. When

exposed to the analyte the sensitive layer undergoes a change in chemistry. The sensitive layer is mounted on a platform which translates the chemical change of the sensitive layer after exposure to the analyte into electrical signals. Chemical sensors are divided into two domains, physical transducers and chemical interfaces. The chemical interface refers to the chemical interaction of the analyte with the surface which facilitate changes in either the physical or chemical properties of the sensor[62]. Biochemical gas sensors have achieved success in detecting H_2 by means of gas-permeable membranes with immobilised bacteria and achieving satisfactory selectivity. However, these devices are not functional at elevated temperatures. Semiconductor sensors have two types of sensors: either semiconductor metal oxide films or mixtures of semiconducting oxides and metal phthalocyanine organic semiconductors. Poor selectivity to different gases is still a major limitation with these systems. Solid electrolyte sensors are well known for its quality performance and has been the most promising of the lot for commercial applications due to its high selectivity, simplicity and rapid response time. Major advances were made in galvanic cells and accelerated with advancements in the fields of solid-state ionics and electronics. The performance of solid-state electrochemical gas sensors were rated on response time, thermodynamic stability, operating temperature, gas-sensing ability and sensitivity. However, the need for cheap, easily deployable sensors that could collect emission data over wide areas were required to better understand NO_2 emissions over broad landscapes.

2.2 Sensors

Electrochemical sensors are analytical devices which can translate analytical information to electronic signals through transduction. Electron transfer is inherent to biological and chemical systems and is mostly associated with energy transduction. In nature basic fundamental processes rely on the electron transfer reactions associated with redox proteins. In electrochemistry the electron transfer between the analyte and electrode surface forms the backbone of analytical detections by converting bio-recognition processes to signals. This process is referred to as electrochemical transduction. In potentiometric devices the former process is characterized by the production of a potential signal. In amperometric systems the subsequent signal response is an expression of the redox activity of electroactive species[63].

Sensors can be classified on their mode of transduction and application. Sensors that are based on transduction are; Potentiometric sensors, which can either be symmetrical or asymmetrical. Potentiometric sensors applied as biosensors incorporating enzymes and antibodies consume or produce species which can be directly monitored by an ion-selective electrode. In amperometric sensor the signals are proportional to the concentration of the analyte specie. Suitable species for detection are electroactive species which are capable of oxidation or reduction. A study by Umaña and Waller (1986) reported on the amperometric detection of glucose. Glucose oxidase enzyme was electrodeposited onto the electrode surface by electropolymerizing pyrrole in the presence of the enzyme. The glucose oxidase could be incorporated into the polypyrrole film during formation for glucose detection. The sensor could determine glucose in an aqueous environment for up to seven days[64].

Polymers serve one of two functions. In sensor devices they either participate in the sensing mechanism or immobilizes the component responsible for sensing[62]. Piezoelectric sensors generate acoustic waves which are propagated by an external alternating current between two electrodes. These sensors are mostly applied for gas-phase monitoring calorimetric sensors. The measured resistance is a function of temperature and is commonly used in thermal enzyme probes. Optical sensors find application in the measurement of light absorbed or emitted during a biochemical reaction. The light waves are guided by optical fibers to suitable detectors and find application in the measurement of pH, O_2, CO_2 etc.

2.3 Advances in sensors

In recent years research and development rendered new classes of polymeric sensor material with properties intrinsic to inorganic systems. Conductive polymers contributes more than a suitable medium for the biological component. These polymers are known as conductive polymers which exhibit unusual electrical and optical properties[62]. Conducting polymers exhibit electrochemical driven expansion and shrinkage that are driven by oxidation/reduction processes under applied potential. During the oxidation reduction processes when conductive polymers are laminated against a second layer, a stress gradient is generated which, can either cause bending away or towards the conductive polymer film. Gaihre et al., (2013) examined the

displacement of bilayer actuators based on three different polymers (polypyrrole (PPy), poly(3,4-ethylenedioxythiophene) PEDOT and poly(3,3-dihexyl-3-4-dihydro-2H-thieno[3,4b][1,4]-dioxepine [PProDOT(Hx)2] synthesized under different conditions. The study found the displacement of the chemically synthesized bilayer actuators were lower than the electrochemically synthesized actuators that showed better displacement. It was found that the conducting polymers that were electrochemically polymerized exhibited greater conductivity. The polymers are arranged from that of greatest displacement to lowest; PPy, PProDOT(HX)2 and PEDOT[65]. Conductive polymers have been reported to be influential in the electrochemical reactions of the system as well expressing selective and transducer properties as well. The contribution of conductive polymers can be explained as follows; in the case of its selectivity the material, when exposed to redox environments, adopts a reduced or oxidized state. The redox environment generally is created by specific analytes, which facilitates the metamorphosis of the conductive polymer affording it an altered electrochemical fingerprint[66].

Electrically conducting conjugating polymers display interesting electrical and optical characteristics. Electrically conductive polymers differ from inorganic semiconductors in that polymers are molecular in nature and lack long-range order. Conducting polymers contain π-electron backbones which are responsible for the electrical conductivity, low energy optical transitions, low ionization potential and high electron affinity. It is this innate property of conducting polymers that makes their application in sensors as attractive. It enhances speed, sensitivity and versatility of sensors. Conductive polymers have shown promise in sensing for gases with acidic, basic or oxidizing characteristics. Conducting polymers in gas sensing applications are polythiophene and its derivatives, polypyrrole, polyaniline and composites of the polymers[67]. In pH sensors polyaniline membranes have improved on sensor stability in the presence of air. In ion-selective electrodes the conducting polymer can either be the conductive system or function as a matrix for the conductive system. When using PANI as a membrane, matrix ionic response signals can be transformed to electronic signals[68]. The conductivity of conductive polymers can be manipulated by doping using electrochemical techniques. The electrical conductivity is also affected by responses to changes in pH, applied potentials or their environments[69]. Polymer materials are generally associated with flexibility and ease of process but they also

possess conducting properties. These properties are associated with a class of polymers, conjugated polymers, with electrical and conducting properties similar to metals and semiconductors. These properties of conductive polymers makes for interesting applications as electrochemical sensors[70].

2.4 Conductivity and electrochemical sensors

Conjugated polymers made up of conjugated π-electron systems delocalize along the polymer backbone. Injection of a charge into the polymer backbone results in a reorganization of the electronic state excitation, where the intruding electron fits into the deformed chain of the polymer. This phenomenon is referred to as the *polaron/bipolaron* state[67] which accounts for the electrical transport mechanism in conducting polymers. The polaron/bipolaron effect was illustrated by Heeger (1985) who performed a series of excitation experiments on polyacetylene and polythiopene systems. The study assessed the mid-gap state and the subsequent changes to the characteristic IR absorption spectra induced by chemical dopants or photoinduced excitation[71]. Conductive polymers not only play a role in charge transfer mediation but also acts as a binding mechanism[66]. The former was illustrated by Swann et al. (1997) whom studied the function of polypyrrole films in enzymatic electrodes, in particular diffusivity. The study was conducted by modifying a Pt electrode containing a film of D-fructose dehydrogenase with polypyrrole. The performance of the electrode was assessed on the basis of standard fructose response. The performance of the composite sensor was enhanced substantially with a charge capacity ranging between 1000 to 2000 nA/cm^2 and a fructose activity reduction from 300 to ~190 mU/cm^2 in comparison to the fructose monolayer electrode. They attributed the performance of the sensor to the charge transfer capacity of polypyrrole. This however was found to be subject to polymer thickness[72].

2.5 Biological integration in electrochemical sensors

There's been extensive reports on electronic communications between functionalised conducting polypyrrole and redox proteins, in solution. What was achieved was an approach to study biological electron transport between proteins and polymeric materials using electrochemically functionalised conducting polymers to produce thin

films[73]. The methods used had potential advantages over more standard techniques used in bioelectrochemistry as found in self-assembled monolayers. By employing this technique polymer films could be used to modify a wider range of electrode materials which allowed for the synthesis of biological significant chemical functionalities at the surface for molecular recognition. The synthesized functionalized interfaces could be introduced to the biological solution as a stable film. It also allowed for altering of the physical character of the film by modifying polymerization conditions[74]. The theoretical study by Del Nero, Galvão and Laks (2003) found electrochemical behaviour of the substituted pyrrole monomers to be unaffected by the absence of carboxylic acid groups when used as a working biosensor for cytochrome-c. Carboxylic acid groups were reported to facilitate the orientation of the protein and enable electron transfer. The study found on the other hand that the structures of the monomers were responsible for the differentiation in electrochemical behaviour[75].

Immobilization of biomolecules often compromise the activity of the enzyme. Losses have been attributed to conformational changes or interactions between the biomolecule and the solid surface. Chah, Kumar, Hammond and Zare (2004) presented a method to quantify the biological activity of the biomolecules attached to solid surfaces. The stability of biomolecules were reported to be a function of its thermodynamic properties which could be expressed through Gibbs free energy. The technique that was used to monitor the enzyme kinetics was surface plasmon resonance. It provided information on the refractive index of the denatured and renatured biomolecule. The reflectivity of the light would in turn affect the dielectric constant and the thickness. The changes were then expressed in the SPR plots. This facilitated the calculation of the Gibbs free energy and allowed for the quantification of denaturation and renaturation changes of the biomolecule[76]. Electronic kinetics of immobilized proteins are slow and slows down further as SAM chain length increases. Experimental work has indicated electrostatic or chemisorptive end-capping of the proteins with gold nanoparticles to improve distant donor-acceptor electronic coupling. A study by Caban, Offenhäusser and Mayer (2009) bovine heart cytochrome-c was electrostatically coupled to an atomically flat Au (111) surface through a monolayer of 11-mercaptoundecanoic acid. AFM and SEM characterisation confirmed the presence of gold nanoparticles on the protein monolayer. Binding of the gold nanoparticles to cytochrome-c was identified with AFM to proceed via two

mechanisms which was identified by changes in magnitude of redox response. It was postulated that the attachment of the nanoparticles might have caused substantial deformation of the protein's ternary structure resulting in increased heme-electrode distance. The changes in response was related to immobilization time of the particles and their size. Binding of the Au nanoparticles was also found to favourably alter the spatial geometry of cytochrome-c by accelerating the long range electron transfer rate of the protein[77].

2.6 Redox proteins in electrochemical sensors

Cytochrome-c has been reported to loose functionality once immobilized on an electrode surface. The loss in function has been reported to be attributed to protein denaturation, however modifying the electrode surface by chemisorbed self-assembled monolayers (SAM) appears to have overcome that limitation. The interaction between the protein and the SAM has been found to be paramount in the enhancement of the electron transfer capabilities. Modifying the electrode surface with a self-assembled monolayer of alkanethiols, an approach by Tanimura et al., (2002), would see the orientation of the enzyme align the positively charged lysine residues with the negatively charged carboxylate head group, enhancing the electron transfer capabilities[78]. Other methods that have also been applied involve modification of the enzymes with reactive groups. Tümer et al., (2008) constructed an amperometric biosensor capable of real-time non-invasive detection of extracellular H_2O_2 released by aquatic microorganisms. The sensor was constructed by first modifying cytochrome-c lysine derivatives with carboxyl-terminated thiol derivatives mercaptopropionic acid (MPA) or mercaptoundecanoic (MUA). This was achieved by carbodiimide/N-hydroxysuccinimide (EDC/NHS) activation. The capping terminals were prepared in phosphate buffer saline (PBS) at pH 7 mixing 0.5 M of MPA or MUA with equimolar concentration of EDC and NHS under stirring. 5 ml of 500 µM cytochrome-c in PBS was then mixed with 50 µL of the MPA/MUA solution at room temperature whilst stirring. After 2 hours ascorbic acid was added to the mixture to reduce the protein which was then purified in a separatory column. The electrodes were modified by dipping them in PBS electrolyte containing the protein solution. Prior to this step the electrodes were treated with hot “Piranha” a mixture made up of concentrated H_2SO_4 and 30% H_2O_2 in a 7:3 ratio. Modification of the electrodes with

the thiol derivatives allowed for fast absorption onto the electrode surface. The sensor in its application exhibited high affinity for H_2O_2 with limits of detection ranging from 1 µM to 250 µM. What was most impressive was the real time analysis of H_2O_2. Addition of 1µM H_2O_2 displayed an immediate spike in the cathodic current demonstrating that cytochrome-c based amperometric sensors are well capable of real-time analysis[79].

Previous studies have shown carbon materials can be used as mediators to promote electron-transfer reactions of cytochrome-c. Therefore, Zang (2008) investigated the electron transfer between horse heart cytochrome-c and carbon by immobilizing cytochrome-c in and on 3D ordered macroporous active carbon electrode (MPCE). The study also looked at the electroactivity of cytochrome-c when immobilized on the substrate surface and its pseudo peroxidase activity. Cyclic voltammetry of cytochrome-c/MPCE confirmed the successful immobilization of cytochrome-c on the surface of MPCE. The results identified a negative shift for the redox reaction of cytochrome-c. It was speculated that the interaction was an electrostatic interaction between the positively charged cytochrome-c and negatively charged carboxylic groups on the surface of MPCE, and the intercalation interaction of cytochrome-c with the 3D porous active carbon itself. The interactions were confirmed by spectral characterisation, FTIR absorption spectra identified shifts in absorption peaks for cytochrome-c; 1647.9 to 1657.6, 1556.6 to 1545.5, 1462.4 to 1448.6 and 1407.0 cm^{-1} to 1402.8 cm^{-1} respectively[80].

The electron transfer properties of proteins and enzymes at electron surfaces have been found to be inconsistent and specie specific. Certain amino acid sequences of some species identified variations in electron transfer kinetics in cytochrome-c oxidase/ cytochrome-c. The study by Rhoten, Burgess and Hawkridge (2002) identified a difference in surface morphology of cytochrome-c. Tuna cytochrome-c displayed higher hydrophobicity. Their findings suggested cytochrome-c oxidase possess the ability to distinguish between cytochromes from different species, essentially the ability for an electrode to distinguish between proteins. The electron transfer kinetics were a function of current and was also found to be a possible indicator for oxidative damage to the components of the mitochondrial electron transport system. Myocardial damaged has been linked to cytochrome-c reductase as a marker. A reduced oxidative

activity in cytochrome-c reductase was identified as an indicator for ischemic injury[81]. Caban, Offenhäusser and Mayer (2009) investigated the morphological changes displayed by cytochrome-c when exposed to denaturants. The natural structure of cytochrome-c has been found to protect the heme of the protein, inhibiting solvents from reaching the active site. However, once the pH was agitated the structure unfolded to expose the heme of the enzyme. This was quite significant as it afforded the protein peroxidase activity. The catalytic reduction of H_2O_2 was electrochemically identified. However, the peroxidase activity was only observed in the pH range of 3 to 7. It was speculated that with increased pH the peroxidase activity decreased. The denaturation process was also found to be irreversible. When the pH was raised back to 7.5 only the charging current was displayed which was indicative of the loss of the native confirmation[82].

One of the prerequisites for reagentless biosensors is to facilitate adequate communication between the electrode and the biocatalytic system. The primary objective is to maintain adequate distance between the electrode surface and enzyme as this will allow for electron transfer processes with high rate constants. Biocatalyst with small molecular weights can facilitate better electrochemical communication between the electrode and the environment with its redox active sites[83]. It's been suggested that the electrochemical behaviour of enzymes are altered when adsorbed onto electrode surfaces. The reason for the specific occurrence, in the case of cytochrome-c, the enzyme adsorbs irreversible on electrode surfaces and subsequently denatures[84]. Szücs and Novák (1995) investigated the interaction between electrode surfaces and cytochrome-c. The study found experimental conditions to be imperative on the electrochemical characteristics of cytochrome-c. By altering the experimental conditions they were able to retain the reversible character of the enzyme adsorbed onto the bare electrode surface. The electrochemical response was found to be stable and near reversible near 60 mV with a scan rate of 20 mVs^{-1}. However, reproducibility of these results were not as straight forward and was dependent on very intricate methodologies. Good reversible electrochemical response was found to be dependent on a range of conditions. The age of the sample, the dissolution procedure of the enzyme, concentration, type of electrode surface and stabilisation time were all influencing factors. The electrochemical activity was found to improve with time. The electrochemical activity was however compromised by aggregation of the enzyme.

Increased oligomer concentration per unit area was found to deteriorate the electrochemical response. The adsorbed oligomers were suspected to be the cause of a positive shift in the redox potential when compared to the monomeric form. The variation in the electrochemical response of adsorbed cytochrome-c on both gold and glassy carbon electrodes was suggested to be related to the structure of the adsorbed state. Adequate anchoring to the electrode surface inhibited aggregation, maintaining monomeric molecular layers. The monomeric forms of the enzyme was found to facilitate reversible electron exchange of cytochrome-c. The complexes on the other hand were reported to block the reversible chemistry and cause shifts in potentials[8584].

Bonanni et al., (2003) performed a study on yeast cytochrome-c (YCC) which makes up a key component of the mitochondrial respiratory chain. It plays a role in electron transfer between membrane-bound enzyme complexes. In order to integrate these unique functions of the proteins with bioelectronic systems the proteins were required to be immobilized onto an electrode, preferable through chemisorption in order to preserve the unique functions of the protein. The study found no cluster formation or mobility on the surface of the electrode. On the gold substrate yeast cytochrome-c proteins bound covalently with the surface of the electrode with up to 84% coverage of the gold electrode substrate. The proteins were found to retain their redox-activity whilst preserving morphology[86].

Chen et al., (2002) probed the non-destructive adsorption of cytochrome-c on electrode surfaces whilst maintaining maximum potential of electron exchange between the electrode surface and the protein. Numerous studies have reported on the destructive effect of adsorption of cytochrome-c on electrode surfaces which subsequently compromised the electrochemistry of the enzyme. This was attributed to the manner in which the enzyme adsorbed that lead to conformational changes and in the end denaturation. The use of self-assembled membrane layers (SAMs) is almost explicitly associated in literature with protein conformation on organic surfaces, and the influence on the protein. SAMs terminating in specific functional groups were selected that was based on the environmental conditions they represented. Cytochrome-c was reported to undergo substantial conformational change when adsorbed onto hydrophobic surfaces. This resulted in the denaturation of the enzyme. The report goes on to discuss how SAMs provided a measure of control over the function of cytochrome-c. From facilitating rapid exchange of electrons on SAMs

surfaces terminating in trimethylammonium, to denaturation of the enzymes on hydrophobic surfaces terminating in methyl and phenyl groups[87].

Cytochrome-c was found to possess the ability to improve on its electron transfer capability by incorporating certain promoters. These promoters were reported to facilitate cytochrome-c binding in such a manner that influenced the orientation of the protein promoting electron transfer. However, these findings were disputed shortly thereafter which led to controversial findings.

Rhoten, Burgess and Hawkridge (2000) investigated the performance of cytochrome-c relative to its environment. The study reported cytochrome-c to preserve its electron transfer capabilities when mounted to an electrode. Even in temperatures exceeding 80 ^{o}C the enzyme maintained its electron transfer capabilities. The study was performed by simulating the natural environment of cytochrome-c oxidase, the mitochondrial membrane, and was incorporated into an electrode-supported lipid bilayer membrane. The cells exceptional performance was attributed to its environment. Cyclic voltammetry was used to characterize the immobilized oxidase. The rate of mediated electron transfer between the solution and the electrode was also observed to be specie dependent. The system was able to detect reduced cytochrome species at concentrations as low as 25 µM[88].

Direct enzyme immobilization on the electrode surface is not a simple procedure and presents technical difficulty. Lötzbeyer, Schuhmann and Schmidt (1996) proposed monolayer enzyme composite systems to improve the reduction capabilities of the enzymes. The enzymes were peroxidase-reducing enzymes, horseradish peroxidase, myoglobin, cytochrome-c and microperoxidase MP11, selected on the bases of size differentiation. The catalytic activity of the enzymes were evaluated individually to assess the limiting factors for enzyme communication, by suspending the enzymes in a homogenous solution. Thereafter the enzymes were immobilized on self-assembled thiol-monolayers. What they found was a significant difference in catalytic performance of the enzymes and concluded what was called ‘productive binding’. This is where the hemin groups orientate towards the monolayer prior to immobilization facilitating efficient direct electrochemical communication [83].

2.7 Cytochrome-c

Cytochrome-c is one on the most studied redox proteins for its electron transfer capabilities. The role of cytochrome-c is to transfer an electron from cytochrome-c reductase to cytochrome-c oxidase which is the terminal enzyme in oxidative phosphorylation. Electron transfer has been reported to take place at the exposed heme edge surrounded by positively charged lysine[89]. In the mitochondrial respiratory chain cytochrome-c functions as a single electron carrier. It has a prosthetic heme group which is covalently attached to the surrounding ligands that affords cytochrome-c the ability to adopt a ferrous or ferric state. These structures may be similar in structure but differences in the oxidation states directly impacts the biochemical properties of the protein[54]. The most important reactions of NO are the reactions with O_2 in aqueous and gas phase. NO has a very short half-life and is highly dependent on initial concentration. Nitric oxide reacts with O_2 radicals to form peroxy nitrite[90]. NO easily coordinates with transition metal ions such as metalloproteins. There's been substantial research on the interaction of nitric oxide with haemoglobin. NO binds to haemoglobin at a rate more rapid than O_2. NO binds to Fe(III)-porphyrins. Upon binding the complex undergoes a charge transfer to form $Fe(II)NO^+$ as result of a subsequent attack by ambient nucleophiles[90]. In the presence of NO, respiratory inhibition was circumvented by alternative oxidase which facilitated electron flow[56]. Studies have reported on the risks of certain cancer types associated with continuous inflammation. NO free radicals have been associated with inflammatory conditions associated with malignancies. NO has also been demonstrated to induce cellular damage and mutations[47]. NO in its free form is highly reactive in biological systems and is converted to nitrite and nitrates in water in the presence of oxygen. S-nitrosothiols have been reported to play a key role in transnitrosation reactions. Amino acids such as cysteine plays a key role in the production of S-nitrosothiols through the degradation of GSNO (S-nitrosoglutathione) resulting in higher NO concentrations[58].

In biosensors enzymes are utilized to translate biological signals generated by a specific biological process, into an electrical signal. Redox enzymes are naturally designed to administer control over the redox state of the embedded cofactor, but maintaining the integrity of the enzyme pose major difficulties. Immobilization of enzymes therefore play a major role in the construction of amperometric biosensors. The most commonly utilized enzymes in biosensors belong to the group

oxidoreductases. These enzymes are designed to incorporate redox cites coupled to electron receptors such as heme moieties. The ideology was for the design of superior architecture that will minimize any additional reagents within the biological matrix while maintaining electron transfer (ET) integrity. Thus far reports on reagentless biosensors explored ET through direct tunnelling and securely immobilized redox relays. According to the Marcus theory ET between redox sites depend on; the reorganization energy qualitatively reflecting structural rigidity of the redox compound in oxidized and reduced form, potential difference between involved redox centres, and the distance between redox cites. Substantial efforts have been committed to the advancement of redox relays to overcome the limitations of tunnelling probability and reducing ET distance. Very recent research suggested the application of redox mediators with fast and reversible electrochemical responses. This was speculated to allow for the shuttling of electrons to protein redox centres. Redox mediation perpetuate redox process on electrode surfaces. Where a voltage is applied, electrochemically, the electrode support layer facilitate direct oxidation and reduction processes of solution phase redox species[91].

Cytochrome-c's redox electron reaction capabilities in the mitochondrial cell makes it the most widely studied protein for its electrochemical properties. Investigations into the redox behaviour of the protein revealed electron transfer to metal surfaces to be sluggish as result of adsorption denaturation[89]. Part of the problem was to manage a successful approach to the electron transfer surface whilst maintaining the stability of the protein[92]. Direct and quasi-reversible electrochemistry was observed when cytochrome-c was deposited on Pt electrode surfaces. The study found initial electro-kinetics to be slow but the introduction of a monolayer, trans-1, 2-bis (4-pyridene) ethylene, greatly enhanced the electron transfer rate. ET was believed to have been facilitated by the absorption orientation of the monolayer. This facilitated terminal nitrogen interactions with cytochrome-c[8993]. Further studies, on the effect of mediators on the redox behaviour of cytochrome-c, were conducted by a number of researchers. Song, Clark and Bowden (1993) immobilized cytochrome-c on gold electrodes coated with SAM of $–S-(CH_2)_{n-1}-COOH$. On the premise of their findings a series of deductions were made. The electronic coupling strength between electrode and proteins can be varied by changing the length of the alkane chain. The mono SAM thickness has a direct impact on the electron-transfer rate constant. This was ascribed

to the electron tunnelling and associated distance[94]. In cytochrome-c the iron heme is covalently linked to the enzyme at cys14 and cys17 by thioether bonds. During electron transfer processes the redox state of the iron changes between Fe^{2+}/Fe^{3+}. The formal potential of the redox state is sensitive to the environment of the heme group. It provides information about the conformational state of cytochrome-c[94].

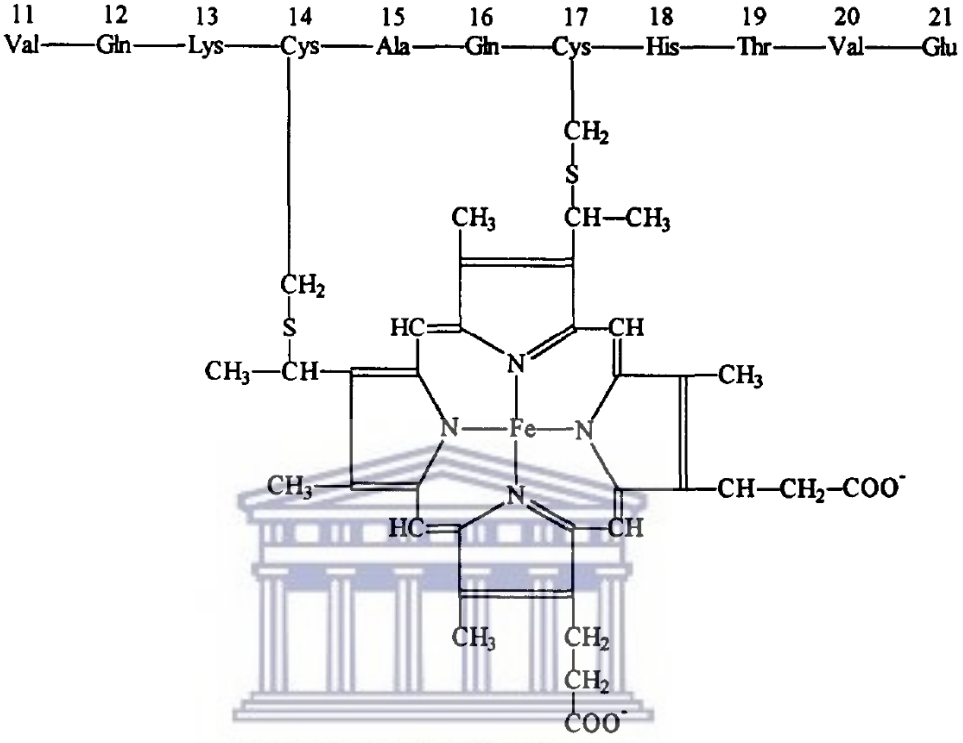

Figure 5: Diagram of microperoxidase (Hanrahan, MacDonald and Roscoe 1996)

The architecture of cytochrome-c affords the enzyme exceptional specificity and selectivity in electrochemical catalysed interactions. Although these attributes could not be replicated on bare electrodes. However, by functionalizing the working electrodes researchers such as Bianco and Lattuca (1997), who experimented with membrane-microelectrode assembly entrapped redox proteins, for the detection and study of proteins. The particular electrode assembly successfully yielded electrochemical responses with the entrapped cytochrome-c[95]. Bond et al., (1992) investigated the mass transport mechanisms associated with redox processes of cytochrome-c at gold electrodes modified with 4, 4'-bipyridyl disulphide (SS-bpy). They discovered the modifications to provide electroactive sites under applied potentials. It was rationalized that the modifiers unblocked parts of the electrode surface. This would displace adsorbed cytochrome-c and provide sites for electron transfer[96].

Eguílaz et al., (2010) constructed a cytochrome-c based biosensor by drop-coating cytochrome-c on a hybrid glassy carbon electrode modified with poly-(3-methylthiophene) and multiwall carbon nanotubes. The hybrid GCE was subsequently coated with a SAM of l-cysteine that was subsequently drop-coated with cytochrome-c. The system was evaluated against H_2O_2. Cytochrome-c type biosensors have previously been used for H_2O_2 determination and other analytes related to H_2O_2 quantification. Hemeproteins don't need redox mediators. They facilitate direct electron transfer to the electrode surface[97]. However, recently cytochrome-c found application in the biocatalytic oxidation of nitrite. The reaction is follows;

$$Fe^{2+} - Cyt\ c \rightarrow Fe^{3+} - Cyt\ c + e^- \quad (2.1)$$

$$Fe^{3+} - Cyt\ c \rightarrow [Fe^{4+} - Cyt\ c]^{\bullet} + 2e^- \quad (2.2)$$

$$[Fe^{4+} - Cyt\ c]^{\bullet} + NO_2^- + H2O \rightarrow Fe^{3+} + -Cyt\ c + NO_3^- + 2H^+ \quad (2.3)$$

In the above reactions ferrous cytochrome-c was oxidized to ferric iron at a low potential. It was further oxidized to $[Fe^{4+} - Cyt\ C]^{\bullet}$ at higher potentials. The intermediate specimen, $[Fe^{4+} - Cyt\ c]^{\bullet}$, was very reactive. It facilitated the oxidation of NO_2^- to NO_3^- in solution[98]. The sensor displayed good performance in the amperometric determination of H_2O_2. For the biocatalytic determination of nitrite the system displayed superior sensitivity.

In order to determine the complete function of NO in living systems the behaviour of NO had to be analysed. However, the detection of NO always proved difficult. This was as a result of NO's instability and high reactivity with other molecules in aqueous solutions. Heat-denatured cytochrome-c and radical scavenger 2-(4-carboxyphenyl)-4, 4, 5, 5-tetra methyl imidazoline-1-oxyl-3-oxide (C-PTIO) are amongst the most reviewed materials for the detection of in-situ NO systems. Heat denatured cytochrome-c deposited on 4-mercaptopyridine gold electrodes, respond to NO in aqueous environments with a cathodic current due to an electrochemical reduction of the oxidative form of cytochrome-c (Fe^{3+}). The study by Haruyama et al., (1998) assessed two types of electrochemical systems for NO based on heat-denatured cytochrome-c and C-PTIO sensing material. Denaturation of cytochrome-c was achieved by heating a 20 mg/ml dissolved cytochrome-c solution in a hot water bath in an Eppindorf tube for 15 minutes. Heat-denatured cytochrome-c/4-mercaptopyridine modified gold electrodes were prepared by submerging gold

electrodes in a 3% mercaptopyridine solution for 10 minutes. Heat-denatured cytochrome-c self-assembled on the electrode by adsorption[99].

A study on ferredoxin-nitrite reductase by Yamada et al., (2002) unexpectedly revealed the heat treated enzyme to reduce NO_2^-. The target enzyme was identified as denatured cytochrome-c-553. The study reported heat treatment of cytochrome-c to induce uncharacteristic catalytic activity in the enzyme when complexing it with NO[100]. When compared to the native enzyme the protein exhibited similar traits. The heme of denatured cytochrome-c on the other hand displayed higher NO_2^- reducing activity. Heat treatment appeared to induce functional changes to the structure of the heme of cytochrome-c. The heme formed a His-Fe-Met octahedral coordination and a thioether bond with two cysteine residues of the peptide chain. The peptide chain of haemoglobin or myoglobin bound only the histidine residue as a fifth ligand revealing unfolding of the peptide chain. The physiological changes induced by heat to denature cytochrome-c were as follows; unfolding of the peptide chain resulted in the exposure of the iron heme as methionine-sulphur coordination disappeared. This exposed the heme to water and resulted in the heme's newly acquired autoxidation ability[101].

2.8 Electrochemical sensors and nitric oxide detection

Nitric oxide is a free radical found both inter- and extracellularly, and is involved in variety of biological processes. However measuring nitric oxide is still relatively difficult due to the myriad of biochemical reactions it undergoes. NO can be described as a diatomic hydrophobic gas with the capacity to permeate cellular membranes and other hydrophobic structures. Nitric oxide can be produced by either enzymatic or non-enzymatic reactions.

The most popular technique for real time NO detection is amperometry which manages very low and rapid levels of detection. In this technique the electrode is covered with a NO permeable membrane. NO diffuses across the membrane producing a redox current due to the potential difference and is oxidized at the electrode surface. In addition to amperometry cyclic voltammetry techniques are also employed to detect nitric oxide. Instead of using a NO selective membrane materials electroactive towards nitric oxide is electrodeposited onto the surface of electrodes. Once deposited the electrode can react electrochemically with nitric oxide. The interaction between nitric

oxide and the electrodeposited layers will produce electrochemical signals. The catalytic oxidation of nitric oxide is thus a useful method for nitric oxide discrimination[102].

Since NO's discovery as a biological signalling molecule many donor molecules have been synthesized. These donor molecules all possess different physico-chemical properties and reactivity that facilitates the *in-vitro* and *in-vivo* deliverance in various biological systems. NO oxidation proceeds via an electrochemical mechanism. In the first step NO is oxidized by the solid electrode to form the nitrosonium cation (NO^+). This is a strong Lewis acid which will explain the relatively short lifespan of these species. The NO^+ ion is subsequently converted to nitrite. The oxidation potential of nitric oxide and nitrite is between +60 to 80 mV and forms the basis of NO detection in solid electrode systems. It is this very characteristic that facilitates the discrimination between oxidation products, nitrites and nitrates, of nitric oxide[51]. Electrochemical detection of NO relies on the modification of the electrodes surfaces and exploiting the redox properties of NO. NO can either be oxidized or reduced electrochemically, depending on the nature of the solution. Under cathodic current NO is reduced to nitrosyl, a highly unstable derivative of NO, which is subject to a series of chemical reactions to eventually form NO. Oxygen is present in most biological systems which makes the potential window below oxygen reduction unsuitable for electroanalysis. Due to the interferences presented by the electrochemical reduction of NO, the electro-oxidation of NO is therefore the methodology of choice for NO detection. The electrochemical oxidation of NO occurs at positive potentials around 800 mV vs. Ag/AgCl and proceeds via a three electron oxidation mechanism. This potential is however not only favourable to NO oxidation but can lead to the oxidation of several other biological species. These interfering species are biologically present at concentrations higher than NO. Selectivity is therefore of the highest order when designing these electrode systems[103]. Advancements, in improving sensitivity and selectivity, with these sensors have been established in literacy to evolve around the development of suitable membranes for these electrodes[52]. Badea et al., (2001) designed a sensor that could effectively discriminate against nitrites and nitrates. This was based on nitrite oxidation in acetate buffer using a Pt electrode. The electrode was polarised at +900 mV against AgCl reference. In order to make Pt electrodes selective to nitrite oxidation the electrode was modified with a cellulose acetate membranes.

Although the sensor was never tested for nitrite permeability, it displayed good mechanical stability and selectivity towards nitrite, though low. Modification of the electrode with an electropolymerized film of 1, 8-diaminonaphthalene, the sensitivity of the system was enhanced five times. It was found that these sensors were quite effective for rapid detection of nitrites and nitrates in water. An interesting observation was the polarization times of the two membranes. The electropolymerized membranes required one night of stabilization in pH 4 acetate buffer at 900 mV[50].

Electroanalytical techniques such as cyclic voltammetry (CV), fast-scan CV and differential pulse voltammetry are quite useful tools for the determination of certain biological specimen. However for short-lived species amperometry offers the best resolution but selectivity is limited. This can be established by running CV which allows for parallel discrimination of the interfering analytes[104]. Shibuki (1990) reported on an electrochemical microprobe which detected NO in brain tissue. According to reports this appears to be one the first probes to effectively detect endogenous release of NO. Using sodium nitroprusside as a NO donor, the probe successfully detected the release of NO and effectively discriminated between O_2 and oxidized NO derivatives [105].

2.9 Motivation

Metalloproteins are proteins that contain metal cofactors. These cofactors are imperative to the function of the protein with innate electron transfer capabilities. Cytochrome-c has long been scrutinized for its electron carrier capabilities. The enzyme consists of a polypeptide chain with 104 amino acid residues arranged in a manner to house a central heme (see figure 5). According to literature electron transfer takes place at the exposed part of the heme. There's been a lot of interest in the direct electrochemistry and electrocatalysis of cytochrome-c immobilized on inert substrates. In order to retain biological significance it is important to design dynamic polymer interfaces that will regulate interactions with the protein[106]. Conductive polymers contribute more than just a suitable medium for biological components. A study by Bedioui and Griveau (2013) reported on the amperometric detection of glucose by immobilization of glucose oxidase to an electrode. The process involved the electropolymerization of pyrrole in the presence of the enzyme. The glucose

oxidase was incorporated into the polypyrrole film during formation, for glucose detection[64]. Pashai, Najafpour, Jahanshahi and Rahimnejad (2018) fabricated an electrochemically reduced graphene oxide gold nanocomposite electrode for NO oxidation. The electrode displayed high selectivity for NO facilitated by the nafion cation-exchange film. This acted as barrier allowing the diffusion of NO to the electrode surface. In the presence of NO oxidation peaks were recorded at +0.8 V. Limits of detection was estimated to be 0.250 µM[107]. Musameh et al., (2018) presented work on the elimination of electron mediators in electrodes. A silk solution was drop-casted on a GC electrode modified with multiwalled carbon nanotubes encapsulated with heme. Well defined electrochemical activity was reported on the Fe^{2+}/Fe^{3+} redox system. The sensor recorded NO anodic potentials above 0.45 V and reduction potentials below -0.7 V with good stability. The sensor managed a lower detection limit of 2 nM with high selectivity for NO[108].

2.10 Rationale

Cytochrome-c has been the subject of extensive research for its redox electron reaction capabilities in the mitochondrial cell. It's been the most widely studied protein for its electrochemical properties. Investigations into the redox behaviour of proteins revealed electron transfer to metal surfaces to be sluggish as result of adsorption denaturation[89]. The reason for the specific occurrence, in the case of cytochrome-c, was as result of irreversible adsorption on the electrode surface and subsequent denaturation[84]. By altering experimental conditions Szück and Novak (1995) were able to retain reversible redox characteristics of enzymes adsorbed onto bare electrode surfaces. However, reproducibility of these results were not as straight forward and is dependent on very intricate methodologies. López-Bernabeu et al., (2017) presented work on silica encapsulation of cytochrome-c. Consequent to literature on the suitability of silica as an ideal matrix for enzymatic compounds. The studies presented preservation of the enzyme but poor conductivity. This work explores the potential of methyl-modified silica as an alternative matrix. The study presented upper limits of cytochrome-c loading. This was circumvented by doping silica with a conductive polymer. Poly(3, 4-ethylenedioxythiophene) (PEDOT) was inserted into the silica pores, this would facilitate adequate charge transfer to the isolated cytochrome-c molecules[109]. Lebègue et al., (2018) reported on a cytochrome-c GC lipid modified

system. Cardiolipin was deposited on a GC electrode. This system was used to model the electroactivity of cytochrome-c in solution. The system provided sufficient electron transfer support between the electrode and redox protein. The cardiolipin also adsorbed cytochrome-c in its native state and retain its electroactivity[61]. Direct enzyme immobilization on the electrode surface is not a simple procedure and presented technical difficulties.

Chapter 3

3. Monomer synthesis: Methodology, results and discussion

The following chapter outlines the methodology applied in the study to answer the research questions posed and objectives as outlined in chapter one. The processes are presented in a comprehensive manner and include all the details of how the study was conducted for independent reproducibility

3.1 Schiff base chelating ligands

Schiff bases have been reported to be excellent as chelating ligands in main group and transition metal coordination chemistry[110]. Transition metal Schiff base complexes possess unusual configuration and are sensitive to the molecular environment. In metalloproteins the surrounding environment, with regards to coordination geometry of ligands and donor groups, lies at the core of the specific physiological functions of metalloproteins[111]. Tümer et al., (2008) synthesised Schiff base ligands and their Co (II), Fe (III) and Ru (III) derivatives. The genotoxicity, antimicrobial and electrochemical properties of these compounds were subsequently studied. Some of

the ligands were mutagenic on salmonella typhimurium, some ligands displayed mutagenic activity on salmonella typhimurium while some ligands were not mutagenic on salmonella typhimurium[110]. Mangamamba, Ganorkar and Swarnabala (2014) synthesized coordination complexes with Cu (II), Ni (II), Co (II), Fe (III), Mn (II), Cr (III) and VO (II) with Schiff base ligands.

All reagents used for synthesis and characterization were analytical grade and were purchased from Sigma-Aldrich and KIMIX chemicals. Millipore deionised water from a Millipore Synergy water system with a resistivity of 18 MΩ was used to prepare all aqueous solutions. The chemicals and reagents used throughout the study is listed below in Table 1.

Table 1: Reagents and materials used for synthesis

Chemical Name	Purity	Chemical Company
2,3-diaminonaphthalene	95%	SIGMA Aldrich
Pyrrole-2-carboxaldehyde	98%	SIGMA Aldrich
cytochrome-c from equine heart	95%	SIGMA Aldrich
iron(II) tetrachloride	99.99% trace metals	SIGMA Aldrich
anhydrous Chloroform	99%	SIGMA Aldrich
Chloroform-d	99.8 atom%	SIGMA Aldrich
1-Propanol	99.65%	SIGMA Aldrich
N,N-Dimethylformamide (anhydrous)	99.8%	SIGMA Aldrich
Methanol	99.9%	SIGMA Aldrich
Sodium nitrite		SIGMA Aldrich
Potassium chloride		SIGMA Aldrich
Sodium chloride		SIGMA Aldrich
DEA-NONOate (diethylammonium (Z)-1-(N, N-diethylamino) diazen-1-ium-1, 2-diolate)		BIOCOM Africa
Absolute Ethanol	99.9%	KIMIX
Silica Gel on TLC plates	Silica gel matrix	SIGMA Aldrich

3.2 Solution preparation

Solutions were prepared using general analytical methods and formulas.

For solutions synthesized from solid materials the following formula was used;

$$C = \frac{n}{V} \qquad (1)$$

Aqueous solutions were prepared as follows;

$$C_1V_1 = C_2V_2 \quad (2)$$

C_1 = initial concentration

V_1 = initial volume

C_2 = final concentration

V_2 = final volume

n = mol

a) $m = 0.1\ x\ 0.50\ x\ 156.01$ (Na_2HPO_4)

= 7.8 g

$m = 0.1\ x\ 0.50\ x\ 177.99$ (NaH_2PO_4)

= 8.9 g

A 500 ml phosphate buffer solution with a pH 7.1 was prepared by adjusting the pH of Na_2HPO_4 with NaH_2PO_4.

b) Phosphate buffer saline was prepared by doping the phosphate buffer solution with NaCl and KCl with 137 mM and 2.7 mM concentrations proportionately to the buffer solution

$m = 0.137\ x\ 0.1\ x\ 58.4$ (NaCl)

= 0.8 g

$m = 0.0027\ x\ 0.1\ x\ 74.551$

= 0.02013 g

3.3 Monomer synthesis - bis((1H-pyrrol-2-yl)methylene)naphthalene-2,3-diamine) – monomer

Conjugated aromatic Schiff bases have received substantial interest for the exceptional thermal stability, semi-conductivity, electrochemical and nonlinear optic properties[112]. These characteristic thermal stability, mechanical strength and opto-electronic properties of Schiff bases have been reported to be resultant of aromaticity and conjugation. Naphthalene incorporation into Schiff bases have been reported to enhance thermal stability and polymer solubility[113]. Poly(pyrrole) has a very low

oxidation potential consequently it can be synthesized from a range of aqueous and non-aqueous solvents where as polythiophene's solubility is limited to organic solvents. Polymerization can be performed on pyrrole using either chemical or electrochemical methods. Water has been identified as the best solvent for polymerisation of polypyrrole and iron chloride as the most ideal oxidant when considering conductivity[114115116]. Schiff bases are a product of the reaction between carbonyls such aldehydes or ketones and generally primary amines. Water is a by-product of these reactions and it is therefore necessary to keep the environment dry to maintain the thermodynamic balance. However, when using aromatic carbonyls the forward reaction is favoured therefore these types of reactions occur with ease and produce high yields[117].

The Schiff-base N, N-bis((1H-pyrrole-2yl)methylene) naphthalene-2,3-diamine was synthesised through the condensation reaction of an amine and aldehyde. The reaction is generally either acid, base or heat catalysed but acid catalysis is generally used to spur on more difficult reactions. The principle mechanism of this reaction is nucleophilic substitution, and the purpose of acid catalysis is to activate the carbonyl carbon for nucleophilic attack provided the presence of a weak nucleophile.

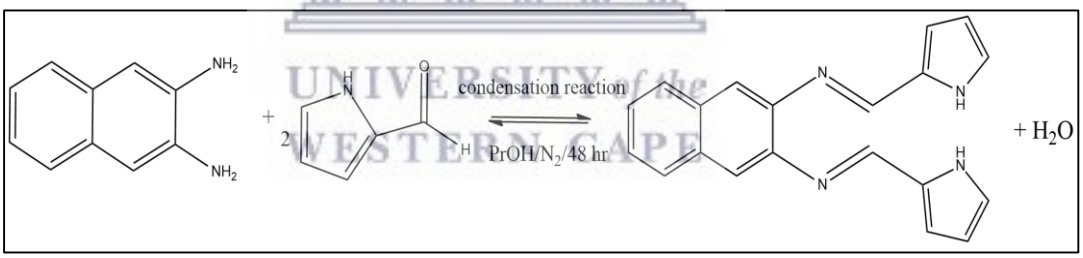

Figure 6: Condensation reaction depicting the Schiff base formation from 2, 3-diaminonaphthalene and pyrrole-2-carboxaldehyde

The reaction setup used consisted of a 250 ml three necked round bottom flask, to which the gas line was attached. The round bottom flask was placed in a hot oil bath on a pre-set IKA ceramic magnetic hotplate stirrer. The reaction was initiated by dissolving 0.5 mM equivalent (395 mg) of the amine, 2, 3-diaminonaphthalene, in 50 ml dried propanol in a 250 ml round bottom flask. The solute was heated to and kept at 60^{o}C in a hot oil bath. In a separate vessel 1mM equivalent (475 mg) of the aldehyde, pyrrole-2-carboxaldehyde, was dissolved in 10 ml dried propanol and heated to 60^{o}C prior to addition. Prior to the addition of the reactants the glassware was dried and purged with Ar. The centre neck of the flask was connected to the nitrogen line in a

fume cupboard whilst the side necks were sealed with septum stoppers. In order to prevent gas build up the one neck was fitted with a pressure release makeshift valve. Initial trials and previous reports suggested the rate of the reaction to be relatively slow. Addition of the aldehyde was therefore executed over a period of ten minutes through drop-wise addition using a HPLC steel glass syringe. Once the addition of the aldehyde was completed the reaction was allowed to proceed. Considering the nature of the solvent used it was expected to perform the reaction under reflux but this appeared to hinder the reaction equilibrium. The extend of the reaction was measured at the 24 hour mark with thin layer chromatography using 35 mm x 60 mm silica plates in a 1 ml 90:10 ratio hexane ethanol mixed mobile phase. The solvents were immiscible under standard conditions and had to be sonicated for 10 minutes to facilitate mixing. Once the solvents were miscible it was transferred to a 100 ml glass beaker and covered with a petri dish. Three spots, aldehyde, amine dissolved in ethanol and an aliquant of the reaction, were placed 1 cm from the edge above the level of the mobile phase. This was allowed to run for 15 minutes.

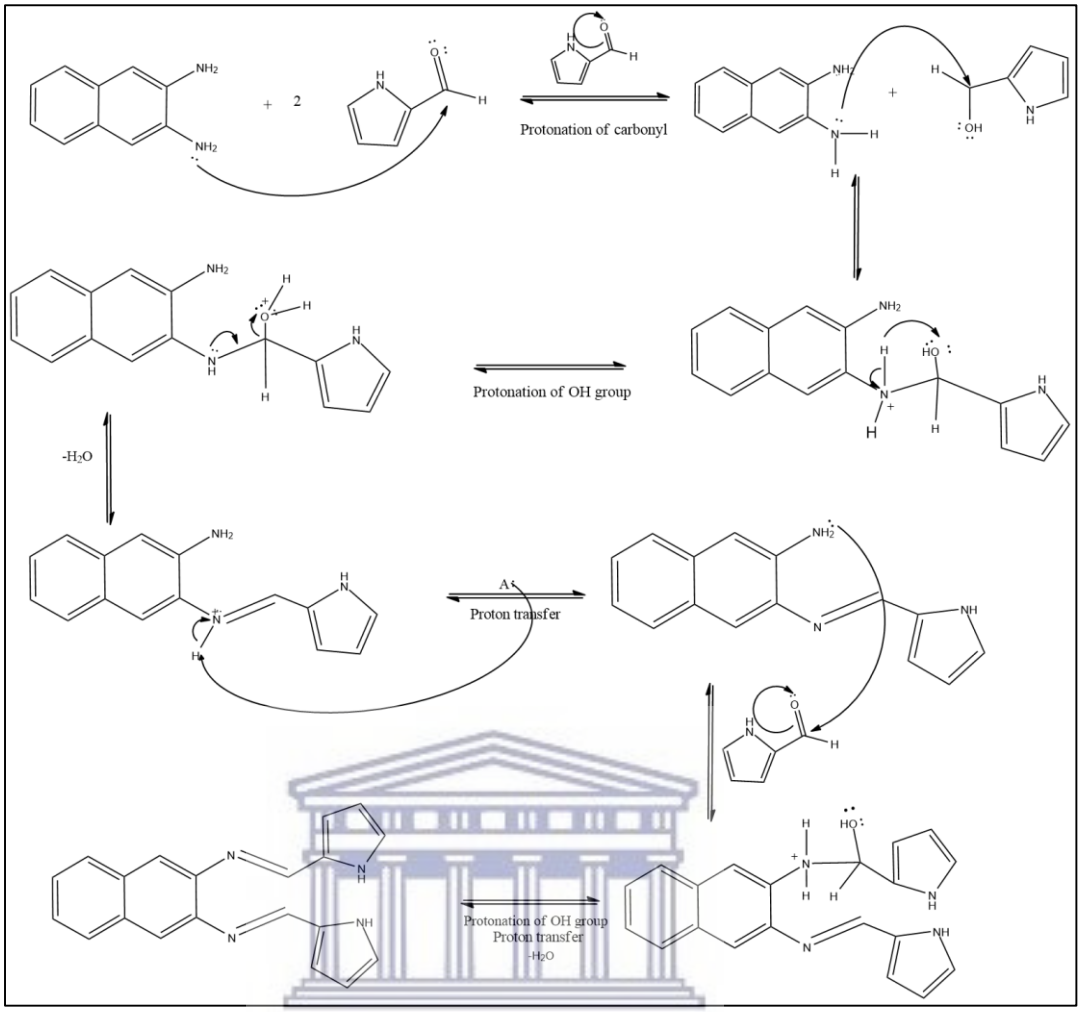

Figure 7: Proposed synthesis mechanism of the monomer bis((1H-pyrrol-2-yl)methylene)naphthalene-2,3-diamine)

The Schiff-base N, N-bis(1H-pyrrole-2yl)methylene naphthalene-2,3-diamine was synthesised through the condensation reaction of 2,3-diaminonaphthalene and the acidic aldehyde pyrrole-2-carboxaldehyde. This reaction is generally either acid, base or heat catalysed but the acidic nature of the aldehyde pyrrole-2-carboxaldehyde negated the need for acid catalysis. The principle mechanism of this reaction is nucleophilic substitution. The purpose of acid catalysis is to activate the carbonyl carbon for attack nucleophilic attack provided the presence of a weak nucleophile. 2,3-diaminonaphthale suffers significant steric hindrance and by virtue thereof is a weak nucleophile. The reaction is marked by the formation carbinolamine succeeding the protonation of the carbonyl. This carbinolamine is a tetrahedral intermediate and unstable, and being an alcohol undergoes acid catalysed dehydration[118]. Condensation reactions are trademarked by their production of water and considering the reversibility of the reaction keeping the environment dry was imperative. Schiff base

synthesis is considered a high yielding reactions and keeping the environment dry helped the reaction go to completion. Prior to initiation the reaction vessel was purged with nitrogen. The reaction was subsequently performed under nitrogen.

The reaction was initiated by dissolving the amine, 2,3-diaminonaphthalene, in dried propanol. The solute was heated to and kept at 60 ^{o}C in a hot oil bath. In a separate vessel pyrrole-2-carboxaldehyde was dissolved in dried propanol and heat prior to addition. Initial trials and previous reports suggested the rate of the reaction to be relatively slow. Once the addition of the aldehyde was completed the reaction was allowed to proceed. Considering the nature of the solvent used it was expected to perform the reaction under reflux but this appeared to hinder reaction equilibrium.

Figure 8: TLC of (A) pyrrole-2-carboxaldehyde, (B) 2,3-diaminonaphthalene, (C) N, N-bis((1H-pyrrole-2yl)methylene) naphthalene-2,3-diamine at 48 hours (D) and 24 hours in 90:10 hexane ethanol mixed mobile phase

In comparison to hinge reactions performed by Ward et al., (2014) on pyrrole accordion type polymers, where the diamine displayed similar stereochemistry the reaction displayed retarded kinetics[119]. At the 24 hour mark thin layer chromatography (TLC) was performed to monitor the progress of the reaction. Distinction was based on differences in absorption activity of the material. TLC was performed on silica plates using a mixed mobile phase with a 90:10 ratio. The reaction appeared to be incomplete under UV light at 254 nm wavelength, there was very poor distinction in retention between reactants. At the 48 hour mark another TLC was performed. Four spots, pyrrole-2-carboxaldehyde (A), 2,3-diaminonaphthalene (B), aliquots of the reaction at 24 hours (C) and at 48 hours (D) were placed 1 cm from the edge above

the level of the mobile phase. There appeared to be a clear distinction in retention times between the starting materials and reaction mixture (see figure 8). At the 24 hour mark it was evident, compared to running the experiment for 48 hours, the reaction was incomplete and starting materials were still present.

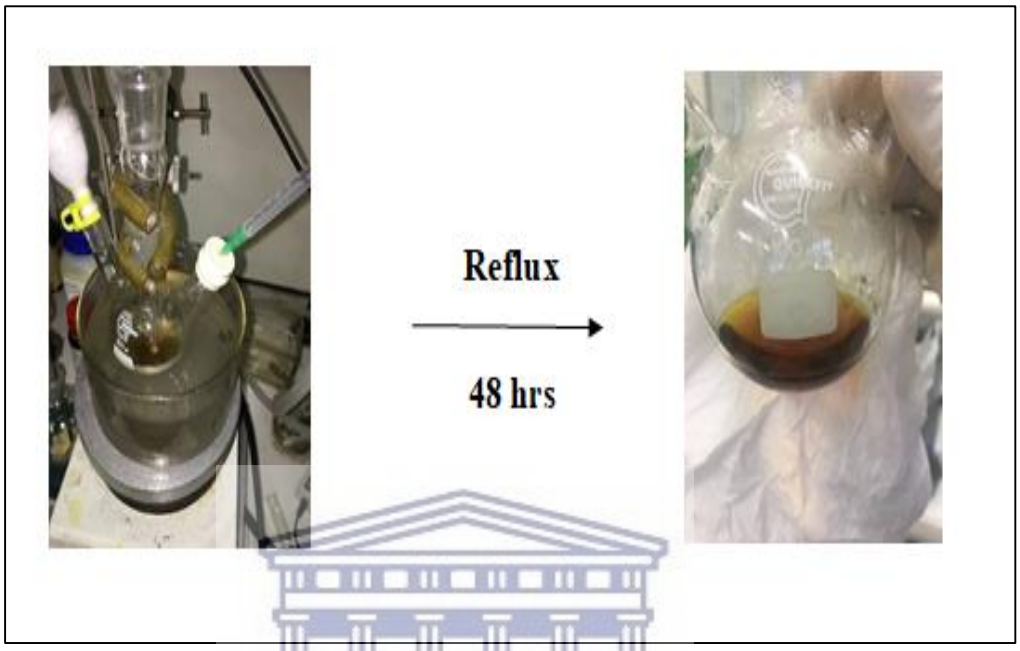

Figure 9: Reflux synthesis of N, N-bis(1H-pyrrole-2yl)methylene naphthalene-2,3-diamine

At the 48 hour mark the reaction mixture had turned from its initial orange brown colour to a deep red brown solution (see figure 9). The reaction was stopped and allowed to settle for several hours at room temperature. This step was critical as it allowed the product to precipitate and separate. At this stage of the synthesis the product had to be separated from the mother liquor. This was achieved through roto-evaporation. Following the removal of the mother liquor the compound was dissolved in chloroform and cooled in the freezer for one hour to facilitate separation. Thereafter, the solution was roto-evaporated and dried in the vacuum oven over night. A 65% yield was recorded.

The degree of solubility which measures the maximum amount of a solute which can dissolve in a given amount of solvent. Solubility of solutes can generally be influenced by temperature and pressure. Where the solute can no longer dissolve in the solvent under a given temperature and pressure the solution is regarded as saturated. The solubility testing of the monomer was performed by dissolving 1 mg of solute in 1 ml of ethanol and subsequently adding 1 mg aliquots of the solute until the solution was

saturated. The saturation concentration was established at 10mg of the solute in 1 ml of ethanol.

3.4 Characterization of Schiff base monomer

3.4.1 Proton Nuclear Magnetic Resonance

In NMR nuclei in a strong static magnetic field is disturbed by an oscillating magnetic field and produces an electromagnetic signal with a characteristic frequency of the magnetic field. This is followed by resonance from the specific magnetic properties inherent to certain atomic nuclei. Proton NMR analysis was performed on N, N-bis(1H-pyrrole-2yl)methylene naphthalene-2,3-diamine with a Bruker BioSpin GmbH Fourier 300 instrument. Solubility posed a major hurdle therefore a diluted sample was used for analysis. A 5 mg sample was dissolved in 2 ml deuterated chloroform, the sample was filtered through cotton wool and transferred to the NMR tube. The sample was analysed by scanning the sample twelve times.

Table 2: Chemical shifts for N, N-bis(1H-pyrrole-2yl)methylene naphthalene-2,3-diamine

Chemical shift (ppm)	Assignment
5.7	Pyrrole N hydrogen
6.2 – 6.7	Pyrrole ring hydrogen
6.9, 7.1	Naphthalene hydrogen
7.4, 7.9	Naphthalene hydrogen
7.7, 8.1	Imine hydrogen

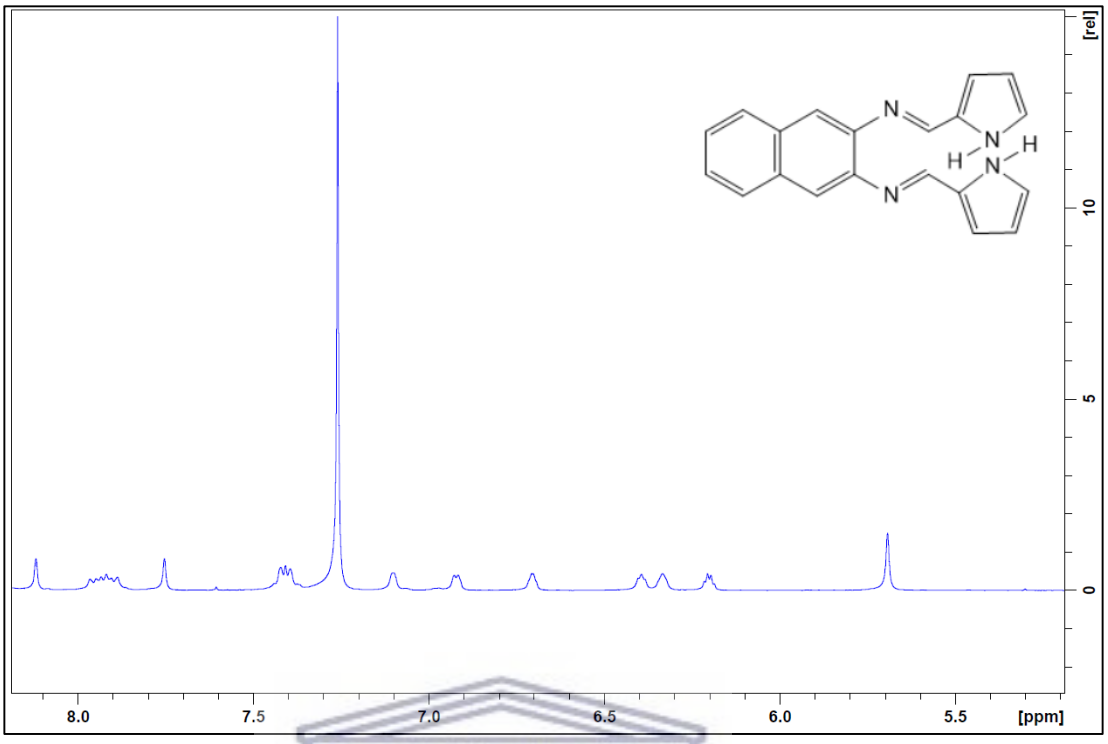

Figure 10: H NMR spectrum of base N, N-bis(1H-pyrrole-2yl)methylene naphthalene-2,3-diamine in deuterated chloroform 12 scans

Table 2 lists the chemical shifts and assigned the peaks of the proton NMR spectrum of N, N-bis(1H-pyrrole-2yl)methylene naphthalene-2,3-diamine. The spectrum shows an absence of the characteristic amine and carbonyl chemical shifts expected for 2, 3-diaminonaphthalene and pyrrole-2-carboxaldehyde respectively. The spectrum does however identify to symmetrical peaks at 8.1 and 7.7 ppm which was evidence of imine formation (-N=CH-). The shift coincided with reports on imines by Simionescu et al., (1998)[113] who synthesized and polymerized pyrrolylidene naphthylamine monomers.

3.4.2 Fourier Transform Infrared Spectroscopy

Fourier transfer infrared spectroscopy (FTIR) is a technique used to obtain an infrared absorption or emission spectrum of a solid, liquid or gas. A FTIR spectrometer collects spectral data over a wide spectral range. It measures the bonding vibrations of a molecule which is dependent on the type of bond. In the technique a 1% (w/w) of sample was mixed with dried KBr. KBr is dried at 100 ^{o}C for one hour and allowed to cool to room temperature. A 4 mg aliquot of N, N-bis(1H-pyrrole-2yl)methylene

naphthalene-2,3-diamine was mixed with dried KBr and compressed into a pellet with a PerkinElmer KBr pellet quick press for 5 minutes. FTIR analysis was performed on PerkinElmer spectrophotometer to record the infrared spectra of the monomer and starting materials in the range of 400 to 4000 cm^{-1}.

Table 3: FTIR bands relevant to N, N-bis(1H-pyrrole-2yl)methylene naphthalene-2,3-diamine

Wavelength, nm	Assignment
3380-3300	Primary amine group, diaminonaphthalene
3150	N-H group, pyrrole
1632-1630	Aromatic carbon-carbon bond,
1595	Imine

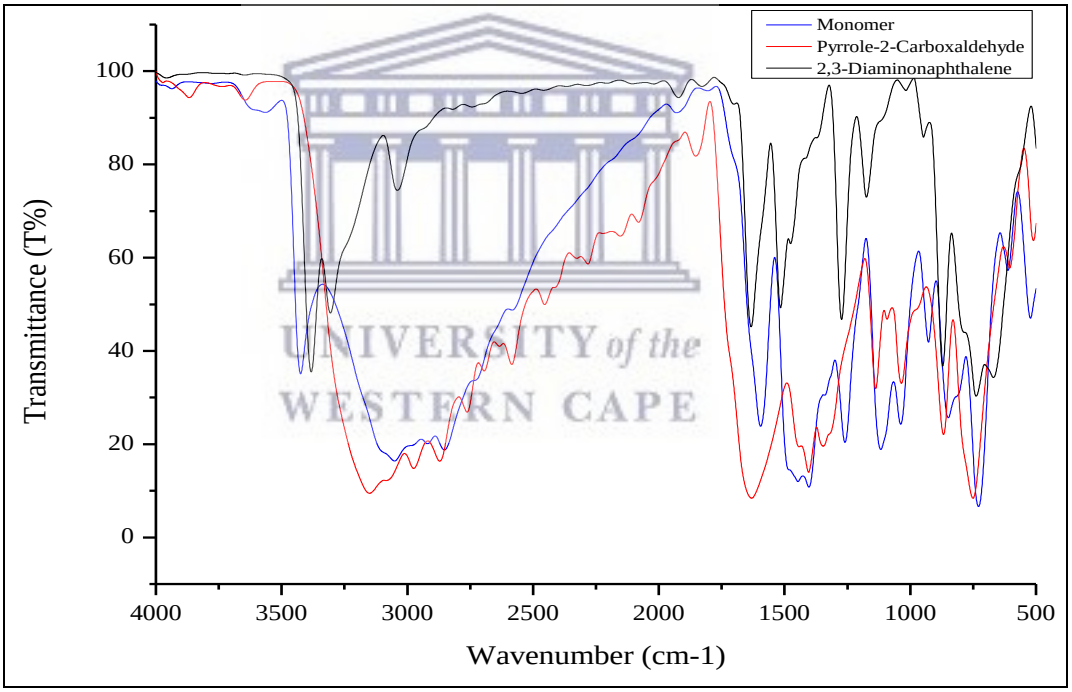

Figure 11: FTIR spectra of starting materials 2,3-diaminonaphthalene, pyrrole-2-carboxaldehyde and monomer N, N-bis(1H-pyrrole-2yl)methylene naphthalene-2,3-diamine in dried KBr.

Infrared analysis was performed on the starting materials and the monomer, and compared as per figure 11. The results identified a spectra with characteristic absorption bands for each compound. The monomer identified molecular vibrations and rotations that was a combination of 2,3-diaminonaphthalene and pyrrole-2-

carboxaldehyde. 2,3-Diaminonaphthalene identified an absorption band at 3380 cm^{-1} which coincided with reports in literature for primary amines[120]. The absorption band at 1595 cm^{-1} coincided with literature reports, and confirmed the formation of the Schiff base which was characterized by formation of an imine bond[113120121]. The shift in the wavelength coincided with findings in literature. Extending pi conjugation has been reported by Barbon, Staroverov and Gilroy (2015) resulted in red shifts[122]. The study investigated the effect of pi conjugation on the properties of boron difluoride. The study found pi conjugation to have a direct impact on wavelength absorption which resulted in a red shift. A theoretical study by Isaiah, Adejoro and Collins (2013) on the effects of substituents, such as cyano and carbonyl groups on pyrrole, found these groups to have an effect on the HOMO and LUMO levels[123]. The groups were found to decrease the band gap and increase the conjugation length of the polymers which impacts absorbance. In the spectra for the monomer a shift in stretch in vibration was evident for pyrrole. This was evidence of successful coordination.

3.4.3 Ultraviolet-visible absorbance spectroscopy

The UV-Vis spectra of pyrrole-2-carboxaldehyde, 2,3-diaminonaphthalene and monomer N, N-bis(1H-pyrrole-2yl)methylene naphthalene-2,3-diamine was measured on a Nicolet Evolution 100 UV-Vis spectrophotometer, over the 200 to 900 nm spectral range, with 10 mm pathlength Hellma absorption cuvettes in ethanol at room temperature. The solubility limit of the monomer was established at 10 mg/ml in ethanol. This was the standard concentration for the materials that were diluted with ethanol in graduated Plastic Eppendorf centrifuge tubes, to concentration levels adequate for analysis. A serial dilution factor of 1:100 000 was used, DF = $\frac{1}{10} * \frac{1}{10} * \frac{1}{10} * \frac{1}{10} * \frac{1}{10} = \frac{1}{100000}$, the final concentrations were $\frac{10mg}{ml} * \frac{1}{100000} = 100\ \mu g/lt.$

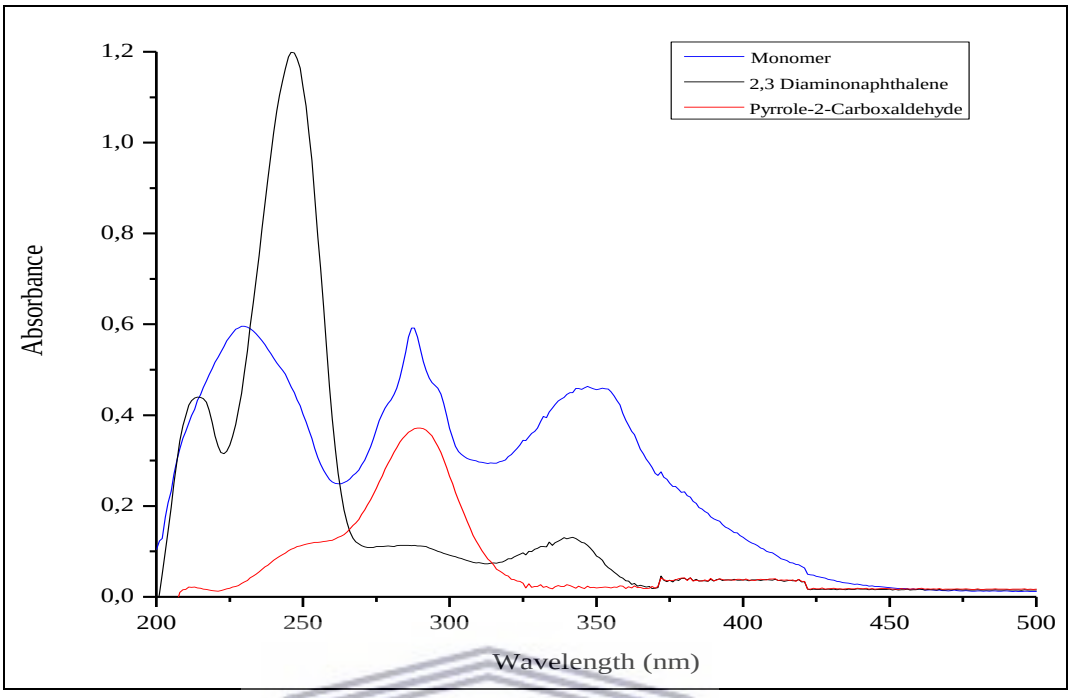

Figure 12: UV-Vis absorbance of starting materials 2,3-diaminonaphthalene, pyrrole-2-carboxaldehyde and monomer N, N-bis(1H-pyrrole-2yl)methylene naphthalene-2,3-diamine in ethanol

The UV spectra for pyrrole-2-carboxaldehyde, 2,3-diaminonaphthalene and the monomer are presented in figure 12. For the monomer three bands were detected, at 230, 288 and 349 nm. The bands at 230 nm and 288 nm was attributed to the π-π^* transitions of the aromatic rings of pyrrole and naphthalene. The absorption band at 349 nm can be attributed to the π-π^* of the imine[124]. When the spectrum of the monomer was compared to the starting materials a clear broadening of the bands were evident. These changes were attributed to the extended conjugation of the monomer.

3.4.4 Electron microscopy

Electron microscopy uses electrons to provide enlarged images of specimen. These microscopes have the capability to provide imagery with much greater resolution than light microscopes and magnification. Electron microscopes utilize electrostatic and electromagnetic lenses to form images by controlling the electron beam, focussing it at specific planes relative to the specimen. Transmission electron microscopy (TEM), energy dispersive X-ray spectroscopy (EDS) and electron energy loss spectroscopy

(EELS) data were collected using an FEI Tecnai F20 field emission gun TEM (FEG-TEM) operated at 200kV, equipped with a liquid nitrogen cooled Si(Li) detector for x-ray detection and a Gatan GIF-2001 energy filter for EELS analysis. Each spectrum was collected in normal parallel beam, bright-field TEM mode for 5 seconds. Scanning electron microscopy (SEM) and EDS data were collected using the Auriga FEG SEM. It is a fully digital 30 kV Hi Resolution FEG SEM unit equipped with EDS. The samples were coated with carbon using the sputter coater Emitech k950x.

SEM analysis can provide valuable information about topography and qualitative elemental analysis. SEM analysis were performed on both the starting materials and product.

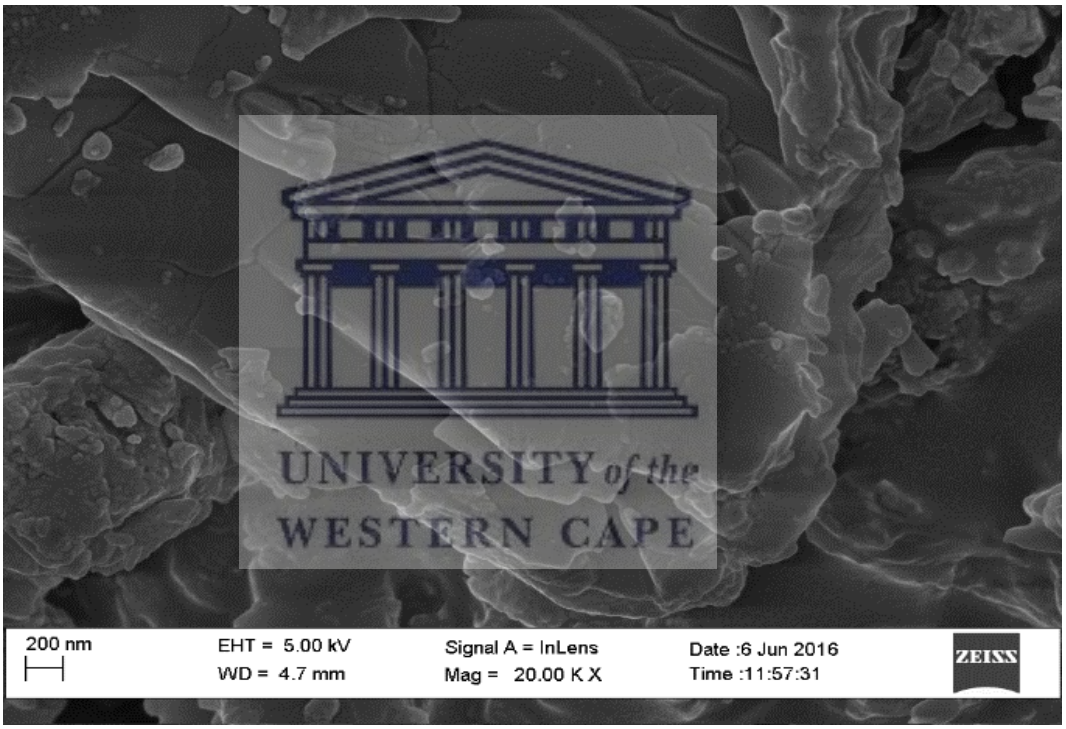

Figure 13: HRSEM images of (A) pyrrole-2-carboxaldehyde

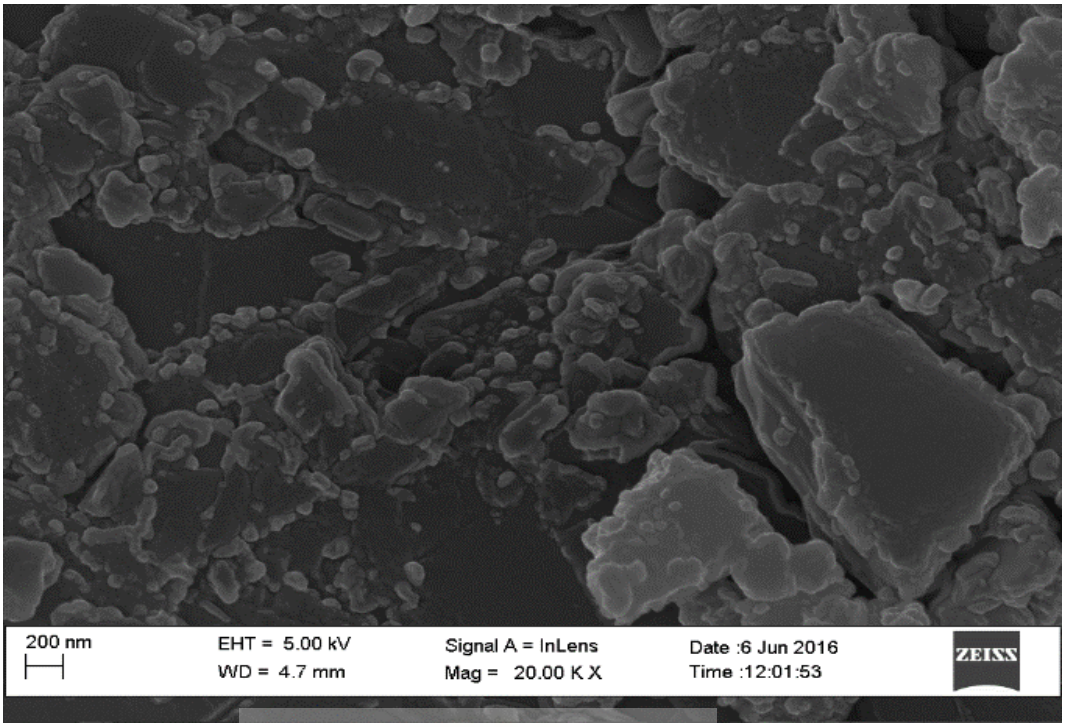

Figure 14: HRSEM images of 2,3-diaminonaphthalene

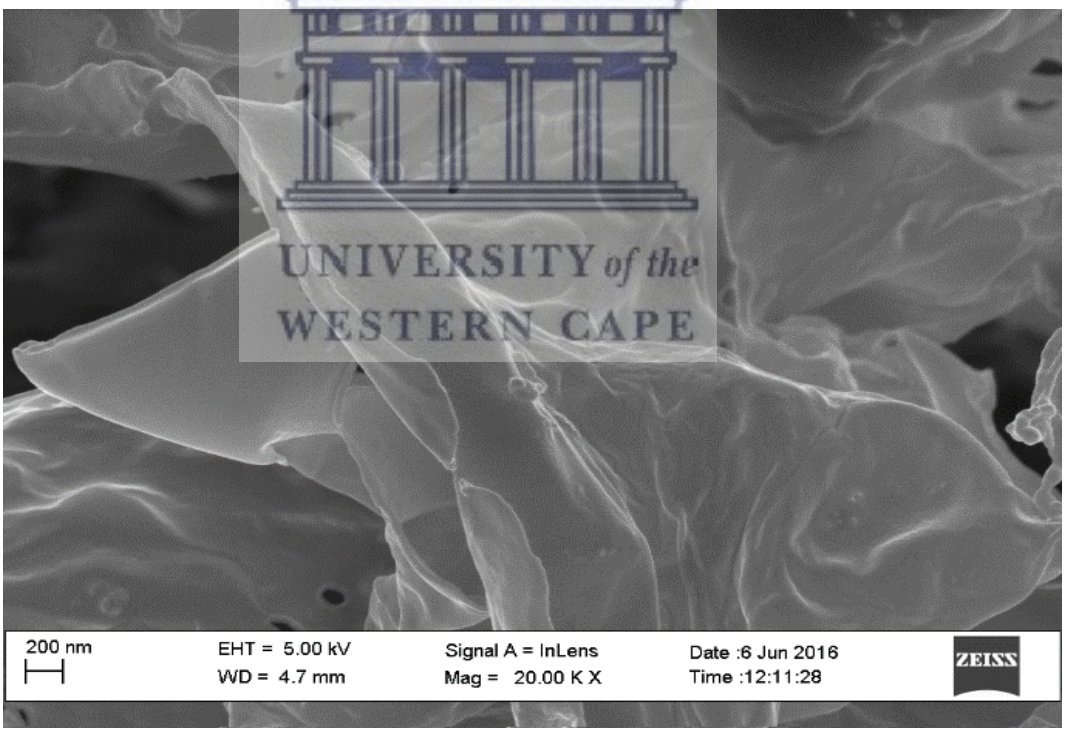

Figure 15: HRSEM images of N, N-bis(1H-pyrrole-2yl)methylene naphthalene-2,3-diamine

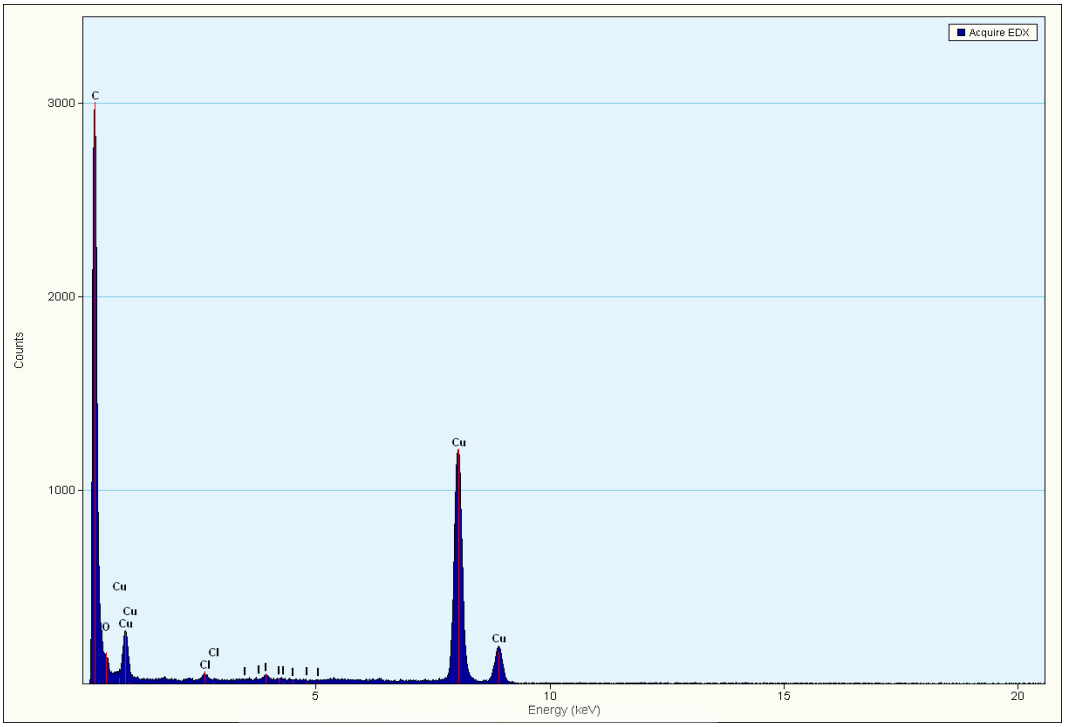

Figure 16: Energy-Dispersive X-ray (EDS) analysis of N, N-bis(1H-pyrrole-2yl)methylene naphthalene-2,3-diamine

The HRSEM results are presented in figures 13 to 16. At 20 000 magnification the materials display distinct difference in appearance. The image of N, N-bis(1H-pyrrole-2yl)methylene naphthalene-2,3-diamine (see figure 15) is much brighter than 2,3-diaminonaphthalene (see figure 14) and pyrrole-2-carboxaldehyde (see figure 13). The yields of secondary electrons in heavier elements are larger than lighter elements therefore the contrast of the monomer is brighter than the starting materials. Heavier nuclei are more effective at light scattering. EDS analysis in figure 16 shows the elemental analysis of N, N-bis(1H-pyrrole-2yl)methylene naphthalene-2,3-diamine. From the excitation data recorded it is evident that the composition of the monomer is carbon based. EDS has been reported to be less sensitive to low atomic number elements therefore detection of imine nitrogen is not expected.

3.5 Electrochemistry background

Electrochemistry is one of the leading techniques to probe electron transfer in reactions. Electrochemistry relates the electron exchange with the chemical reaction which is generally associated with oxidation or reduction of complexes. The transfer of electrons in a reaction between two molecules in solution proceeds from high energy to low energy state. The difference in energy states facilitates the reaction. In electrochemistry heterogeneous electron transfer occurs between an electrode and its environment. The driving force of the electron exchange is facilitated by an external power source, when the electrons in the electrode are at a higher energy than its environment an electron is transferred from the electrode to the conductive layer or electrolytic solution[125].

3.5.1 Electrochemistry of ligand

Electrochemistry has become an essential tool to monitor electron transfer processes of electroactive materials[125]. Research on the redox behaviours of Schiff bases have found the redox properties to be of sizable importance. It's been reported that the electrochemical properties of Schiff bases play a role in the biological characteristics of the material[126]. Whether it is chemical reduction or electrochemical reduction, the energy difference is the driving force of these reactions. In chemical reduction reactions electron transfer takes place between two molecules in solution. In electrochemical reduction reactions electron transfer takes place between the electrode and solution. Electrochemical reactions however makes provision for the manipulation of electron energy in the electrode which will facilitate electron transfer[125].

In order to investigate the redox properties of the ligand cyclic and square wave voltammetry was performed on screen print carbon electrodes modified with N, N-bis(1H-pyrrole-2yl) methylene naphthalene-2,3-diamine (monomer). The electrodes were prepared as follows; A 10 mM equivalent solution of N, N-bis(1H-pyrrole-2yl)methylene naphthalene-2,3-diamine was prepared by dissolving 6.2 mg of the monomer in 2 ml of dimethylformamide in an electrochemical cell. The solution was stirred for 5 minutes to facilitate adequate mixing. 2 ml of degassed 0.1 M HCl supporting electrolyte was added to the solution and stirred. The electrodes were then immersed in the monomeric solution to which a potential was applied using a

PalmSense potentiostat. Cyclic voltammetry (CV) was applied to deposit the material by cycling the potential between -0.600 V to 0.700 V at the working electrode for five cycles. This potential window was found to generate adequate charge to facilitate the electrochemical deposition of the monomer on to the working electrode. Thereafter the material was characterized in phosphate buffer solution with a pH of 7.1. Cyclic and square wave voltammetry was performed on the modified screen print carbon electrode (SCPE) over the potential -1 V to 1 V varying the scan rate between 10 mV/s and 500 mV/s.

Table 4: Redox properties of N, N-bis(1H-pyrrole-2yl)methylene naphthalene-2,3-diamine

$\sqrt{scanrate}$	Scan Rate	Ip anodic	Potential	Ip cathodic	Potential	ΔE	$E^{o'}$	$\frac{Ipa}{Ipc}$
3,162	10	8,6E-07	0,687	-2,8E-06	-0,676	1,363	0,006	-0,306
4,472	20	3,58E-07	-0,522	-4,9E-06	-0,685	0,163	-0,604	-0,072
5,477	30	7,5E-07	-0,505	-7,6E-06	-0,697	0,192	-0,601	-0,098
6,325	40	7,46E-07	-0,516	-1E-05	-0,701	0,185	-0,609	-0,074
7,071	50	1,11E-06	-0,528	-1,3E-05	-0,695	0,167	-0,612	-0,089
10,000	100	1,12E-06	-0,538	-1,5E-05	-0,73	0,192	-0,634	-0,073
14,142	200	3,68E-06	-0,541	-2E-05	-0,769	0,228	-0,655	-0,182
17,321	300	4,44E-06	-0,539	-1,9E-05	-0,793	0,254	-0,666	-0,228
20,000	400	3,47E-06	-0,53	-1,9E-05	-0,798	0,268	-0,664	-0,184
22,361	500	3,92E-06	-0,531	-1,9E-05	-0,799	0,268	-0,665	-0,210

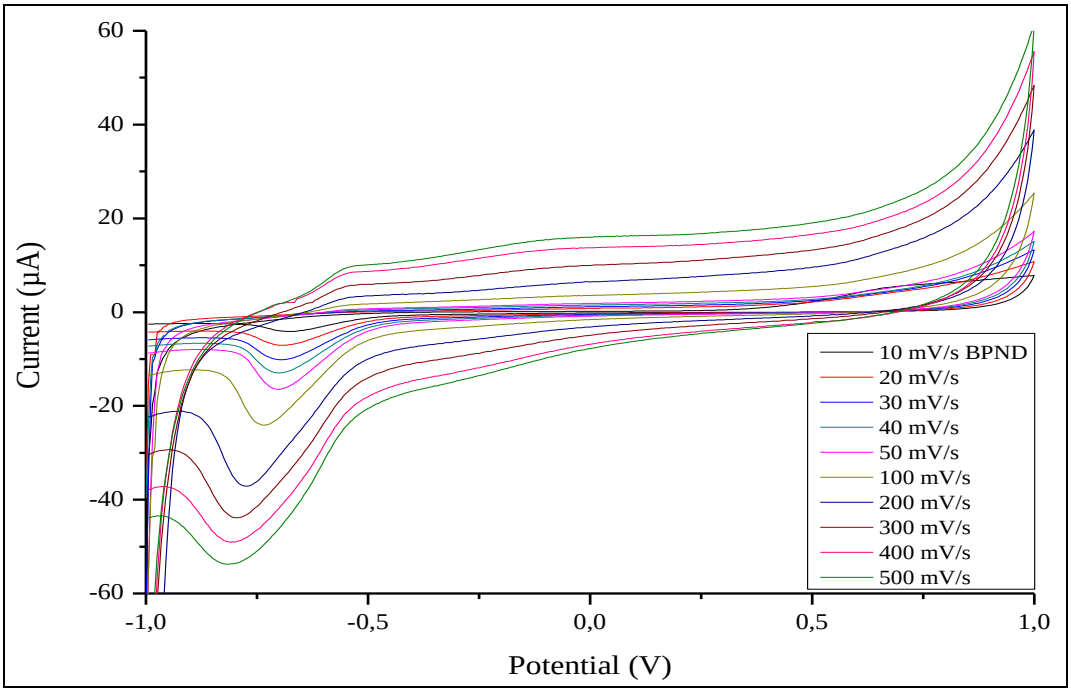

Figure 17: Cyclic voltammetry of N, N-bis(1H-pyrrole-2yl)methylene naphthalene-2,3-diamine deposited on SPCE in 0.1 M PBS vs Ag/AgCl performed at scan rates ranging between 10 and 500 mV/s over the potential window -1V to 1 V

CV (see figure 17) was performed on the material to determine if the material is electroactive. CV also provided data of the potentials at which the electrochemical processes occurred. The redox properties of N, N-bis(1H-pyrrole-2yl)methylene naphthalene-2,3-diamine was investigated following the electrodeposition of the monomer on the SPCE. Electrochemical experiments were initiated at -1 V, where no electrode processes occurred, and scanned linearly in the positive direction until the switching potential was reached at +1 V, and swept back to -1 V. In the forward scan a non-reversible oxidation process was recorded producing a peak current at 0.687 V. This was attributed to production of an anionic radical[127]. A strong reduction peak was observed at -0.676 V in the cathodic scan. This was attributed to the reduction of the anionic radical. At 10 mV/s the electron transfer process appeared to be slow, the peak to peak separation, as per table 3, was ΔE = 1.363 V at 10 mV/s. The initial electron transfer process was determined to be non-reversible. In subsequent scans electron transfer at 0.687 V appeared to be blocked. The oxidation process at 0.687 V was electrochemical in nature, a one electron transfer process that produced $Ph{=}[NHC_5H_7N]^{\cdot+}$ an unstable intermediate[128]. At 20 mV/s an anodic peak was recorded -0.522 V. The anodic and cathodic peak currents increased with increasing

scan rate and identified quasi reversible electron transfer. The initial oxidation process would suggest electron transfer to proceed via a heterogeneous chemical reaction, transforming from and insulating to conductive layer. The product of the initial oxidation reaction was reduced and available more rapidly for reoxidation[129]. The subsequent electron transfer processes depicted in the CV can be ascribed to adsorption and diffusion processes.

It's well accepted that a diffusion controlled current for CV according to the Randle-Sevcik equation is linear. A plot of the square root of the scan rate vs. the peak current of the monomer is presented in figure 18.

Figure 18: Randles-Sevcik plot of N, N-bis(1H-pyrrole-2yl)methylene naphthalene-2,3-diamine

The plot revealed the electron transfer process to be non-linear. The deviation from linear behaviour could be associated with adsorption phenomena. It is evident that the mass transfer behaviour of the ligand did not display diffusion control characteristics.

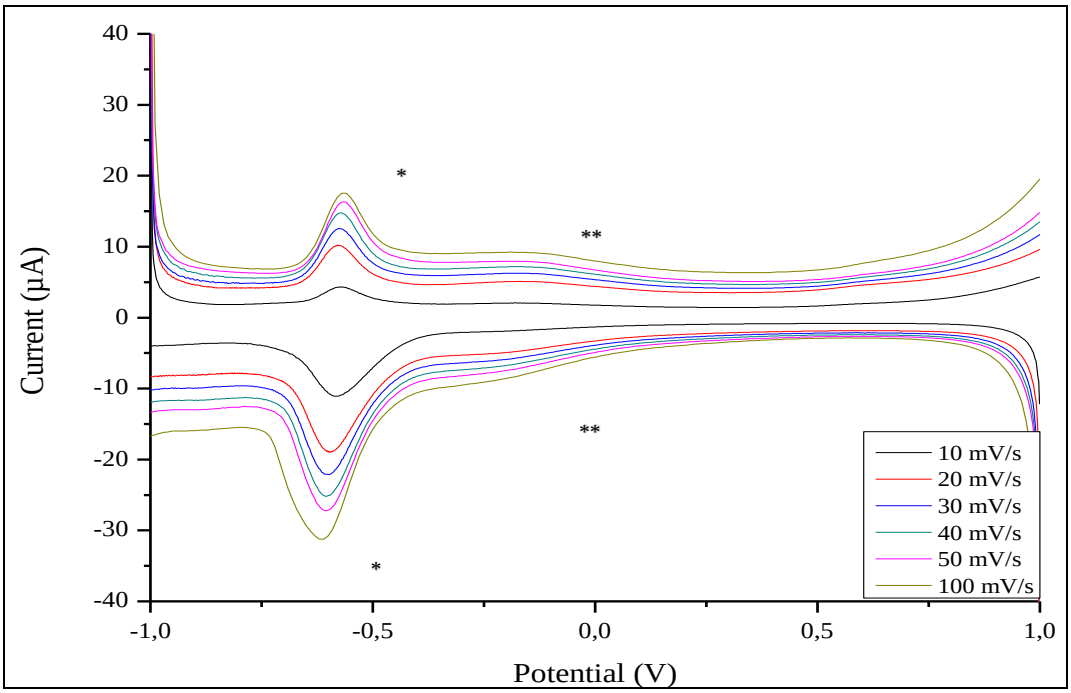

Figure 19: Square Wave Voltammetry, anodic and cathodic, of N, N-bis(1H-pyrrole-2yl)methylene naphthalene-2,3-diamine deposited on SPCE performed in 0.1 PBS vs Ag/AgCl performed at scan rates ranging between 10 and 100 mV/s over potential window -1V to 1 V

*Table 5: Square wave Redox properties of N, N-bis(1H-pyrrole-2yl)methylene naphthalene-2,3-diamine (Peak *)*

$\sqrt{scanrate}$	Scan Rate	Ip anodic	Potential	Ip cathodic	Potential	ΔE	E$^{o'}$	$\frac{Ipa}{Ipc}$
3,162	10	1,82E-06	-0.572	8,22E-06	-0.582	10	-0.577	0,221
4,472	20	5,78E-06	-0.577	1,22E-05	-0.592	15	-0.584	0,474
5,477	30	7,23E-06	-0.573	1,39E-05	-0.600	27	-0.586	0,521
6,325	40	8,66E-06	-0.572	1,54E-05	-0.603	31	-0.587	0,562
7,071	50	9,39E-06	-0.565	1,65E-05	-0.605	40	-0.585	0,570
10,000	100	9,76E-06	-0.568	1,83E-05	-0.614	46	-0.591	0,533

*Table 6: Square wave Redox properties of N, N-bis(1H-pyrrole-2yl)methylene naphthalene-2,3-diamine (Peak **)*

$\sqrt{scanrate}$	Scan Rate	Ip anodic	Potential	Ip cathodic	Potential	ΔE	E$^{o'}$	$\frac{Ipa}{Ipc}$
3,162	10	3,1E-07	-0.150	7,7E-08	-0.172	22	-0.161	4,026
4,472	20	8,85E-07	-0.141	3,87E-07	-0.187	46	-0.164	2,287
5,477	30	9,62E-07	-0.137	4,69E-07	-0.179	42	-0.158	2,051
6,325	40	1,12E-06	-0.135	5,11E-07	-0.190	55	-0.162	2,192
7,071	50	1,08E-06	-0.132	5,65E-07	-0.196	64	-0.164	1,906
10,000	100	1,15E-06	-0.126	5,96E-07	-0.192	66	-0.159	1,936

Square wave voltammetry is a more sensitive technique than cyclic voltammetry and is generally performed to eliminate background interferences such as capacitive current. Figure 19 above illustrates the square wave voltammograms of N, N-bis(1H-pyrrole-2yl)methylene naphthalene-2,3-diamine electrodeposited on screen printed carbon electrodes in 0.1 M phosphate buffer at different scan rates. Square wave voltammetry was initiated at -1 V and scanned in the positive direction. At this point the material was unreactive in the electrolyte and the current stable. In both anodic and cathodic scans the currents recorded over the potential window was a function of scan rate. The frequency was kept constant, at 10 Hz, changing only the potential step. The anodic peak currents recorded for N, N-bis(1H-pyrrole-2yl)methylene naphthalene-2,3-diamine was assigned to the redox processes of Ph=$[NHC_5H_7N]_2^{2-}$ (-0.572 V) and Ph=$[NHC_5H_7N]_2^{\cdot-}$ (-0.582 V) following the formation of an anion intermediate. Investigations of the second peak indicated the peak to be asymmetric and indicative of electrochemical reaction coupling. This was substantiated by the peak current ratios in table 6. This phenomena has been reported to be indicative of electroactive molecules with more than one isomer[129]. The two electron transfer process recorded could possibly confirm this with the two isomeric forms having different redox properties.

Chapter 4

4. Macromolecule synthesis: Methodology, results and discussion

In an attempt to mimic the electrochemical behaviour of cytochrome-c, a new molecule was designed based on Schiff base chemistry and the incorporation of an iron centre. Different sensor strategies were employed to isolate and optimise the reactivity of the metal ligand complex towards NO detection.

4.1 Electrochemistry of Fe^{2+}/Fe^{3+} in situ

Potassium Ferricyanide is commonly used to calibrate voltammetric systems in aqueous media. Voltammetric experiments on 5 mM potassium ferricyanide $K_3Fe(CN)_6$ will give a characteristic current response at which iron is oxidized and reduced at the working electrode. The electrochemical measurements were performed by dissolving potassium ferricyanide in a 0.1 M KCl supporting electrolyte solution. Cyclic voltammetry was recorded over the potential window -1V to 1V in PBS. The square wave redox voltammetry of ferricyanide was recorded at 10 Hz, changing only the potential step.

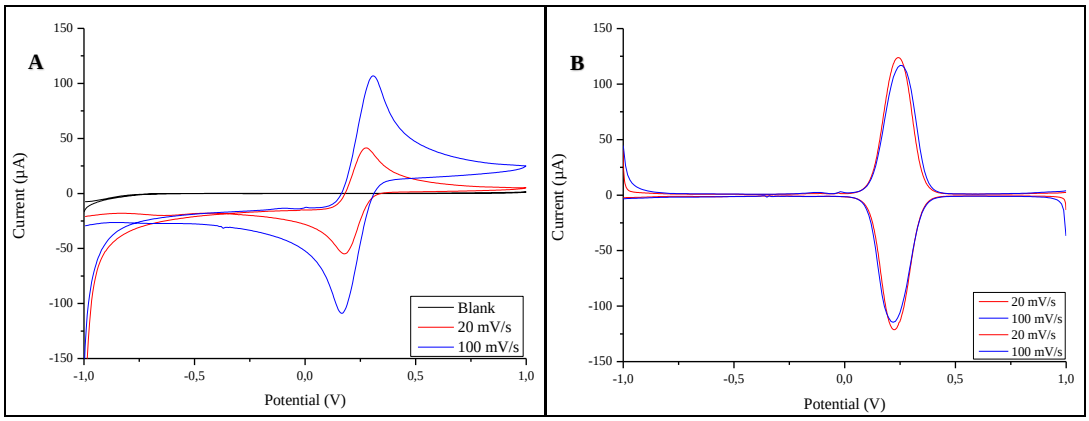

Figure 20: (A) Cyclic voltammetry (B) Square Wave Voltammetry of $K_3Fe(CN)_6$ on SPCE in 0.1 M KCl vs Ag/AgCl at 20 and 100 mV/s over potential window -1V to 1 V

Table 7: Cyclic voltammetry study of ferricyanide redox couple

Oxidation potential (V)	Reduction potential (V)	Scan rate (mVs^{-1})	$E^{0'}$ (V)
0.275	0.177	20	0.226
0.308	0.166	100	0.237

Table 8: Square wave voltammetry study of ferricyanide redox couple

Oxidation potential (V)	Reduction potential (V)	Scan rate (mVs^{-1})	$E^{0'}$ (V)
0.242	0.223	20	0.232
0.258	0.220	100	0.239

As the potential is scanned in the forward direction ferricyanide is oxidized to;

$$Fe(CN)_6^{-4} \longrightarrow Fe(CN)_6^{-3} + e^- \qquad (4.1)$$

The anodic peak current formed at 0.275 V. For the purpose of illustrating reversibility the scan rate was increased to 100 mVs^{-1}. The anodic current was recorded at 0.308 V, where oxidation peaked and gradually decreased until the switching potential was reached. On the reverse scan ferricyanide was reduced to;

$$Fe(CN)_6^{-3} + e^- \longrightarrow Fe(CN)_6^{-4} \qquad (4.2)$$

The cathodic current reached a potential where reduction of Fe reached a maximum at 0.177 V at 20 mVs^{-1}. When the scan rate was increased to a 0.100 Vs^{-1} the reduction of Fe peaked at 0.166 V at 0.100 Vs^{-1}. The formal potential was calculated at 0.226 V at 20 mVs^{-1} and 0.237 V at 0.100 Vs^{-1} and accounts for the activity coefficients for oxidation and reduction at these potentials.

Square wave voltammetry is more sensitive than cyclic voltammetry. The potential windows for both oxidation and reduction processes ranged from -1 to 1 V. At a scan rate of 20 mVs^{-1} an anodic peak current was recorded at 0.242 V and a cathodic peak current at 0.223 V. When the scan rate was increased to a 0.100 Vs^{-1} an anodic peak was recorded at 0.258 V and a cathodic peak at 0.220 V. ΔE_p was subsequently calculated to be 0.038 V. A process, by definition, is reversible if the peak potentials are separated by 0.059 V for a one electron transfer process. It was also evident that the peak current potentials correlated to the scan rate. The peak currents were recorded as follows 5.145 µA (I_{pa}) and 5.118 µA (I_{pc}) with a peak current ratio of 1. These results correlated with literature reports on systems that display ideal behaviour for chemically reversible systems in aqueous solutions[130131].

4.2 Sensor synthesis strategies

Three electrode synthesis strategies were adopted. In synthesis strategy (A) denatured cytochrome-c was used as a redox element. The denaturation of cytochrome-c was induced by heating 1 ml solution of horse heart cytochrome-c, 1 mg/ml, for 1 hour at 70ºC. Sensor strategy A involved the electrochemical deposition of the denatured cytochrome-c on a bare SPCE. In sensor strategy B, the chemically synthesized Schiff base ligand was electrodeposited onto the SPCE. This step was followed by drop coating the denatured cytochrome-c onto ligand modified SPCE. Sensor strategy C involved modification of the bare SPCE with the synthesized Fe centred Schiff base ligand complex (FeL_4) (see figure 21).

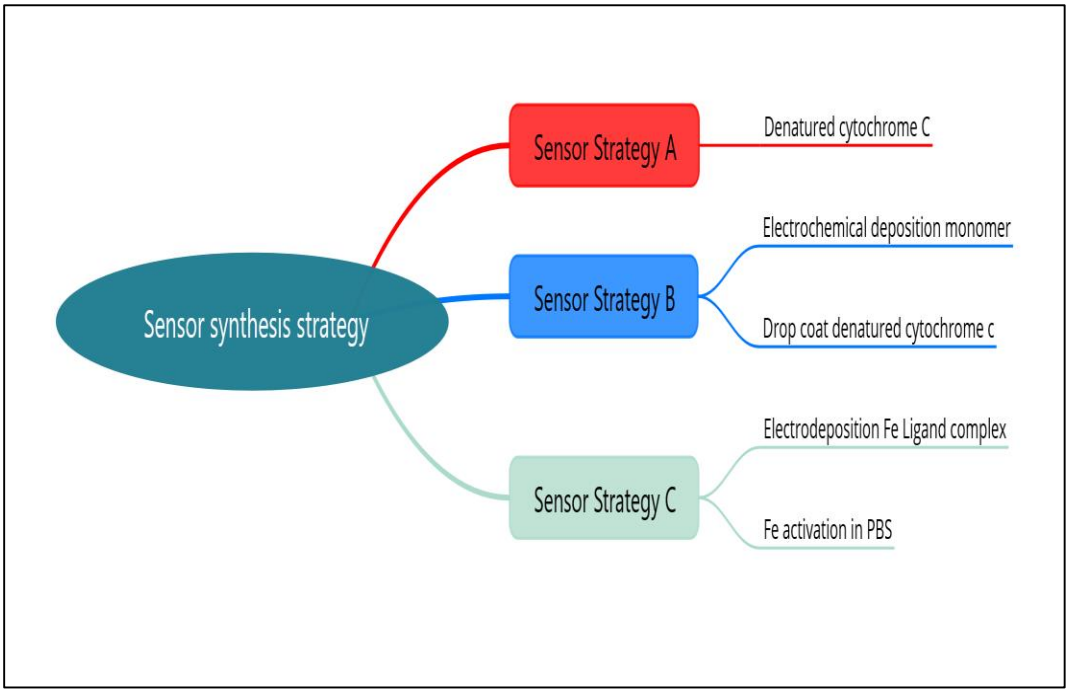

Figure 21: Schematic design of sensor fabrication strategies

4.2.1 Sensor synthesis strategy A

For sensor strategy A denatured cytochrome-c was electrodeposited onto a SPCE by cycling a current, once, over the potential window -0.600 V to 0.700 V at 50 mV/s. This was performed in a 1mg/ml solution of denatured cytochrome-c. These studies were conducted with SPCEs to assess the electrochemical response of the enzyme in its denatured state. Past studies, which investigated structural aspects of the protein, found the environment of the protein to have a direct impact on the electron transfer capabilities of the heme. The electrochemistry of denatured cytochrome-c was examined in PBS by performing cyclic voltammetry over a potential window of -1 V and 1V.

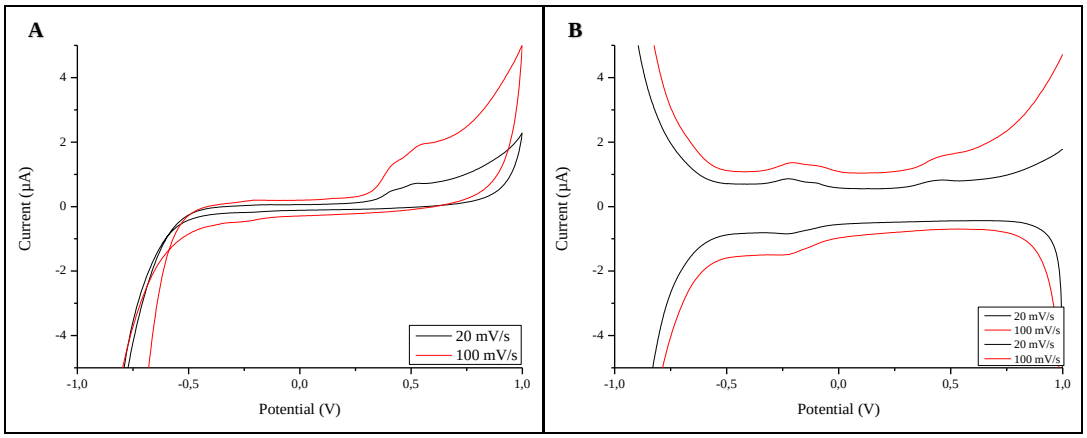

Figure 22: (A) Cyclic voltammetry (B) Square Wave Voltammetry of SPCE/denatured cytochrome-c in 0.1 M PBS (7.1) at scan rates 20 mV/s and 100 mV/s

An inspection of the electron transfer behaviour of the enzyme subjected to an applied potential showed the denatured enzyme to be electroactive (figure 22A). In the anodic scan a Faradaic current was produced, as a function of applied potential, with a moderate oxidation peak observed at 0.410 V. The electron transfer appeared to be irreversible as only an oxidation peak was observed on the forward scan. This suggested changes to the conformational structure of the enzyme, akin to denaturation of the enzyme. Previous reports sited quasi-reversible electrochemistry of cytochrome-c deposited on glassy carbon and pyrolytic graphite electrodes. When looking at the heme structure of cytochrome-c lysine has been reported to facilitate redox processes within the enzyme but high temperature denaturation deprotonates lysine. This results in changes to the redox behaviour of the enzyme[92132]. CV revealed strong conformational changes represented by a shift in native formal potential previously reported at 0.060 mV[133]. The oxidation peak observed at 0.410 V was attributed to the oxidation of Fe^{2+}. The shift in the oxidation potential was attributed to a conformational change in the heme due to heat induced unfolding. The peak broadening effect observed was interpreted as fluctuations in the stability of adsorbed denatured cytochrome-c. The stronger the molecule adsorbed the more the negative the oxidation potential[132]. This phenomena coincides with a report by Clark and Bowder (1997) whom investigated the voltammetric peak broadening for cytochrome-c monolayers adsorbed onto self-assembled monolayer (SAM) modified gold electrodes[134]. The interpretation of this phenomena was that cytochrome-c underwent

considerable conformational changes upon adsorption on to the hydrophobic surface resulting in the denaturation of the enzyme[135136137].

Square wave voltammetry a technique much more sensitive than cyclic voltammetry was performed. This technique rejects interference by charging currents. A two-step redox process, a reversible one electron transfer process at -0.250 V and a non-reversible electron transfer process at 0.435 V, was revealed (see figure 22B). The peak currents increased with increasing scan rate indicating a diffusion controlled process. The reversible couple at -0.250 V could have originated from a weak interaction between denatured cytochrome-c and the electrode surface. The oxidation peak current corresponded to -0.250 V and reduction -0.350 V. No redox couple was observed for the oxidation of Fe^{2+} at 0.435 V. This finding coincided with investigations into the influence of SAMs terminating in functional groups. These simulated different surface conditions and the impact thereof on the conformation of cytochrome-c[87]. A study by Szucs and Novak (1995) reported on reversible and irreversible electrochemical behaviour of cytochrome-c deposited on bare electrodes[84]. The irreversible electron transfer behaviour was ascribed to the presence of oligomers on the electrode surface that oxidizes monomeric forms of cytochrome-c. Monomeric forms on the other hand facilitates redox chemistry on the electrode but decreases as oligomeric forms increase. This can be identified by voltammetric peaks forming shoulders. When deposited on bare electrodes the enzyme undergoes conformational changes with possible loss of transfer capabilities but when immobilized on a monolayer it can retain near native conformation[84]. These findings were also reported by Sagara et al., (1990) who investigated the redox behaviour of cytochrome-c deposited on gold electrodes modified with 4-pyridyl derivatives that served as surface modifiers[133]. The electron transfer behaviour of cytochrome-c was investigated when immobilized on the modified gold electrodes. The study reported on shifts to more negative formal potentials in comparison to native cytochrome-c.

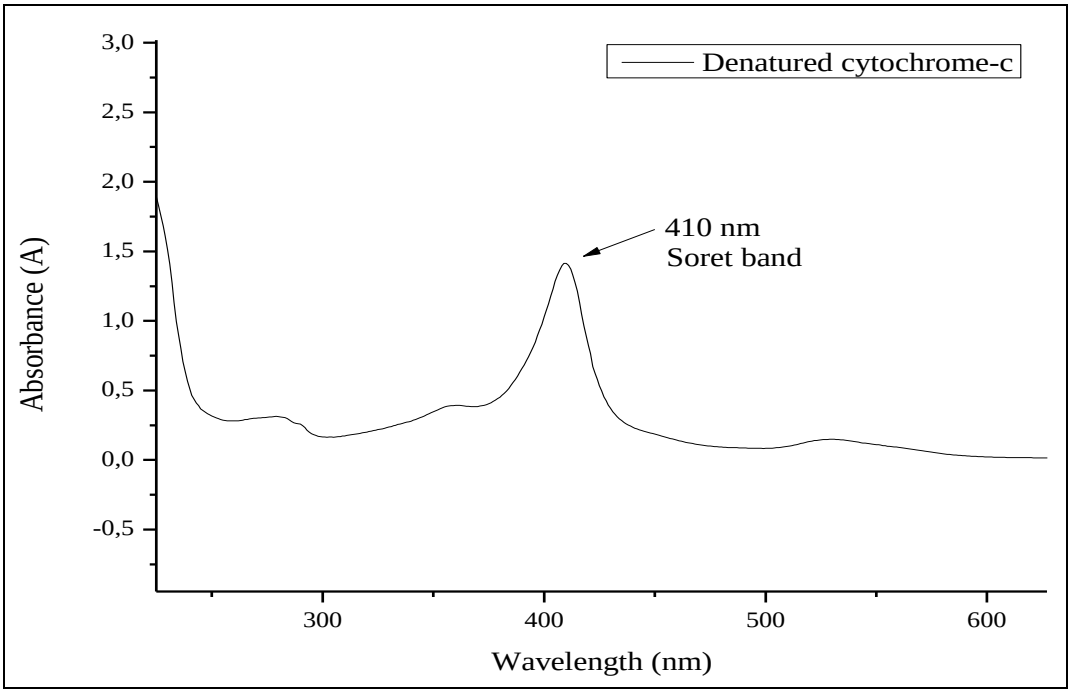

Figure 23: UV Vis spectroscopy of 4ml 1mg/ml denatured cytochrome-c solution in deionised water

UV Vis analysis of the cytochrome-c solution confirmed the solution to be denatured as indicated by the Soret band of the iron heme 410 nm in figure 23. The position of the Sorbet is an indicator used in literature to provide information of the heme protein, when denatured the absorption band shifts or disappears[106]. The presence of the peak confirmed the availability of the heme for electron transfer interactions.

4.2.2 Sensor synthesis strategy B

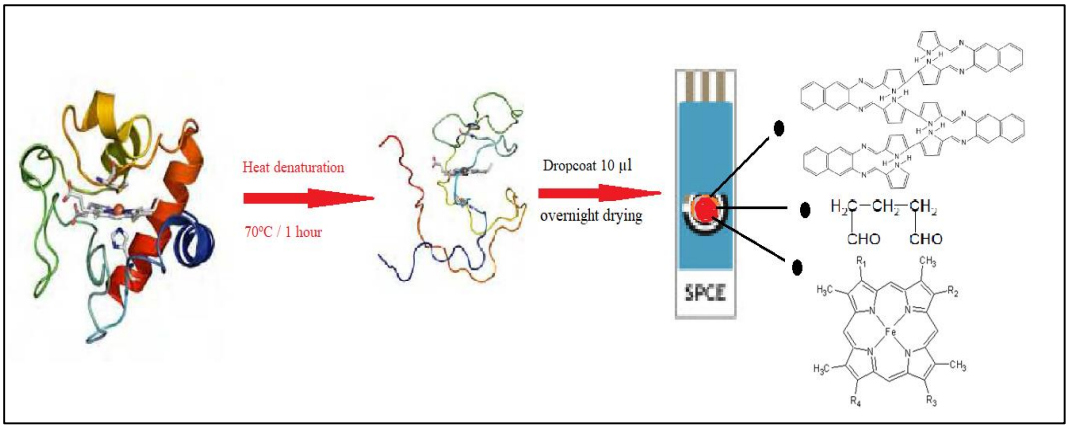

Figure 24: Schematic design of sensor fabrication strategy B

In the second sensor strategy, sensor fabrication strategy B, a Schiff base was synthesized and used as a transducer layer. It served as a redox mediator to allow for the investigation of the electron transfer behaviour of denatured cytochrome-c. 5 mM of the Schiff-base bis((1H-pyrrol-2-yl)methylene)naphthalene-2,3-diamine) (6.2 mg weight equivalent), was deposited on to the SPCE surface electrochemically in a mixed electrolyte system. The monomer was dissolved in 2 ml DMF and mixed with 2 ml of degassed 0.1 M HCl supporting electrolyte solution. The solution was bubbled with Argon gas for 5 minutes to remove dissolved oxygen. The Schiff base monomer was electrodeposited onto the electrode surface using CV with the following parameters; a potential window of -0.600 V to 0.700 V was cycled 5 times at a scan rate of 50 mVs^{-1}. A stock cytochrome-c solution with a concentration of 10 mg/ml was prepared by dissolving 10 mg of the enzyme in 1 ml deionized water in an Eppindorf tube. The enzyme was denatured in a hot water bath (75 ^{o}C) for 1 hour. From this solution a 1 mg/ml solution of the denatured enzyme was prepared. The denatured enzyme was anchored on the ligand with 10 µl of a 1% gluteraldehyde solution that was drop coated on the SCPE and dried for approximately 1 to 3 hours. Thereafter 10 µl of the 1 mg/ml denatured cytochrome-c solution was deposited on the surface and dried overnight. Cyclic and square wave voltammetry was used to investigate the electron transfer behaviour. The diffusion coefficient was calculated using the Randles-Sevcik equation $i_p = (2.69 \times 10^5)\, n^{\frac{3}{2}} A D^{\frac{1}{2}} C v^{\frac{1}{2}}$: A is the electrode area (cm^2), D diffusion coefficient (cm^2/s), C is the concentration of the electrolyte in bulk solution (mol/cm^3) and v scan rate.

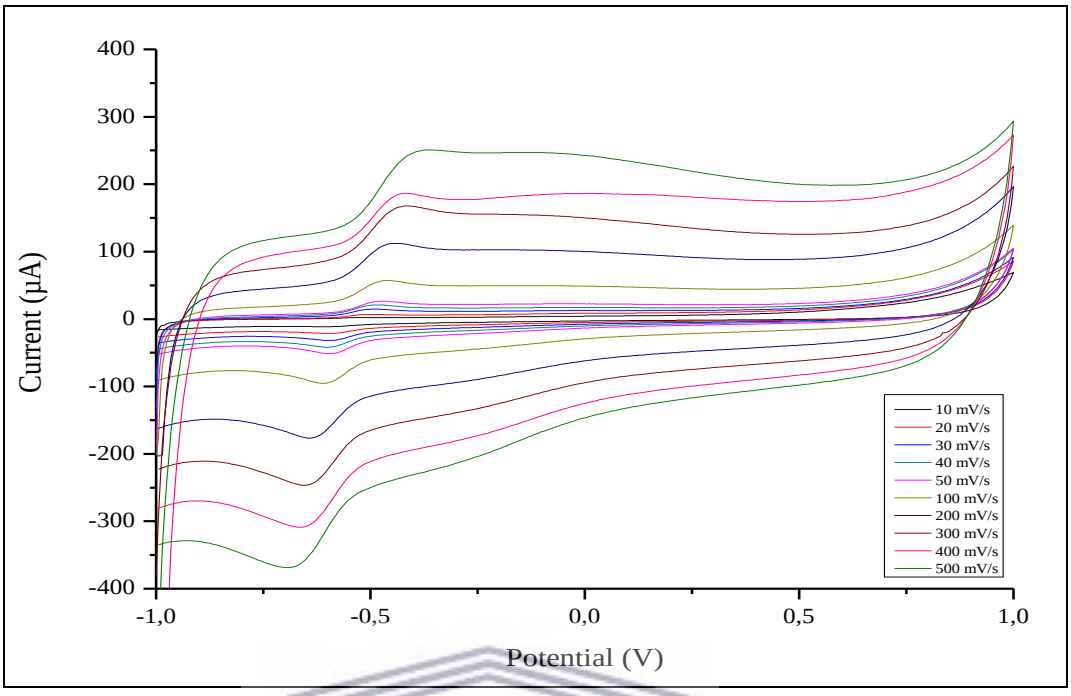

Figure 25: Cyclic voltammograms of denatured cytochrome-c, sensor strategy B, at the modified SPCE vs Ag/AgCl, in 0.1 M PBS at scan rates using 10-500 mV/s

Table 9: Cyclic voltammetric study of denatured cytochrome-c redox couple

$\sqrt{scanrate}$	Scan Rate	Ip anodic	Potential	Ip cathodic	Potential	ΔE	$E^{o'}$	$\frac{Ipa}{Ipc}$
3,162	10	2,575E-06	-0,524	-2,57E-06	-0,587	0,063	-0,556	-1,000
4,472	20	6,718E-06	-0,506	-6,34E-06	-0,59	0,084	-0,548	-1,060
5,477	30	8,137E-06	-0,5	-1,08E-05	-0,593	0,093	-0,547	-0,753
6,325	40	1,156E-05	-0,486	-1,37E-05	-0,598	0,112	-0,542	-0,841
7,071	50	1,458E-05	-0,472	-1,71E-05	-0,592	0,12	-0,532	-0,851
10,000	100	2,644E-05	-0,465	-2,86E-05	-0,608	0,143	-0,537	-0,926
14,142	200	5,041E-05	-0,443	-5,61E-05	-0,638	0,195	-0,541	-0,899
17,321	300	6,195E-05	-0,417	-6,05E-05	-0,647	0,23	-0,532	-1,024
20,000	400	5,910E-05	-0,424	-6,91E-05	-0,657	0,233	-0,541	-0,855
22,361	500	8,997E-05	-0,368	-9,23E-05	-0,675	0,307	-0,522	-0,975

Table 10: Square wave voltammetric study of denatured cytochrome-c redox couple

Oxidation potential (V)	Reduction potential (V)	Scan rate(mVs^{-1})	$E^{0'}$ (V)
-0.540	-0.570	10	-0.555
-0.090	-0.170	10	-0.130
-0.508	-0.582	50	-0.542
-0.126	-0.220	50	-0.173
-0.504	-0.610	100	-0.538
-0.098	-0.244	100	-0.171

The inspection of the electron transfer behaviour of denatured cytochrome-c stacked on the ligand subjected to an applied potential revealed a one redox couple. At low scan rate the forward scan showed evidence of electron transfer that took place with a very poorly defined oxidation peak. In subsequent scans the oxidizing peak increased with increasing scan rate as illustrated in figure 26. Ferrous iron in cytochrome was oxidized to ferric iron. The ligand modified with denatured cytochrome-c displayed oxidizing potentials more negative than denatured cytochrome-c on bare SPCE (see figure 25). Comparing the two systems at 10 mVs^{-1} an oxidizing peak current was recorded at -0.524 V vs Ag/AgCl for the SPCE modified with the ligand and denatured cytochrome-c. The bare SCPE immersed in a denatured cytochrome-c solution with a concentration of 1 mg/ml recorded an anodic peak current at 0.420 mV. At 10 mVs^{-1} the formal potential of -0.555 V suggested the material can be readily oxidized under standard conditions. As the scan rates increased the current response increased and the formal potential shifted and simulated a diffusion controlled one-electron response system. The changes in the formal potential of denatured cytochrome-c adsorbed on to the ligand was evidence of conformational changes of the denatured enzyme. The cyclic voltammetric response of denatured cytochrome-c deposited on the ligand identified a quasi-reversible electron transfer system. The ligand appeared to have minimized destructive adsorption of denatured cytochrome-c onto the SPCE. The ligand allowed for orientation of denatured cytochrome-c onto the electrode surface in a manner that allowed for rapid exchange of electrons. These findings coincide with reports in literature. Sagara et al., (1990) found electron transfer reactions to be facilitated by surface modifiers in their investigation of the behaviour of cytochrome-c deposited on gold electrodes modified with 4-pyridyl derivatives[133]. Similar findings

were reported by Eddowes and Hill (1979) whom investigated the impact of monolayers on the electron transfer behaviour of cytochrome-c.

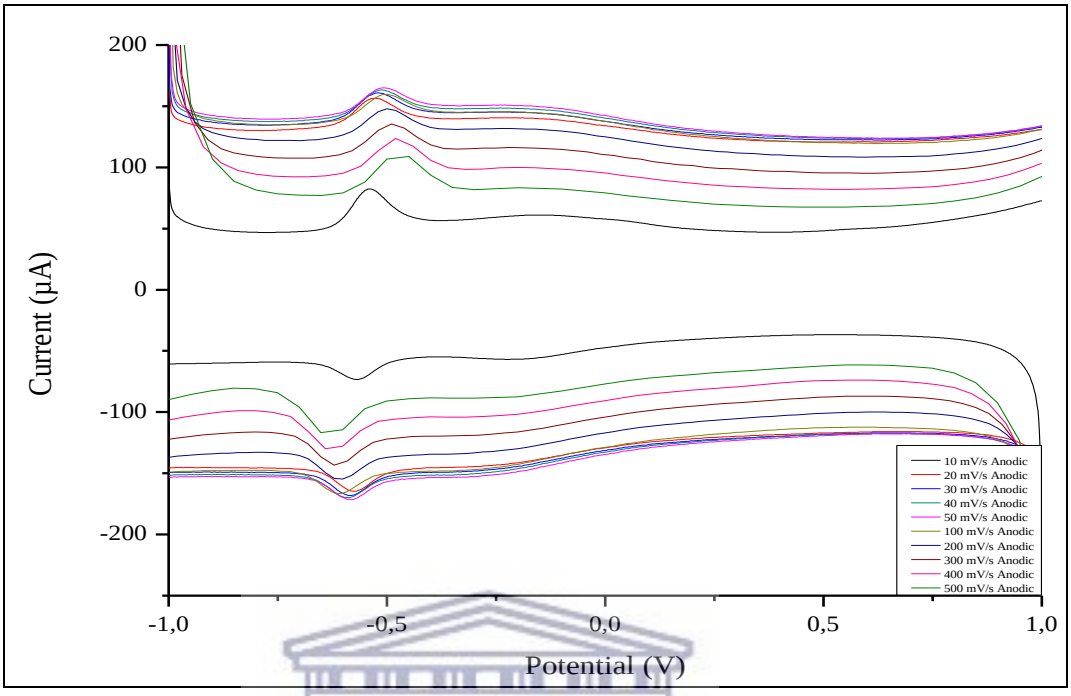

Figure 26: Square Wave Voltammograms of denatured cytochrome-c (sensor strategy B) at the modified SPCE, vs Ag/AgCl in PBS (pH = 7.1) at scan rates 10 – 500 mV/s

Square wave voltammetry (figure 26) identified a one electron-transfer redox system. Although, at low scan rates, two anodic peaks were recorded at -0.540 V and -0.090 V in the forward scan, the secondary peak (-0.090 V) was attributed to lateral interactions of the redox active groups[138]. This phenomenon was observed by Chidsey et al. (1990) who reported broadened voltammograms and positively shifted formal potential values brought about by ferrocene monolayers[139]. The primary redox process recorded at -0.540 V was found to be reversible at low scan rates. However, peak-to-peak separation increased with increasing scan rate rendering the electron transfer process quasi-reversible.

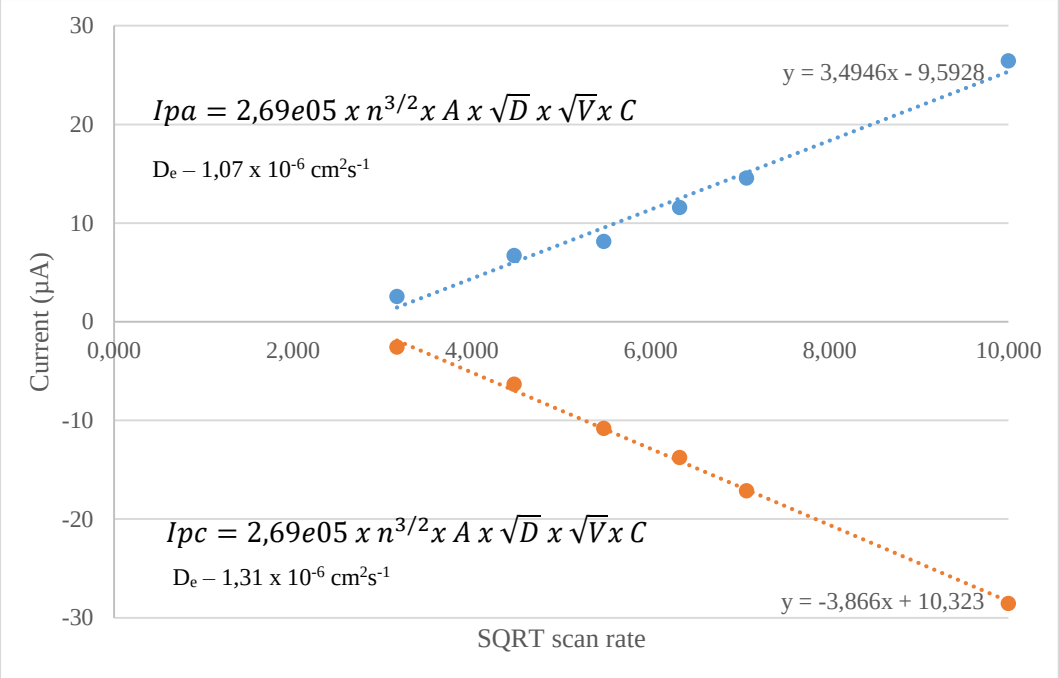

Figure 27: Randles-Sevcik plot of square root vs scan rate for sensor strategy B

The Randle-Sevcik equation was applied to investigate electron transfer at the electrode surface in figure 27. The Randles-Sevcik plots for the oxidation and reduction currents vs. square root of scan rates shows a linear relationship. Based on the peak current ratios calculated in table 9 the redox couple displayed reversible electron transfer behaviour. The systems displayed diffusion controlled kinetics as evidenced by the linear regression lines for scan rates 10 – 500 mV. The diffusion coefficient (De) was calculated to be 1.07 x 10^{-6} cm^2/s for the anodic process and 1.31 x 10^{-6} cm^2/s for the cathodic process. These values were in agreement with a report by Eddowes and Hill (1979). De values of 9.4 x 10^{-7} cm^2/s were reported for 4,4`-bipyridal cytochrome-c systems[135]. Abass and Hart (2001) reported De values of 8.1 x $10^{-7}$$cm^2/s$ for the anodic peak currents, and 8.03 x $10^{-7}$$cm^2/s$ for the cathodic peak currents, in their investigations of cytochrome-c deposited on polycarbonate modified SPCE[140].

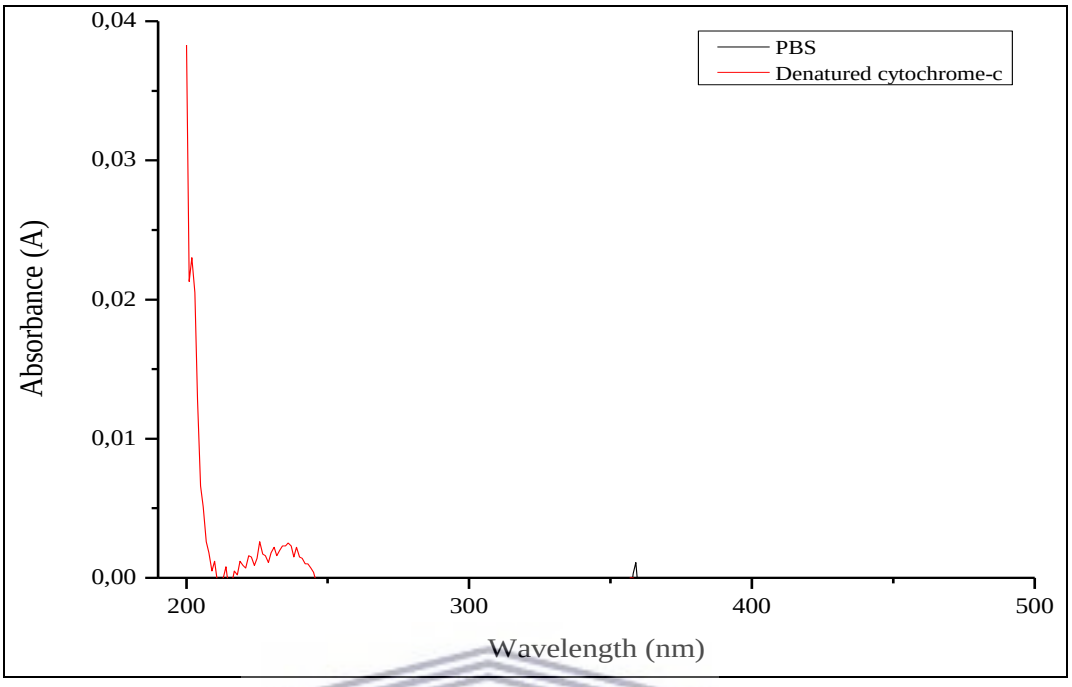

Figure 28: UV Vis spectroscopy of the 4ml PBS solution following characterization of the denatured cytochrome-c ligand system

Stability of the denatured cytochrome-c enzyme on the ligand is vital. Leaching of the material into solution will compromise the integrity of the system rendering it ineffective. Following electrochemical characterization the PBS electrolyte solution was subjected to UV analysis. Two solutions of PBS were analysed, a blank solution (black) and the PBS solution used in the characterization of sensor strategy B (red). From figure 28 it is evident there was no leaching of the material into the electrolyte solution. Hinnen, Parsons and Niki (1983) also cited strong adsorption effects of cytochrome-c corroborating the stability of denatured cytochrome-c. The small absorbance bumps observed were negligible and was mostly noise. The red bump observed 230 nm was ascribed to residual material stuck to the surface of the electrode during synthesis, this was therefore insignificant. The dissolution of the adsorbed layer into the solution is also negligible[141].

4.2.3 Sensor strategy C

In an attempt to emulate the redox chemistry of cytochrome-c iron was chelated with the ligand ((1H-pyrrol-2-yl)methylene)naphthalene-2,3-diamine). The iron chelated

ligand ((1H-pyrrol-2-yl)methylene)naphthalene-2,3-diamine) complex, was prepared by refluxing the ligand in a hot methanol solution of iron (II) chloride tetrahydrate ($FeCl_2.4H_2O$). A 5 mM methanolic solution of $FeCl_2.4H_2O$ was prepared by dissolving 20 mg of $FeCl_2.4H_2O$ in 20 ml methanol. This mixture was added drop wise to a hot 10 mM methanolic solution (30 ml) of the monomer. The molar ratio of the ligand and iron chloride was 2:1. The reaction mixture was refluxed in a 250 ml round bottom flask clamped to a retort stand. Reflux was performed for 3 hours in an oil bath at 70 ^oC on an IKA C-Mah HS 7 magnetic stirrer. The solution was allowed to cool to room temperature which facilitated the precipitation process of the material. The precipitate was then separated from the solvent through rotary evaporation (P-100 BUCHI ROTAVAPOR system). The residue was washed with methanol, chilled and allowed to reach room temperature. This step was followed by rotary evaporation of the solution to produce the metal ligand complex dark brown black in colour with an 84.5% yield. The colour corresponding to a study by Veauthier et al., (2004).

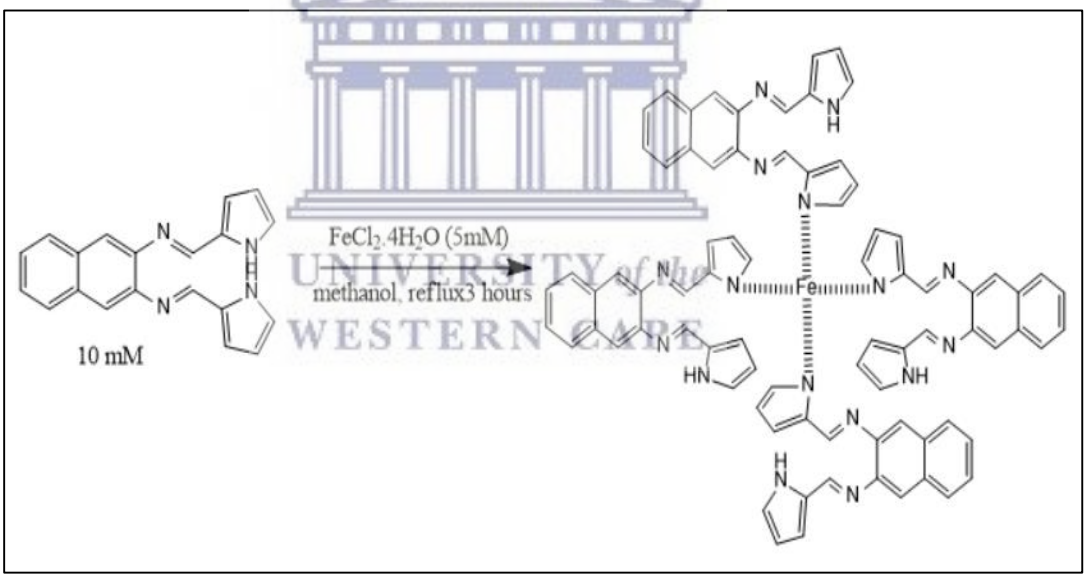

Figure 29: Proposed mechanism for synthesis of the macromolecule

Figure 29 predicts a possible mechanism and structure for the macromolecule based on the chelating and macrocyclic effect of N, N-bis(1H-pyrrole-2yl)methylene naphthalene-2,3-diamine. Coordination of ligands to a Lewis acidic metal ion activates the chloro- substituent to nucleophilic attack by methanol and by other exogenous nucleophiles[142]. Pyrrole in a study by Doddi et al., (1976), who investigated the reactivity of pyrrole in nucleophilic substitution reactions. When compared to furan and thiophene derivatives, pyrrole was reported to be less reactive relative to the other

heteroatoms[143]. Although square planar coordination, for four coordinate compounds, it offers substantial electronic stabilization. Strong field ligands has been reported to adopt square planar geometry in Ni complexes. Square planar coordination for iron (II) compounds have been reported to be limited to complexes containing porphyrin, salicylaldimato, phthalocyanine ligands[144]. Based on the premise of N, N-bis(1H-pyrrole-2yl)methylene naphthalene-2,3-diamine being a heterocyclic macro-cycle organic compound it was postulated that the macromolecule adopted a square-planar geometry.

4.3 Characterization of the iron ligand complex

4.3.1 Fourier Transform Infrared spectroscopy

FTIR analysis was performed on PerkinElmer spectrophotometer to record the infrared spectra of the monomer and starting materials in the range of 400 to 4000 cm^{-1}. A 4mg aliquot of iron ligand complex was mixed with dried KBr and compressed into a pellet with a PerkinElmer KBr pellet quick press

Table 11: FTIR bands relevant to iron ligand complex

Wavenumber, cm^{-1}	Assignment
3200	Pyrrole group
1630	Imine group
473	Metal nitrogen bond

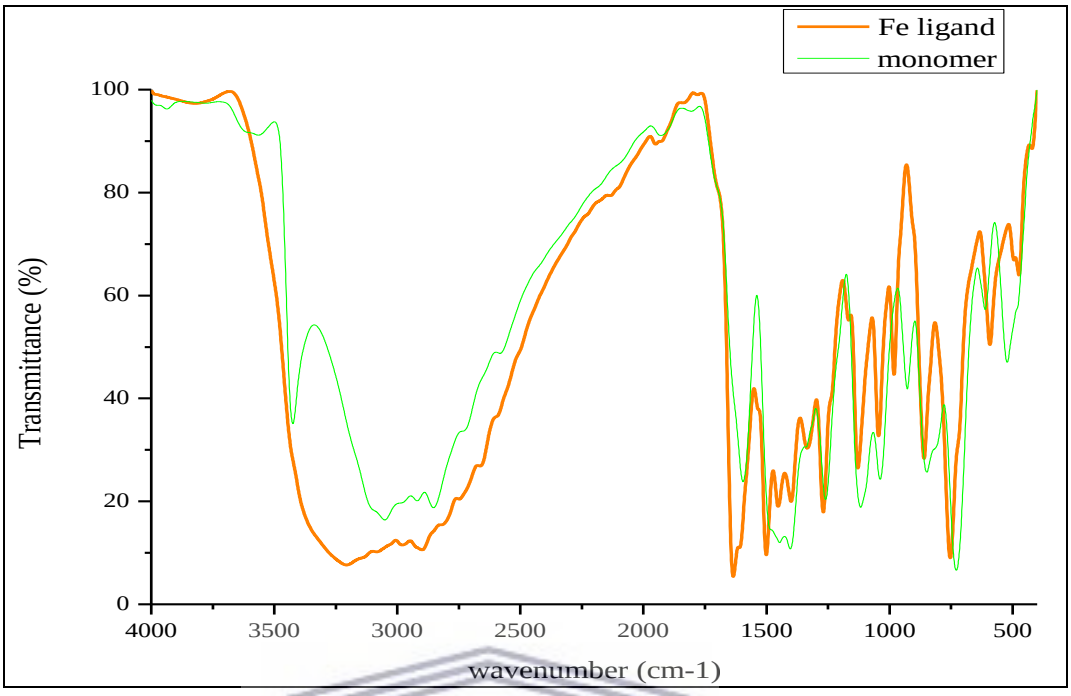

Figure 30: FTIR spectra of the Schiff-base and iron ligand complex in dried KBr

The infrared spectral data of the iron ligand complex is presented in Table 11. The spectra in figure 30 identified the characteristic stretch in vibration at 1630 cm^{-1} which was attributed to the imine bond. The spectra identified a shift in frequency for some bands and also identified a new band 473 cm^{-1} which was attributed to metal ligand complexation. This band was absent in the monomeric form. In the monomer the azomethine (imine bond) stretch in vibration was recorded at 1595 cm^{-1}. Therefore it can be assumed that the metal ligand coordination did not proceed via the imine linkage. According to literature a shift toward lower frequency would have been recorded if the iron complexed through the azomethine nitrogen[145146111]. However, a shift to higher frequency was recorded for the azomethine group at 1630 cm^{-1}. It was interpreted that the iron did not complex with the azomethine group and that complexation occurred at the pyrrole nitrogen. The broad peak at 3200 cm^{-1} was evidence that one of the pyrrole ring nitrogens was not coordinated to the iron[146].

4.3.2 Ultraviolet-visible absorbance

The UV-Vis spectrum of the iron ligand complex was measured and compared with the monomer N, N-bis(1H-pyrrole-2yl)methylene naphthalene-2,3-diamine. The UV-

Vis absorbance was measured on a Nicolet Evolution 100 UV-Vis spectrophotometer over the 200 to 900 nm spectral range with 10 mm pathlength Hellma absorption cuvettes, in ethanol at room temperature. The solubility limit of the iron ligand complex was established at 10 mg/ml in ethanol. This was used as the standard concentration for the materials and was diluted with ethanol in 10 graduated Plastic Eppindorf centrifuge tubes to concentration levels adequate for analysis. A serial dilution factor of 1:100 000 was used, DF = $\frac{1}{10} * \frac{1}{10} * \frac{1}{10} * \frac{1}{10} * \frac{1}{10} = \frac{1}{100000}$, the final concentrations were $\frac{10mg}{ml} * \frac{1}{100000} = 100\ \mu g/lt.$

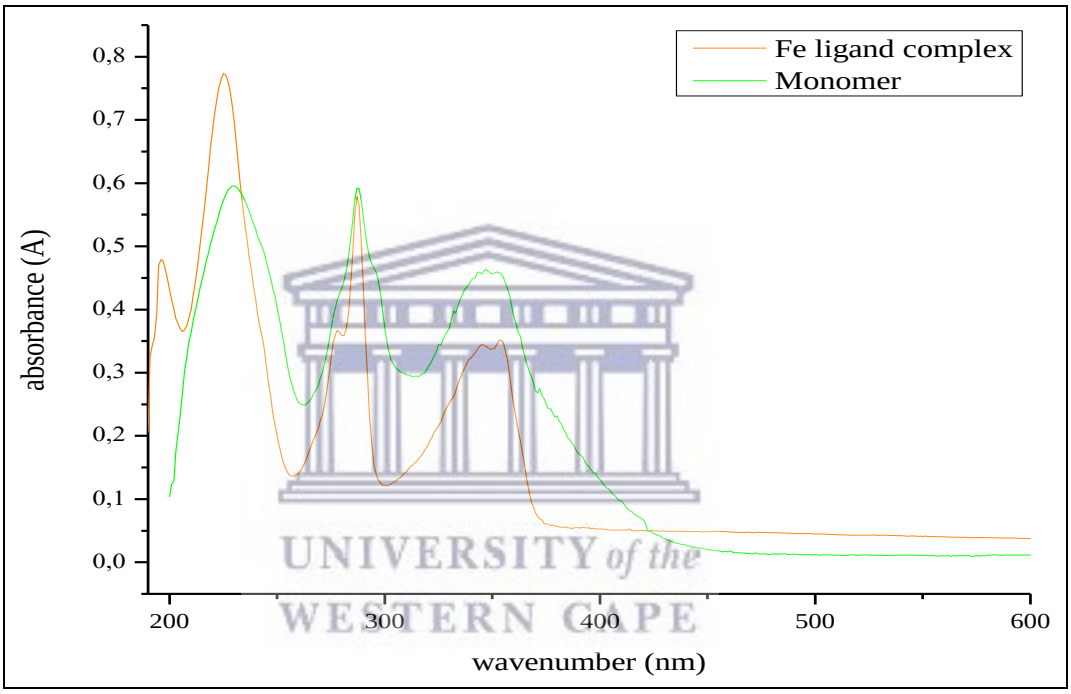

Figure 31: UV Visible spectra of the Schiff-base and iron ligand complex in ethanol 1 mg/ml 100x dilution

The UV spectra of the monomer and iron ligand complex is presented in figure 31. The iron ligand complex displayed three bands at 225, 287 and 350 nm. The bands at 225 nm and 287 nm can be attributed to the π-π* transitions in the aromatic rings of pyrrole and naphthalene. The absorption band at 350 nm can be attributed to the π-π* of the imine[124]. When the spectra of the iron ligand complex was compared to the monomer, a narrowing of the bands were evident. These changes could be attributed to the coordination with the iron. The spectrum identified weak absorbance above 400 nm which could be the d-d transitions of the metal but the intensity of the transitions were very weak[147].

4.3.3 Morphological characterization of iron ligand complex

The information on electron microscopy relating to the microscopes and techniques is contained in section 3.4.4. Metalloproteinase have been reported to catalyse nitric oxide electrochemically[148]. The presence of iron will substantiate the claims that the inhibitory effect was due to the interaction between nitric oxide and iron. The binding of nitric oxide to iron will be reflected by a change in the electrochemistry of the iron ligand complex. Electron microscopy was therefore performed to confirm the presence of iron in the iron ligand complex. High resolution images of the material was obtained using a new Field Emission Tecnai F20. High resolution SEM and EDS analysis were performed on a Zeiss Auriga EMU. These techniques provided high resolution images, up to the nanometer range, that provided detailed structural information about the compounds. The samples were prepared for analysis by sputter coating the compounds with carbon on copper grids.

Figure 32: TEM micrographs of (a) monomer, (b) $FeCl_2.4H_2O$, (c) Iron ligand complex

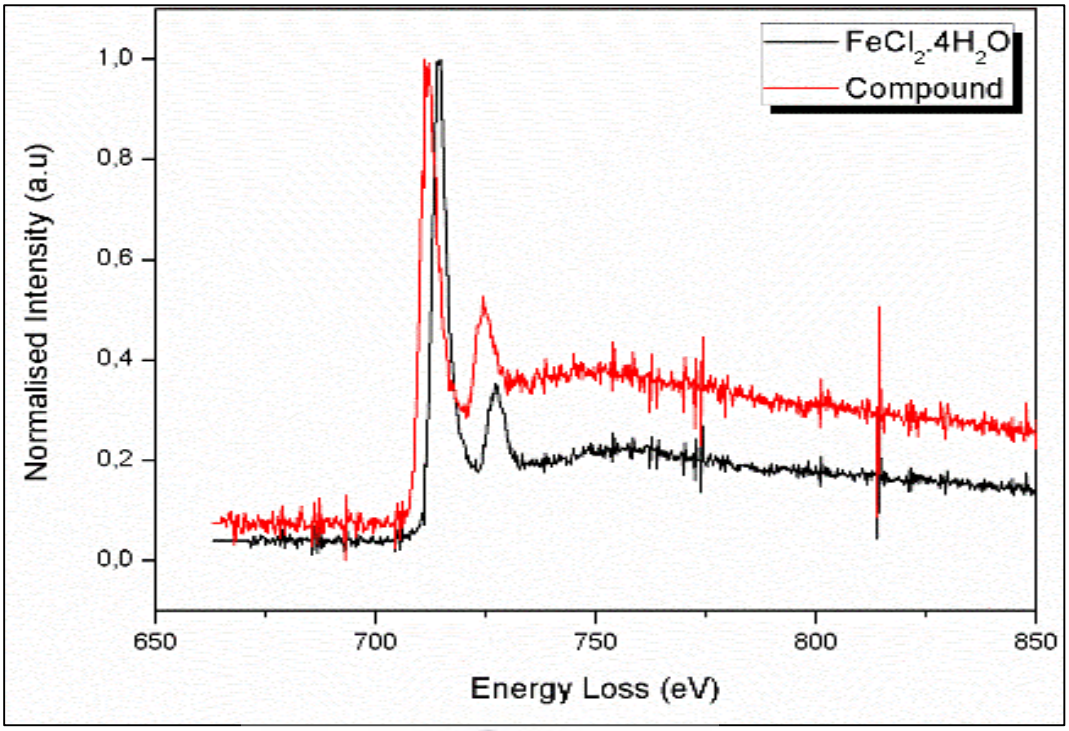

Figure 33: Electron Energy Loss Spectroscopy analysis of metal precursor $FeCl_2.4H_2O$ (black curve) vs. iron ligand complex (red curve)

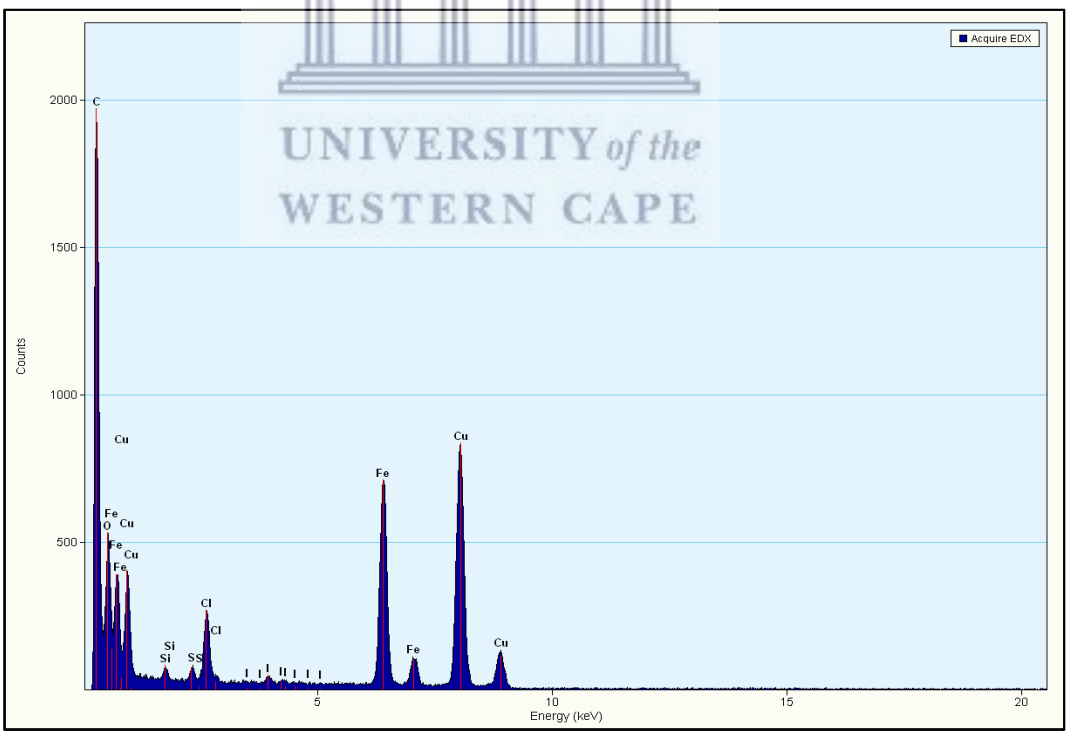

Figure 34: Energy-Dispersive X-ray Spectroscopic (EDS) analysis of iron ligand complex

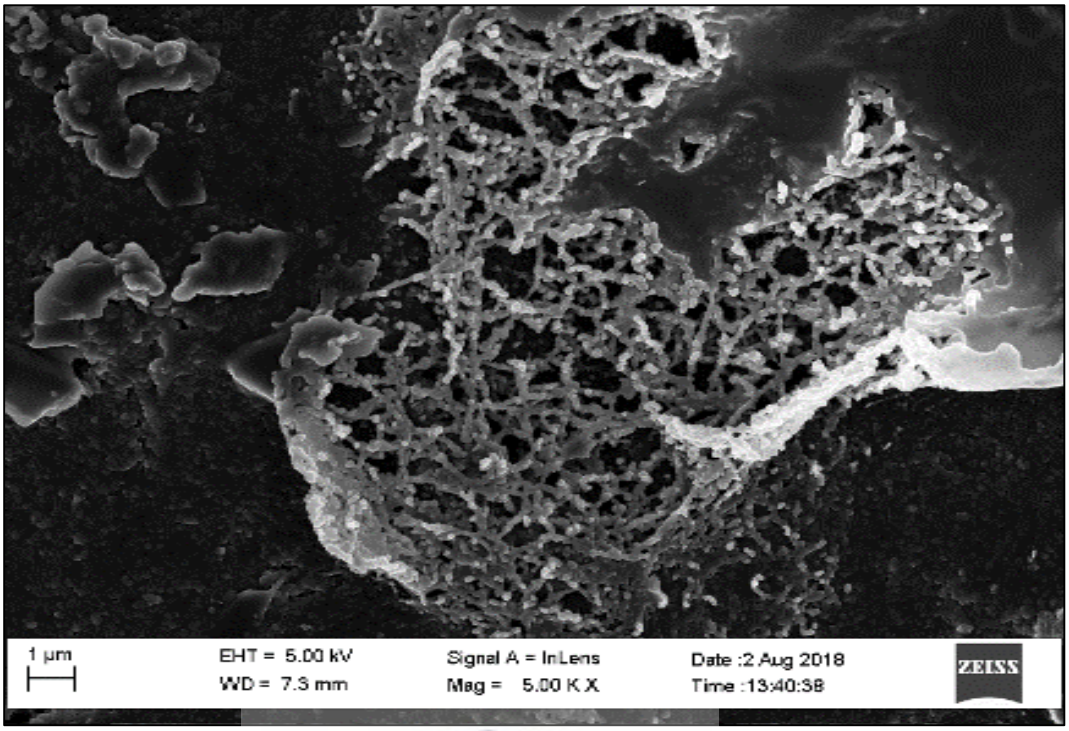

Figure 35: HRSEM of iron ligand complex electrodeposited on SPCE (sensor synthesis strategy C)

The electron microscopy results confirmed successful coordination of the iron to the monomer. In figure 32A, which depicts a high resolution image of the monomer (N, N-bis(1H-pyrrole-2yl)methylene naphthalene-2,3-diamine), a clear distinction can be drawn between the precursor $FeCl_2.4H_2O$ (32B) and the iron ligand complex (figure 32C). Structurally the monomer in figure 32A resembled rod shape morphology whereas in figure 32B the morphology appeared amorphous with the iron particles dispersed throughout. In Figure 32C on the other hand doping monomer with iron to form the iron ligand complex appeared to have altered the morphology of the complex yielding a highly structured morphology.

EDS analysis (see figure 34) was performed on the iron ligand complex to confirm the presence of iron in the complex. EDS provides an absolute measure over a focus area of which several measurements provides a relative measure of specific elements. For confirmation of successful coordination of iron to the monomer (N, N-bis(1H-pyrrole-2yl)methylene naphthalene-2,3-diamine) electron energy loss spectroscopy (EELS) was also performed on the iron ligand complex. Transition metals exhibit L3 and L2 edges which expresses the excitations of electrons from 2p to unfilled 3d orbitals. The orbital transitions are represented by ratios. Variations in L3/L2 intensity ratios are

related to changes to the electronic structure of the d orbitals. In order to monitor changes to the L3/L2 intensity ratios of the iron EELS was performed on iron ligand complex as well as the iron precursor (see figure 33). The EELS spectrum in figure 33 of the iron ligand complex on the other hand provided an absolute measurement of iron in the complex. On first glance there was shift in the peaks of the iron ligand complex and the precursor. Further analysis of the peak intensity revealed a change in the peak ratio. Changes to the peak ratios were an indication of a change in electron density surrounding the iron[149150]. Based on these two findings, coordination of iron to the monomer was confirmed. The results also revealed iron to remain in the Fe^{2+} oxidation state.

Figure 35 illustrates a high resolution image of the iron ligand complex, sensor fabrication strategy C, once electrodeposited on a SPCE.

4.4 Electrochemistry of the iron ligand complex (macromolecule)

In order to investigate the redox properties of the iron ligand complex cyclic and square wave voltammetry was performed on screen print carbon electrodes modified with the macromolecule. The electrodes were prepared as follows; 2 mM of the iron ligand complex was dissolved in 2 ml DMF and mixed with 2 ml of degassed 0.1 M $NaBF_4$ supporting electrolyte solution. The iron ligand complex was electrodeposited onto the SPCE using cyclic voltammetry. The parameters used were the same as that used in the electrochemical deposition of the monomer on to SPCEs. Electrochemical deposition was performed over a potential window of -1V to 1V and was cycled for 5 times at a scan rate of 50 mVs^{-1}. Cyclic and square wave voltammetry was performed by recording voltammograms over a potential window of -1 V to 1V, varying the scan rates from 0.010 Vs^{-1} to 0.500 Vs^{-1}. This provided insight into the electron transfer behaviour of the iron ligand complex.

Table 12: Cyclic voltammetric study of iron ligand redox couple

$\sqrt{scanrate}$	Scan Rate	Ip anodic	Potential	Ip cathodic	Potential	ΔE	E°'	$\frac{Ipa}{Ipc}$
3,162	10	1,066	-0,414	-1,954	-0,507	-0,093	-0,461	-0,546
4,472	20	3,688	-0,416	-7,909	-0,497	0,081	-0,457	-0,466
5,477	30	6,655	-0,406	-12,321	-0,492	0,086	-0,449	-0,540
6,325	40	9,464	-0,394	-13,76	-0,487	0,093	-0,441	-0,687
7,071	50	11,392	-0,38	-15,184	-0,477	0,097	-0,429	-0,750
10,0	100	22,665	-0,354	-25,257	-0,487	0,133	-0,421	-0,897

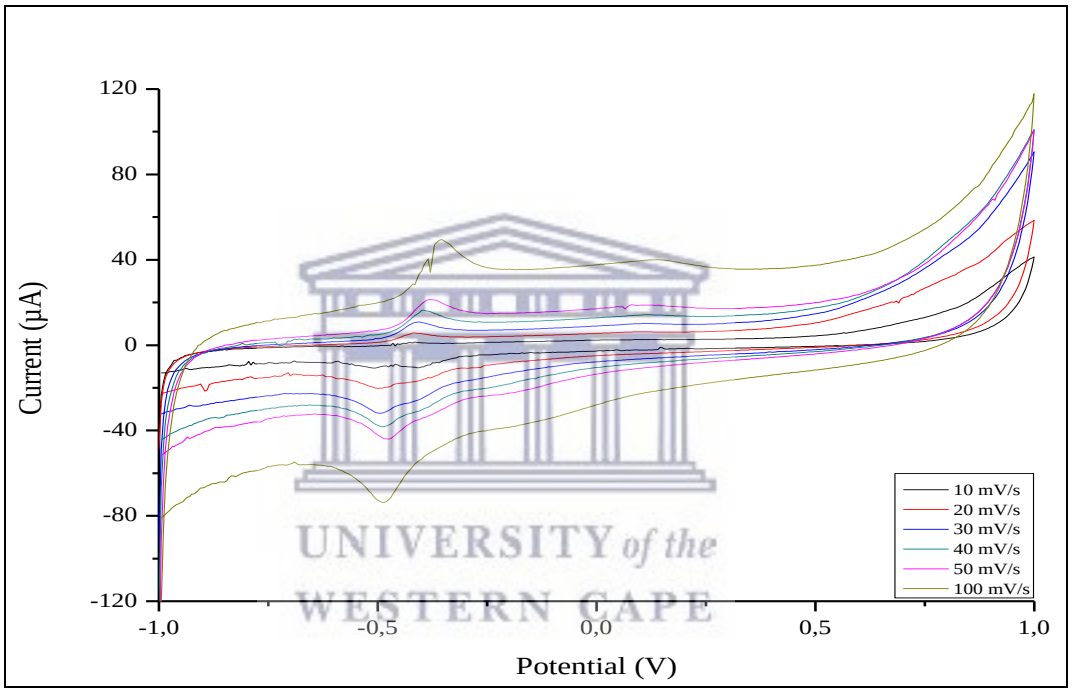

Figure 36: Cyclic voltammograms of iron ligand (sensor strategy C) modified SPCE vs Ag/AgCl, in 0.1 M PBS (pH = 7.1) at scan rates 10 - 100 mV/s

Cyclic voltammetry of the deposited iron ligand complex showed the system to be electroactive (see figure 36) in the electrochemical window between -1V to 1 V vs Ag/AgCl, where a well-defined redox couple was recorded at -0.429 V. Coordination of iron to the ligand system appeared to have shifted the potential at which oxidation and reduction occurred. Cyclic voltammetry of the iron ligand system identified electrochemical properties characteristic to reversible electrochemical systems. Investigation into redox properties of the iron ligand system revealed the redox system to be reversible. In the forward scan an anodic peak current was recorded at -0.414 V and cathodic peak current at -0.507 V in the reverse scan. The electron transfer

processes were associated with the redox processes of iron Fe^{2+} to Fe^{3+}. In both anodic and cathodic scans secondary redox processes were observed that might be interpreted as residual material being oxidized/reduced.

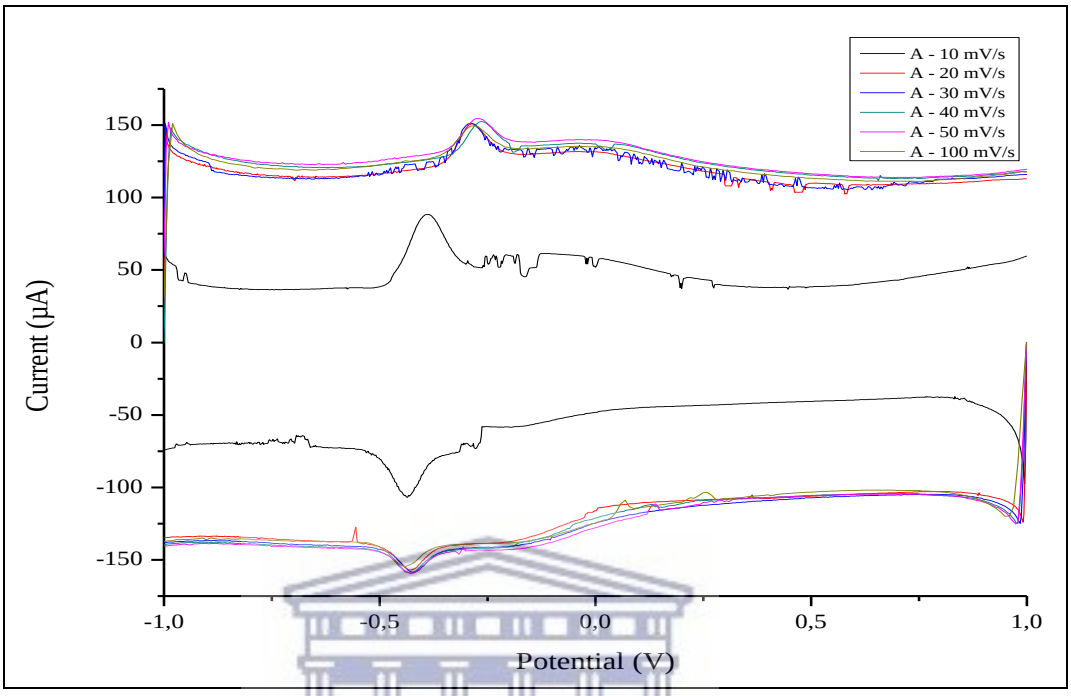

Figure 37: Square Wave Voltammograms of iron ligand (sensor strategy C) modified SPCE vs Ag/AgCl, in 0.1 M PBS (pH = 7.1) at scan rates 10 - 100 mV/s

A series of square wave analysis were performed on sensor strategy C (see figure 37). A two electron transfer process was observed. The primary peak displayed reversible redox chemistry whilst the secondary process displayed quasi-reversible electron transfer characteristics. However, as previously cited the secondary electron transfer process was attributed to non-ideal lateral interactions of the redox active groups.

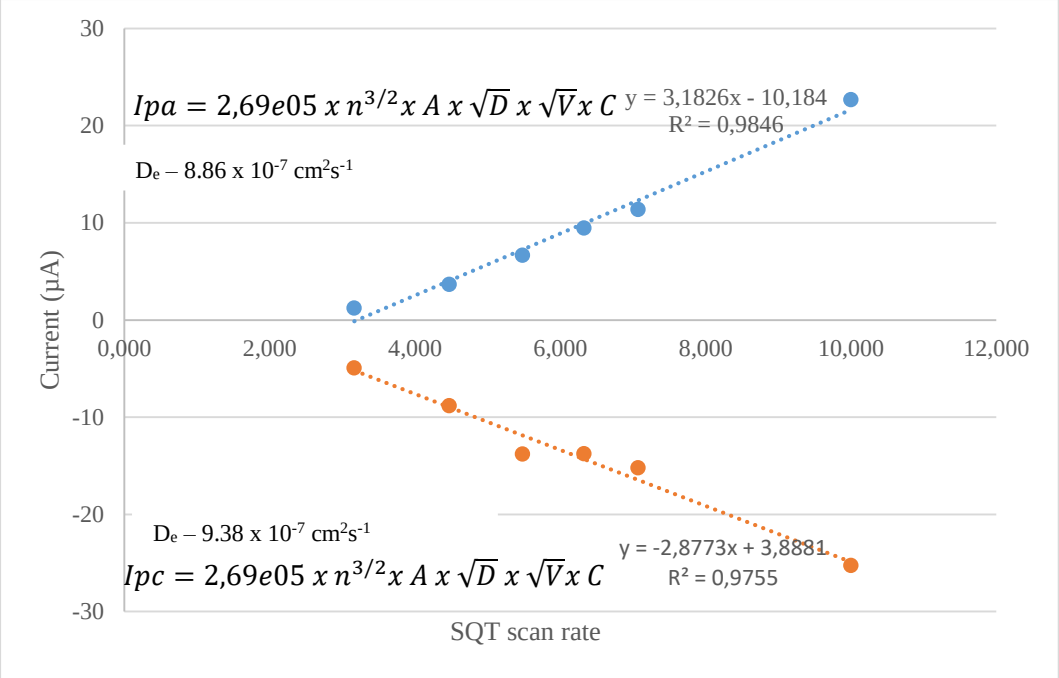

Figure 38: Randles-Sevcik plot of square root vs scan rate for sensor strategy C

The Randle-Sevcik equation was applied to investigate the electron transfer at sensor strategy C in figure 38. The Randles-Sevcik plots for the oxidation and reduction currents vs. square root of scan rates shows a linear relationship. Calculated peak current ratios, presented in table 12, suggested electron transfer of the redox couple to become reversible at higher scan rates. Diffusion coefficient values for sensor strategy C were 8.86 x 10^{-7} cm^2s^{-1} I_{pa}, and 9.38 x 10^{-7} cm^2s^{-1} I_{pc}. When compared to phenazine-2,3-diimino(pyrrole-2-yl) (PPDP), a similar type hinge system, doped with 1,4-naphtaquinone sulphonic acid (NQSA) and polyvinylsulfonic acid (PVSA) the diffusion rates were competitive. The following diffusion rate values for PPDP doped with NQSA were reported; D_e – 4.62 x 10^{-7} (I_{pa}) and D_e – 4.39 x 10^{-7} (I_{pc}). PDDP doped with PVSA on the other hand reported superior diffusion rates, D_e – 9.28 x 10^{-3} (I_{pa}) and D_e – 1.60 x 10^{-2} (I_{pc}). Reversible electron transfer was identified for sensor strategy C coupled with diffusion controlled electron transfer characteristics. This corresponds with reports by Zaheer et al., (2011) who investigated introduction of ferrocene moieties into Schiff bases. The compounds displayed mass transport characteristics controlled by diffusion[151]. De values of 2.66 x 10^{-5} cm^2/s were reported, diffusion coefficient values were found to decrease with molecular weight. Compared to De values calculated (see section 4.2.2) for the denatured cytochrome-c ligand

modified SPCE (sensor strategy B), 1.07 x 10^{-6} cm^2/s, electron transfer appears to be slower.

Sensor strategy A displayed non-reversible electrochemistry and was not considered for comparison. The secondary peak formation was attributed to non-ideal lateral interactions of the redox active iron groups[138].

4.5 Fe ligand complex stability

Biosensors convert biological responses into electrical signals. The function of the transducer membrane is to relay the interaction with the analyte, and to do so needs to be in contact with the electronic circuitry. The material is therefore deposited onto the electrode surface by conventional methods. Stability of the material deposited onto the SPCE is vital and is one of the key constraints of biosensors.

Concerns regarding the Fe stability chelated with the conductive membrane prompted the need for a stability assessment of the SPCE modified with the iron ligand complex. The objective of the test was to investigate if the iron leaches into solution once subjected to electrochemical currents. A stock solution of the iron ligand complex was prepared by dissolving 13.5 mg in 2 ml dimethyl formamide. From this solution a 1 ml aliquot was mixed with 1 ml of 0.1 M $NaBF_4$ supporting electrolyte to yield a 5 mM equivalent iron ligand solution. The solution was then dropcoated onto SPCE with adequate coverage of the working, reference and counter electrode area and inserted into a cylindrical glass cell. Cyclic voltammetry over a potential window of -0.600 to 0.700 V at a 50 mVs^{-1} scan rate was used and cycled 5 times to electrodeposit the Fe-Ligand complex. A similar process was used for the electrodeposition of the monomer onto the SPCE.

The stability of the iron ligand modified SPCE, within redox environments is important. Will the iron remain chelated to the ligand or leach under applied potentials. CV was performed on a 0.1M PBS solution using an iron ligand modified SPCE. CV analysis were conducted at three different scan rates 10 mV/s, 50 mV/s and 100 mV/s over the potential window -1 V to 1 V. Spectrometric analysis were conducted on the electrolyte solutions to identify possible leaching of iron into solution. This would be

a good indication of the stability of iron in the complex. This experiment was repeated two more times and subsequently labelled A, B and C.

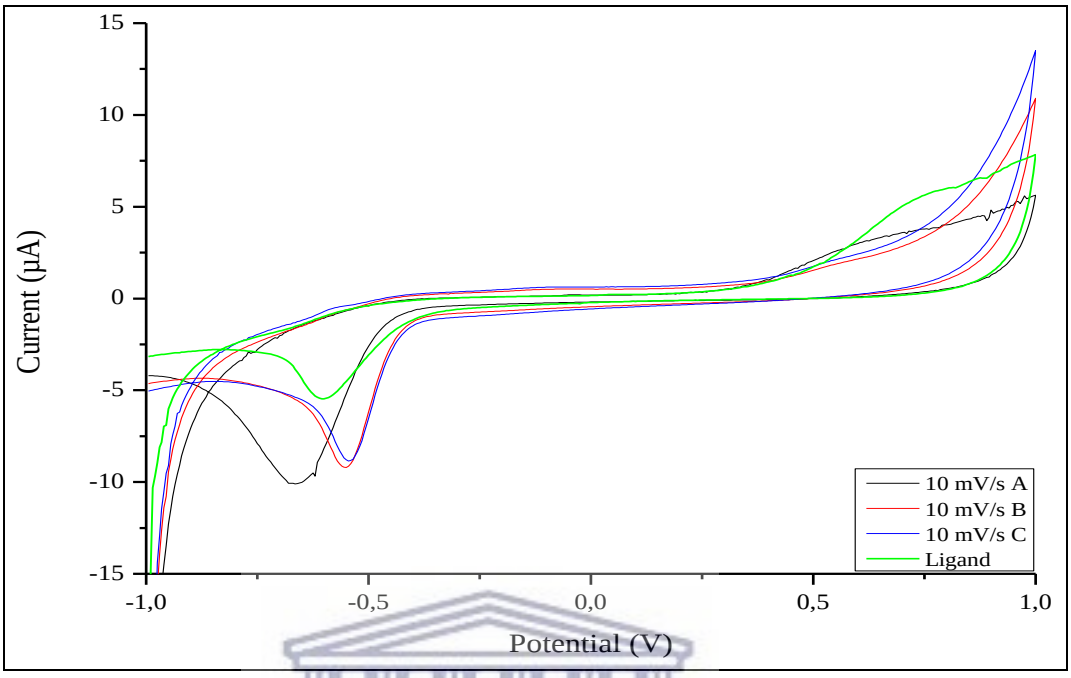

Figure 39: Cyclic voltammograms of iron ligand, sensor strategy C, modified SPCE and ligand modified SPCE in 0.1 M PBS vs Ag/AgCl at scan rate 10 mV/s

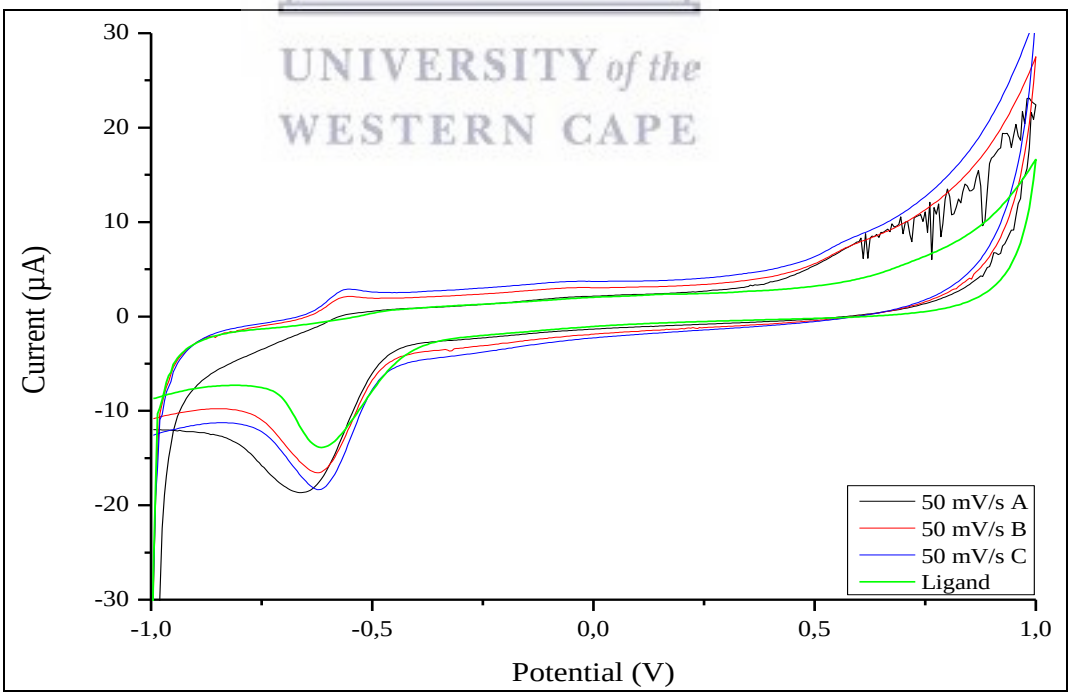

Figure 40: : Cyclic voltammograms of iron ligand, sensor strategy C, modified SPCE and ligand modified SPCE in 0.1 M PBS vs Ag/AgCl at scan rate 50 mV/s

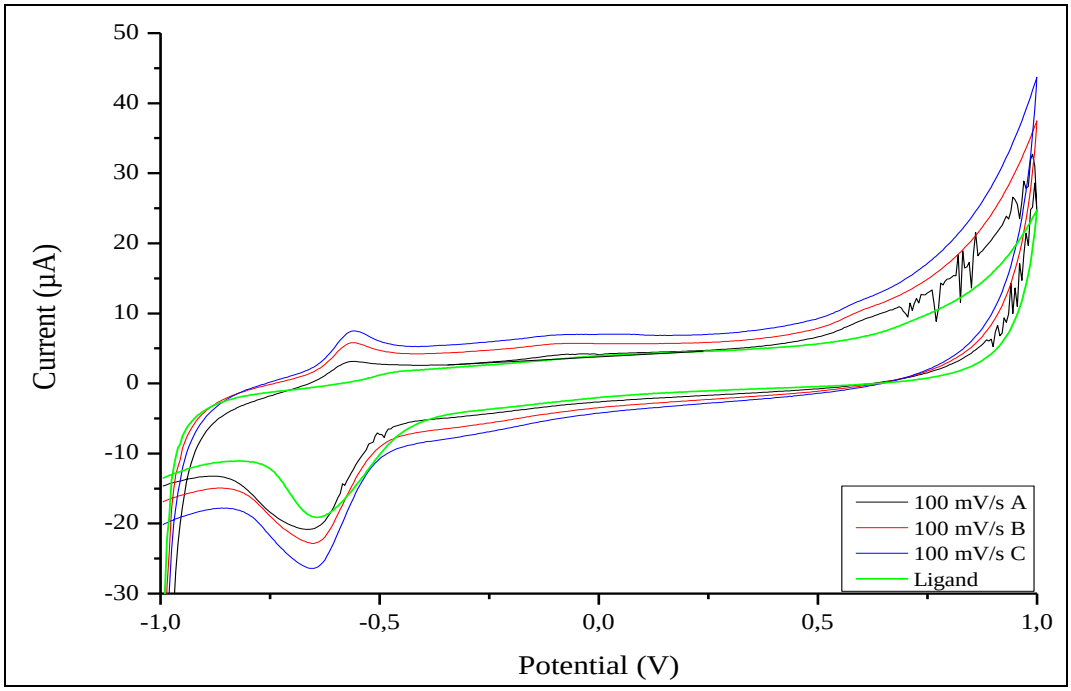

Figure 41: Cyclic voltammograms of iron ligand, sensor strategy C, modified SPCE and ligand modified SPCE in 0.1 M PBS vs Ag/AgCl at scan rate 100 mV/s

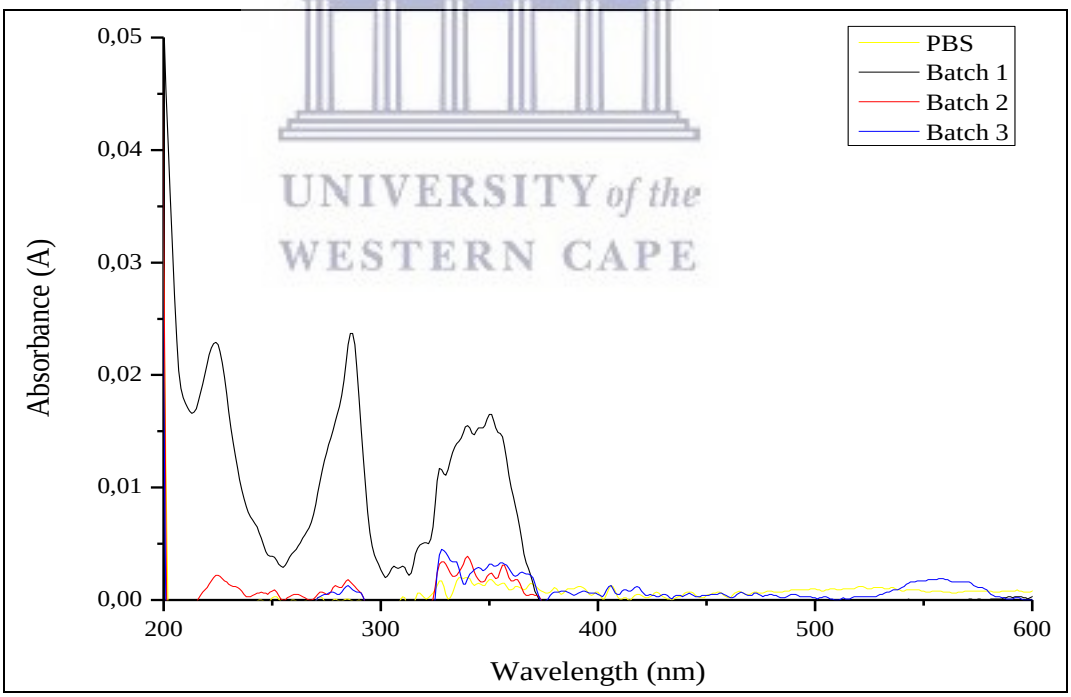

Figure 42: UV spectroscopic analysis of the electrolyte solutions to identify possible leaching of iron ligand complex into solution

Investigation into possible leaching of the material into solution appeared to be limited only to the initial electrochemical characterization (see figure 42). Although the UV

results indicated leaching of the iron ligand complex into solution, it was restricted to the initial scan. The UV spectra in figure 42 identified four bands. The first band was that of PBS (yellow), with a very noisy baseline. Batch 1 (black), where leaching was evident. The absorbance bands for the iron ligand complex can clearly be observed, albeit weak in intensity. However, in subsequent analysis no evidence of leaching could be observed. No changes were observed to the CV profiles of the iron ligand complex (see figures 39, 40 and 41). The leaching observed was therefore ascribed to residual material present on the electrode surface following preparation. It is safe to assume that the iron remains chelated to the Schiff base and does not particulate into iron under reduction and leach into solution.

Electrochemical analysis show no changes to the redox profile of the material. Oxidation and reduction potentials were reported as follows; reduction of iron Fe^{2} + $2e^{-} \longrightarrow Fe(s)$ at +0.44 V and oxidation of iron $Fe^{3+} + e^{-} \longrightarrow Fe^{2+}$ +0.77 V [152]. The redox potentials corresponded to values published in literature for iron. In figure 40 the CV for the ligand displayed passivating behaviour with an oxidation peak at 0.580 V, where electron transfer occurred on the initial scan. Subsequent scans showed electron transfer to be blocked at that potential for the ligand. This behaviour takes after claims by Mostany and Scharifker (1997) whom alluded to polypyrrole displaying insulating properties in its reduced state. Whereas oxidation of the polymer backbone endowed the polymer with electronic conductivity and changed its properties[153]. For the iron ligand complex there appeared to be evidence of electron transfer on all subsequent scans. Doping the ligand with iron appeared to mitigate the passivation observed in the ligand. This finding coincides with views published in an article by Wang et al., (2017) whom stated highly conjugated polymer chains can be endowed with reversible electrochemical properties by doping[154]. Examining the redox behaviour in figures 39 to 41 the ligand displayed a weak oxidation peak and a strong reduction peak. On the other hand the iron ligand complex displayed a modified voltammetric response when the potential was swept from -1 V to 1 V. Three oxidation peaks (-0.560 V, -0.075 V and 0.600 V) and two reduction peaks (-0.660 V and -0.320 V) was observed. The peak observed at -0.560 V could possibly be assigned to the oxidation process of Fe^{2+} to Fe^{3+} [152]. The shift in potential could be a result of the metal chelating with the ligand. The voltammograms showed increased current density response which can be attributed to increased roughness[155].

Chapter 5

5. Detection studies

The following section is an attempt at improving NO detection and discriminating against interfering analyte NO_2^-. The analytical performance of sensor strategy B, denatured cytochrome-c sensor, and sensor strategy C, iron ligand complex sensor, for the detection of NO will be assessed. Sensor strategy A was excluded from DEANONOate studies in phosphate buffer solution (PBS) based on the electrochemical analysis of the sensor. The scope of this chapter is therefore limited to the electrochemical analysis, by cyclic voltammetry, of nitric oxide at the iron ligand complex modified electrodes, in PBS.

5.1 Preparation of NO standards

Since NO's discovery as a biological signalling molecule many donor molecules have been synthesized. These donor molecules all possess different physical and chemical properties as well as reactivity. Each of these properties influence the *in vitro* and *in vivo* deliverance in various biological systems. The past decade has seen the development of diazeniumdiolates also referred to as NONOates. Diethylamine NONOates (DEANONOate) spontaneously hydrolyses to physiological regulating radical nitric oxide when dissolved in aqueous media. These compounds decompose in a 2:1 stoichiometric fashion which is dependent on the pH of the solution and temperature, as this strongly influences the half-life[156].

The commercial DEANONOate was dissolved in 0.1 M NaOH to prevent spontaneous decomposition of the diethylammonium salt to produce a 50 mM parent stock solution. This parent stock solution was split over 10 vials each containing 100 µl aliquots of

the donor. On the day 0.5 mM and 0.05 mM sample aliquots of DEANONOate were prepared from a 50 mM stock solution. DEANONOate dissociate in a 2:1 ratio producing 2 mole of nitric oxide per mole of NONOate.

$$[RNONO]^- + H_3O^+ \longrightarrow {}_{\nu NO}NO^{\cdot} + RH + H_2O \qquad (5.1)$$

DEANONOate dissociates into nitric oxide and the parent amine as per (eq) 5.1. The decomposition process has been reported to be spontaneous and acid catalysed[157].

5.2 UV measurement of DEANONOate decomposition

DEANONOate are nitric oxide donor compounds that are stable in alkaline solutions but readily decomposes in neutral or acidic conditions. Decomposition of DEANONOate can be observed by changes in the UV absorption bands. Therefore, to evaluate the NO donor capability of DEANONOate UV measurements were performed over the 200 to 400 nm ultraviolet wavelength range. The decomposition of the donor was illustrated by DEANONOate absorbance which was a reflectance of the transient nitric oxide concentration. The released nitric oxide reacted with molecular oxygen to produce nitrite as illustrated in the equations below[158].

$$4\,NO^{\cdot} + O_2 + 2H_2O \longrightarrow 4\,NO_2^- + 4H^+ \qquad (5.2)$$

The release of NO was associated with a decrease in DEANONOate absorbance, which was also reported to be time-dependant[159]. A total of eight 5 mM aliquots of DEANONOate were injected intermittently into 3 ml of PBS and subsequently characterized to validate the NO release rate. In a second study the time dependent decomposition of 5 µM DEANONOate in 3 ml 0.1 M PBS was assessed at 2 minute intervals. The 2 minute intervals were based on the half-life of the donor. Decomposition of the sample was allowed to proceed under aerobic conditions.

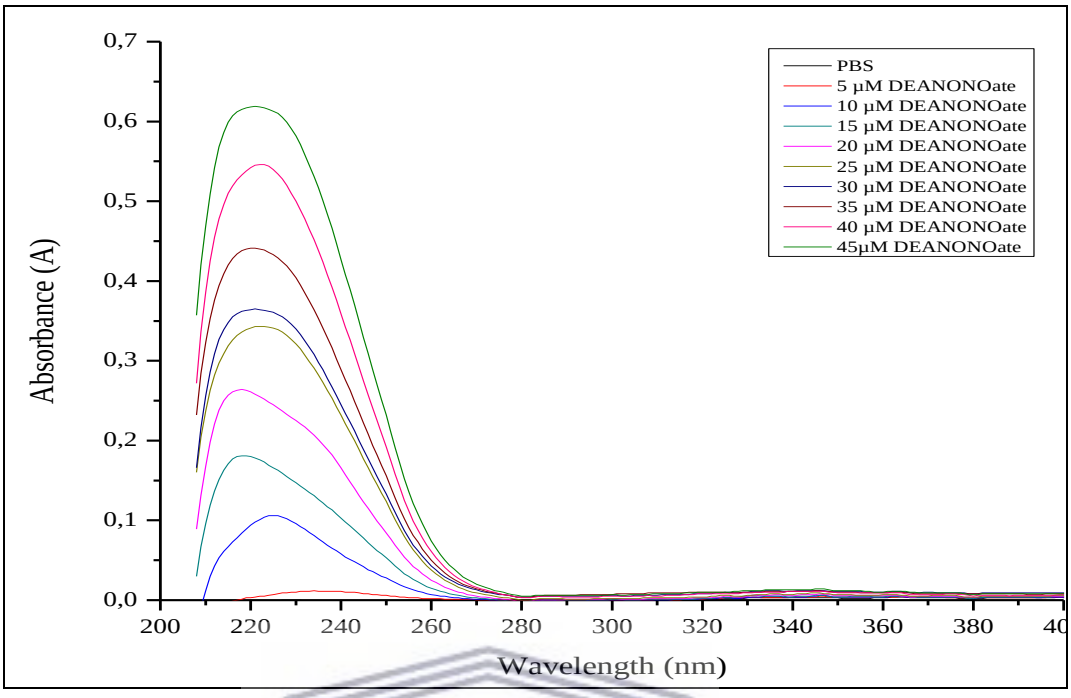

Figure 43: UV absorbance of nitric oxide donor DEANONOate in PBS illustrating the activity of the donor at concentrations ranging between 5 and 45 µM

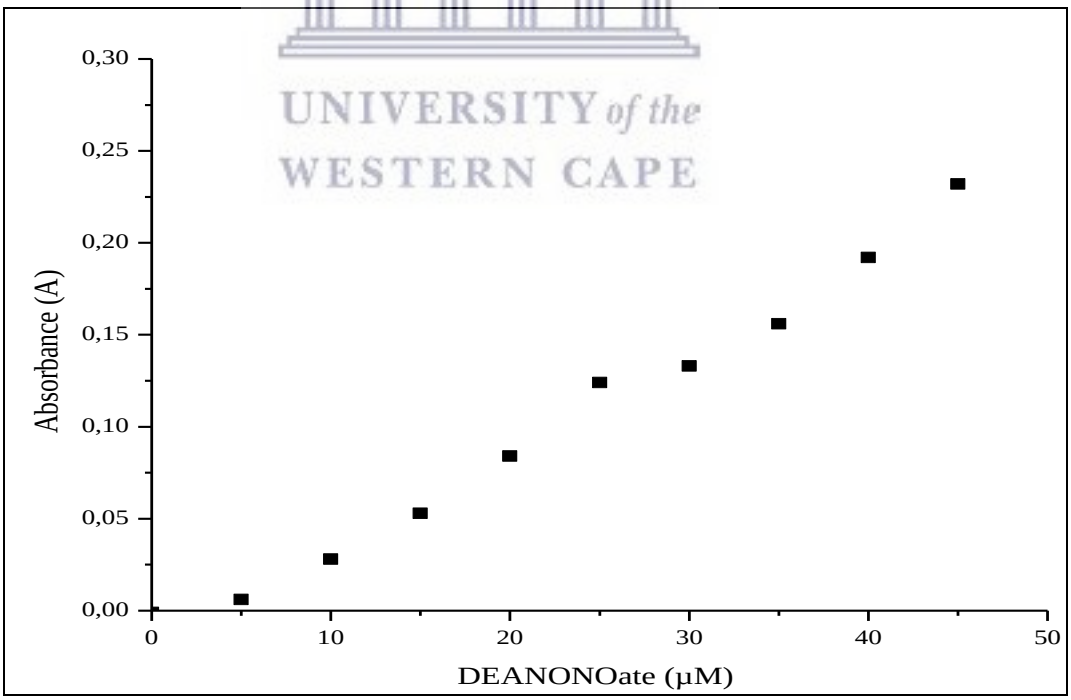

Figure 44: UV absorbance of DEANONOate at 250 nm in PBS to measure donor activity

Figure 43 illustrates the effect of concentration on the absorbance of DEANONOate. The compounding of the donor resulted in an increase in absorbance which was proportional to concentration illustrated in figure 44. However, at the 30 µM mark a change in trend of the slope was observed. However, subsequent additions of DEANONOate saw a continuation in the linear relationship between concentration and absorbance. This phenomena was ascribed to the half-life of DEANONOate, which was reported by Griveau, Dumézy, Goldner and Bedioui (2007) to be 2 minutes at 37^{o}C. The time between each injection was approximately two minutes on account of the range of the scan. And at the 30 µM a total time of ten minutes had lapsed. This experiment was used to determine the ideal time for the initial spontaneous dissociation of DEANONOate.

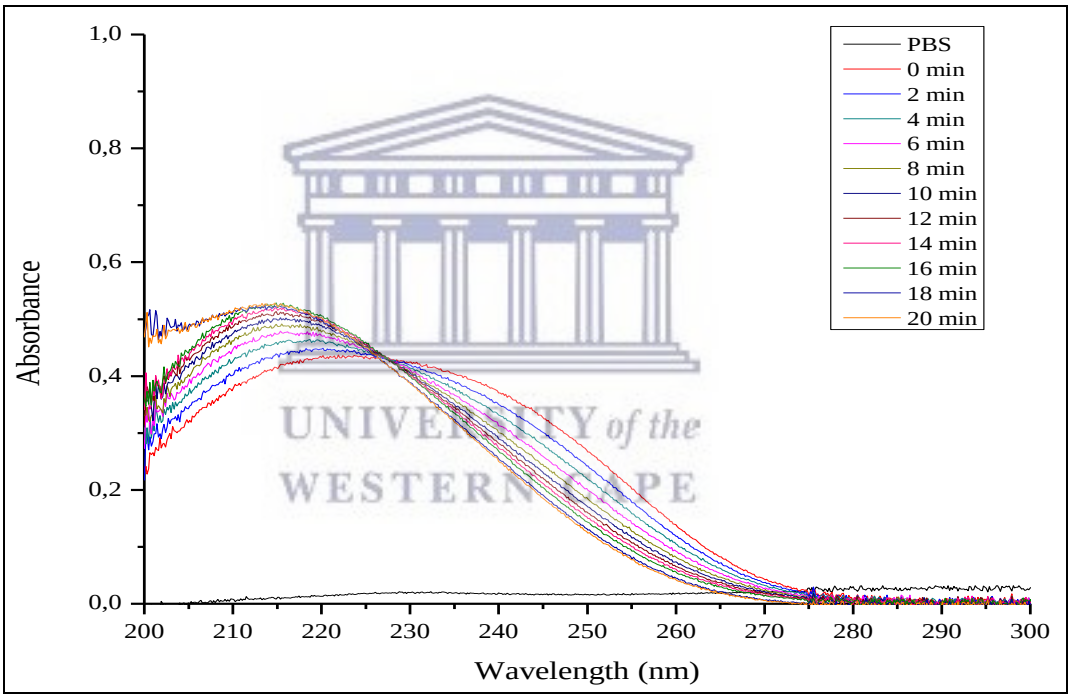

Figure 45: UV absorbance of 5 µM DEANONOate in 0.1 M PBS illustrating the decomposition of the NO donor over time

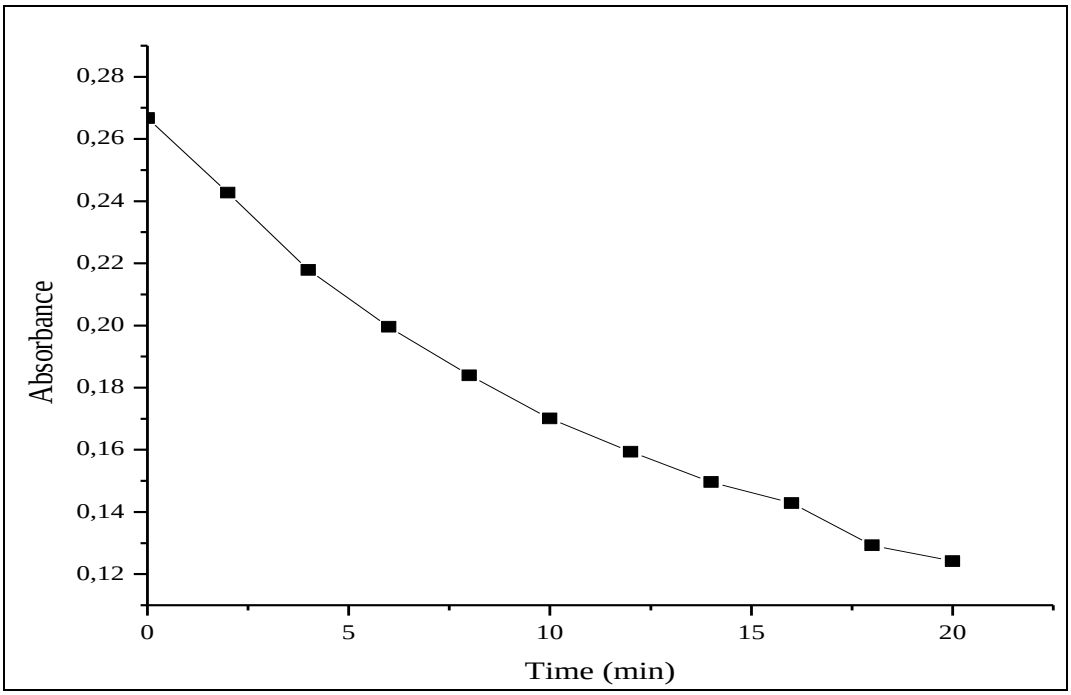

Figure 46: UV absorbance of time dependent decomposition of DEANONOate

Figure 45 illustrates the time dependent decomposition of DEANONOate in solution. A phosphate buffer solution containing 5 µM of DEANONOate was analysed over period of 20 minutes to investigate the decomposition of DEANONOate over time. Phosphate buffer (0.1 M) was used to initiate the decomposition of DEANONOate. The decomposition of DEANONOate is plotted in figure 46 and illustrates the decrease in absorbance over time at 250 nm. UV absorbance was measured at two minute intervals. The decay in UV absorbance corresponded with reports in literature[158].

The experiments were conducted on the commercial NO donor, DEANONOate. Up till now the experiments were preliminary to establish the ideal decomposition time that would allow for maximum NO formation. NO has a short lifespan before it spontaneously converts to NO_2. Timing was therefore vital and had to be established before commencing DEANONOate studies with sensor strategies B and C, as described in section 4.2. The decomposition of DEANONOate was calculated over time at 2 minute (120s) intervals. This was achieved by using the absorbance data from figure 46 which correlated decaying absorbance to concentration at given time intervals through Beer-Lamberts Law, A= Ɛ.c.l. The decomposition of DEANONOate was reported to follow first order kinetics. The reported stoichiometric ratios

[DEANONOate:NO] were 1:1.5 and decomposition kinetics k =12.9 x 10^{-4} at 250 nm at room temperature.

Table 13: Absorbance vs. concentration over time for DEANONOate and NO at 250 nm

Time (s)	DEANONOate Concentration	Absorbance	NO concentration
120	4,54919E-06	0,24269	4,69476E-07
240	4,08263E-06	0,2178	8,42654E-07
360	3,74053E-06	0,19955	1,15807E-06
480	3,44811E-06	0,18395	1,42338E-06
600	3,18831E-06	0,17009	1,64517E-06
720	2,98624E-06	0,15931	1,84908E-06
840	2,80479E-06	0,14963	2,02618E-06
960	2,6777E-06	0,14285	2,21071E-06
1080	2,42352E-06	0,12929	2,25097E-06
1200	2,32699E-06	0,12414	2,40145E-06

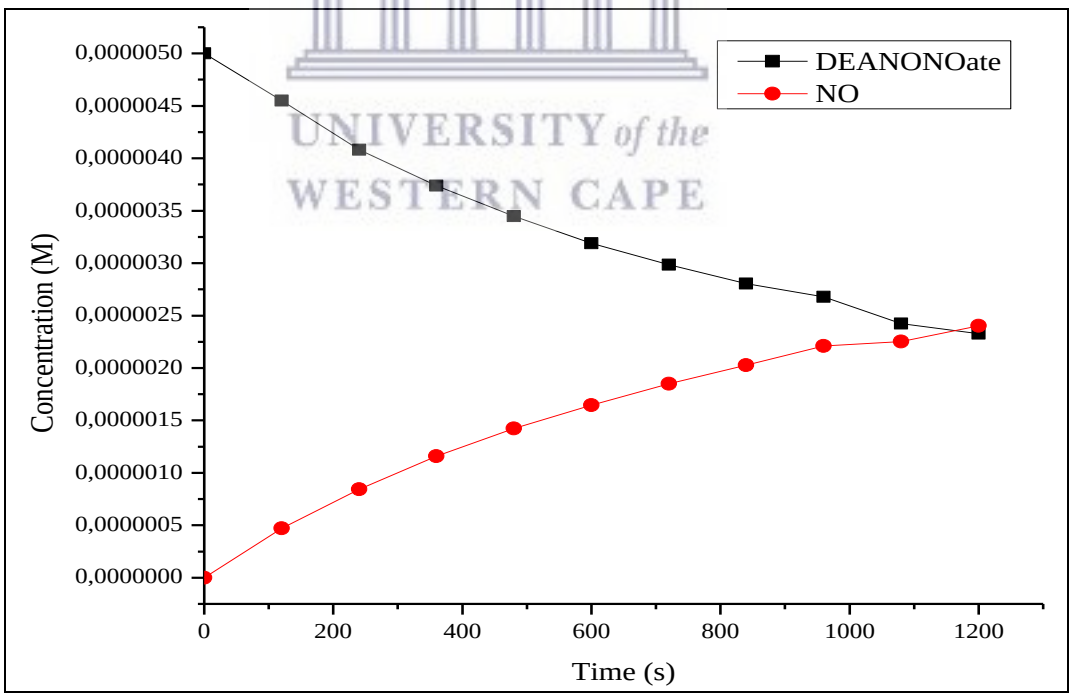

Figure 47: DEANONOate decomposition (black line) and nitric oxide formation (red line) over time in 0.1 M PBS

Figure 47 illustrates the nitric oxide formation as a function of DEANONOate dissociation in PBS over 120s intervals. It is evident that NO formation reduced overtime, and that the highest rate of nitric oxide formation was at the initial concentration of DEANONOate. At 600s the dissociation of DEANONOate and production of NO was the highest. Thereafter the amount of NO produced over 120s reduced. By virtue of these findings, and considering NO's fleeting existence, a 600s decomposition time was selected.

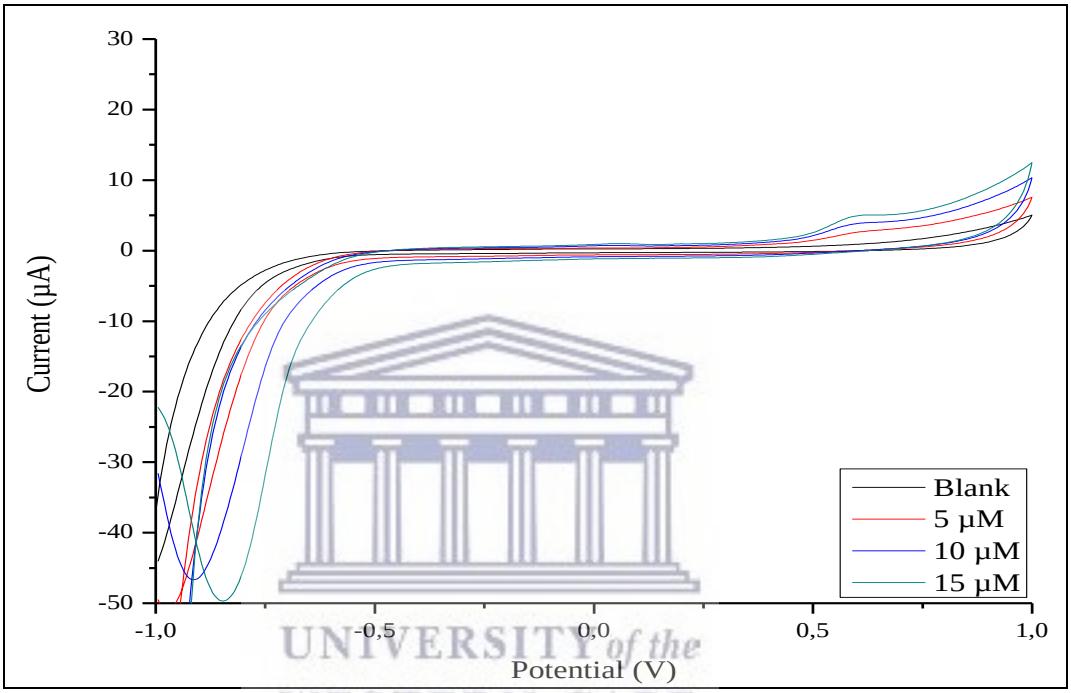

Figure 48: Cyclic Voltammograms of DEANONOate dissociation in 0.1M PBS with SPCE vs Ag/AgCl at a scan rate of 50 mV/s

Figure 48 shows the electrochemical behaviour of DEANONOate at different concentrations on blank SPCE. Three 5µM aliquots of DEANONOate was injected into 8 ml PBS. The anodic current recorded at ~0.610 V for DEANONOate was assigned to nitric oxide oxidation. The growth in the anodic peak current recorded at 0.610 V indicated an increase in NO production.

The aim of these experiments were to establish baseline redox profiles for both DEANONOate and $NaNO_2$ on screen printed carbon electrodes in 0.1 M PBS.

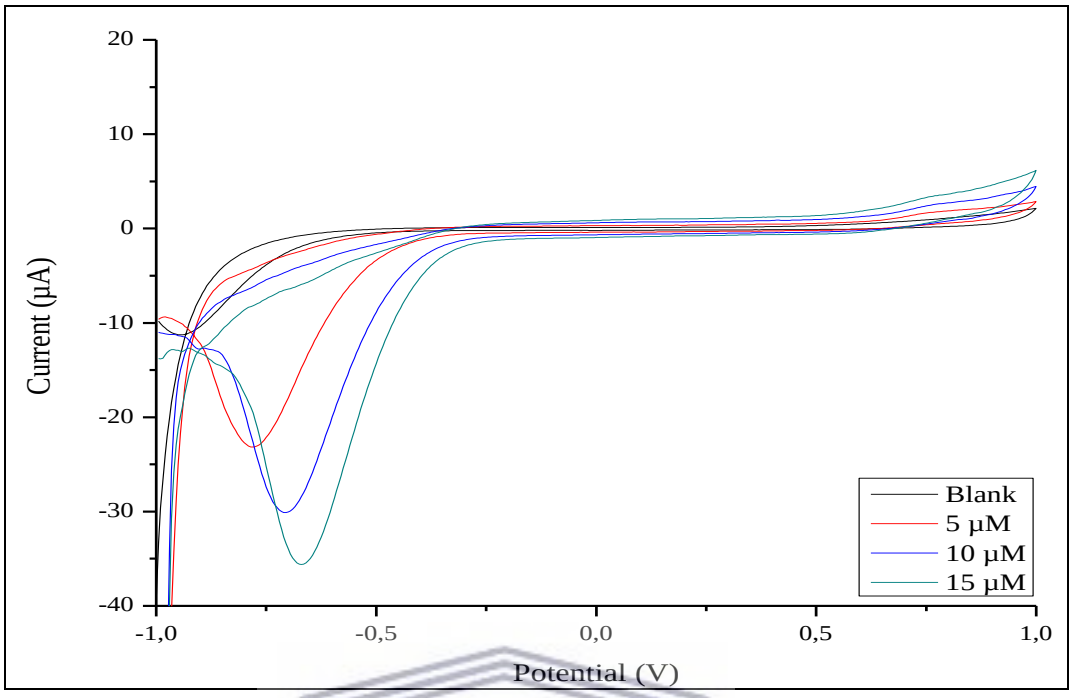

Figure 49: Cyclic Voltammograms of $NaNO_2$ in 0.1M PBS with SPCE vs Ag/AgCl at a scan rate of 50 mV/s

In figure 49 the redox behaviour of $NaNO_2$ is illustrated over the potential range -1V to 1V. An anodic current was recorded at ~0.770 V which increased with $NaNO_2$ concentration. The oxidation process recorded in figure 49 for $NaNO_2$ was assigned to the oxidation of nitrite ions to nitrogen dioxide gas (see eq 5.3)[160]. In all media the oxidation of nitrite is believed to proceed by the formation of nitrogen dioxide gas (NO_2)[161].

$$NO_2^- \longrightarrow NO_2\,(g) + e^- \qquad (5.3)$$

5. 3 Electrochemical detection of nitrogen dioxide with sensor strategy B and C

From (eq) 5.3 nitrite ions form nitrogen gas when it undergoes oxidation, however this is dependent on the media it is in[160]. The electrochemical behaviour of $NaNO_2$ was assessed by injecting 10 µM aliquots of $NaNO_2$ into 8 ml PBS. The experiment was conducted by running CV over the potential window -1 V to 1 V recording the current response after each injection. This procedure was followed for sensor synthesis strategy B and C to model and assess the redox behaviour of the sensors in the presence of nitrite ions.

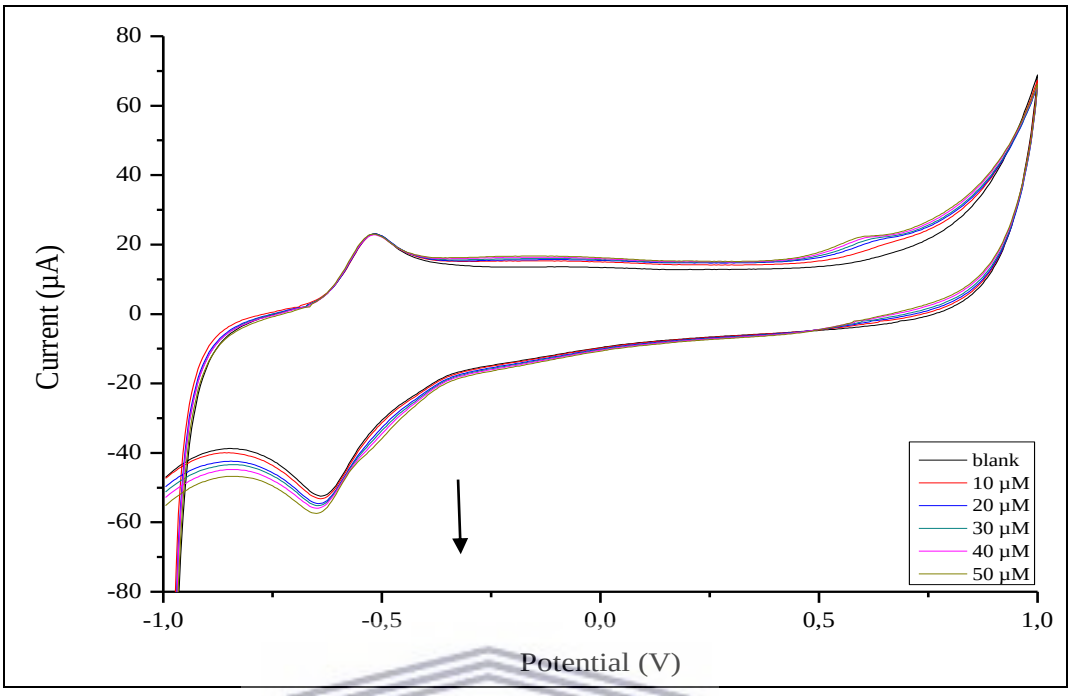

Figure 50: Cyclic voltammograms illustrating the electrochemical response of denatured cytochrome-c, sensor strategy B, deposited on modified SPCE, to $NaNO_2$ in 0.1M PBS vs Ag/AgCl at 50 mV/s

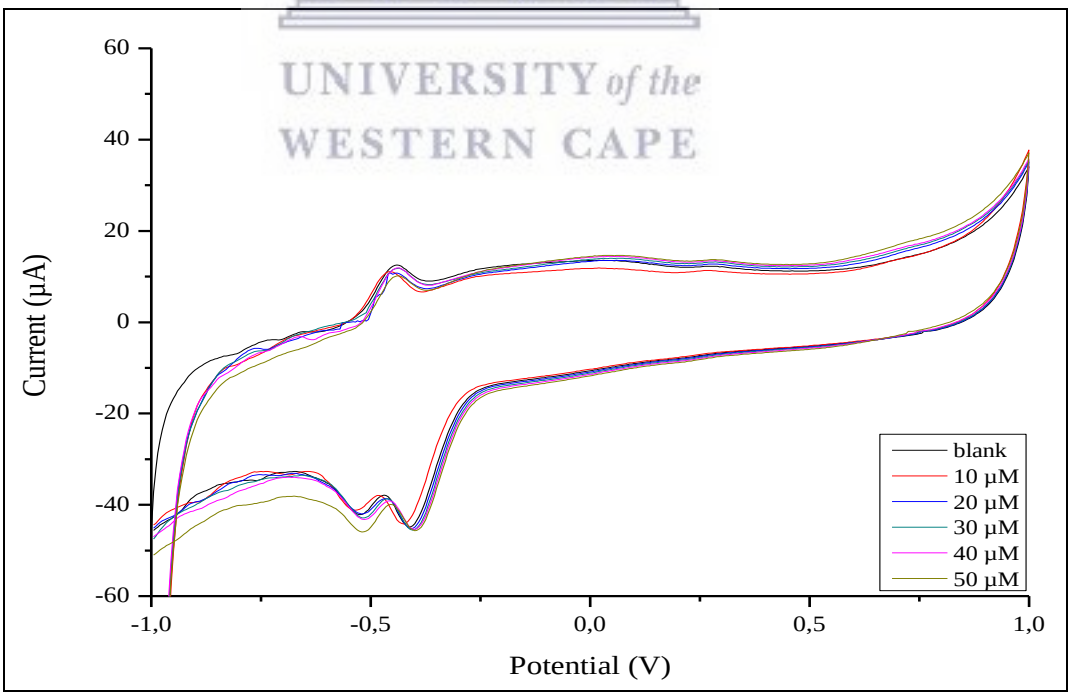

Figure 51: Cyclic voltammograms illustrating the electrochemical response of iron ligand, sensor strategy C, modified SPCE, to $NaNO_2$ in 0.1M PBS vs Ag/AgCl at 50 mV/s

In figure 50 the electrochemical oxidation of $NaNO_2$ was recorded at different concentrations for sensor strategy B in PBS. Analysis of the CV recorded in figure 50 identified negligible interference by the nitrite ions on the anodic iron peak at ~ -0.500 V for sensor strategy B. An anodic current was however recorded at ~0.650 V that increased with concentration. A shift in the anodic peak potential was also observed. At 10 µM an oxidation potential for $NaNO_2$ was recorded ~ 0.650 V, at 50 µM the oxidation potential shifted down to 0.600 V. This was attributed to catalytic activity of denatured cytochrome-c for nitrite (NO_2^-) oxidation to nitrate (NO_3^-)[162]. The oxidation process was preceded by the reduction of the heme illustrated in figure 50 by an increase in the cathodic current. The catalytic oxidation process of nitrite to nitrate is as follows;

Cyt-c Fe(II) $\longrightarrow$ cyt-c Fe(III) + e^-

Cyt-c Fe(III) $\longrightarrow$ $[\text{cyt-c Fe(IV)}^+]^{\cdot}$ + $2e^-$

$[\text{cyt-c Fe(IV)}^+]^{\cdot}$ + NO_2^- + H_2O $\longrightarrow$ cyt-c Fe(III) + NO_3^- + $2H^+$ [162]

As the analyte concentration increased at the electrode surface the critical potential required to induce oxidation (flow of electrons) decreased. In sensor strategy C catalytic oxidation of NO_2^- was observed. In figure 51 an anodic current was recorded at 0.720 V though weak. A positive correlation was observed between the anodic current response and $NaNO_2$ concentration. At low concentrations the electrochemical oxidation appeared restricted. An increased basal concentration was required. This was assigned to the oxidation of nitrite ions to nitrogen dioxide gas (see eq 5.3)[160]. Subsequently as the concentration increased an increase in the anodic current was recorded. This was complemented by an increased cathodic current at -0.520 V and a reduction in the cathodic current recorded at -0.400 V.

5.4 Electroanalytical detection of nitric oxide with sensor strategies B and C

In the next set of experiments the effect of DEANONOate decomposition on the electrochemistry of sensor synthesis strategy B was investigated. The behaviour of nitric oxide was modelled with the nitric oxide donor DEANONOate which dissociated into nitric oxide and the parent amine (see eq 5.1). Nitric oxide in its free form is highly reactive in biological systems and is converted to nitrite and nitrates in

water in the presence of oxygen. It also reacts rapidly with radicals such as superoxides O_2^-, peroxynitrite and has been reported to react rapidly with heme proteins[163]. Nitric oxide forms a powerful ligand to metal ions and binds much stronger than CO and O_2. It's the understanding that under bioregulatory conditions nitric oxides specifically target metal centres[164].

Cyclic voltammetry was performed to investigate the electrochemical response of sensor strategy B and C to DEANONOate decomposition in PBS (see figure 52). 5 µM aliquots of DEANONOate was injected into an electrochemical cell containing 8 ml of PBS (pH 7.1) electrolyte. The dissociation of DEANONOate was allowed to continue for 10 minutes (600s). Cyclic voltammetry was subsequently performed on the solution over the potential window of -1V to 1 V with a scan rate of 50 mVs^{-1}. The experiment was concluded after five injections of 5 µM DEANONOate aliquots. The study was done in triplicate. At the beginning of the experiment a current was cycled over the potential window -1V to 1V several times until a stabilized current response was achieved.

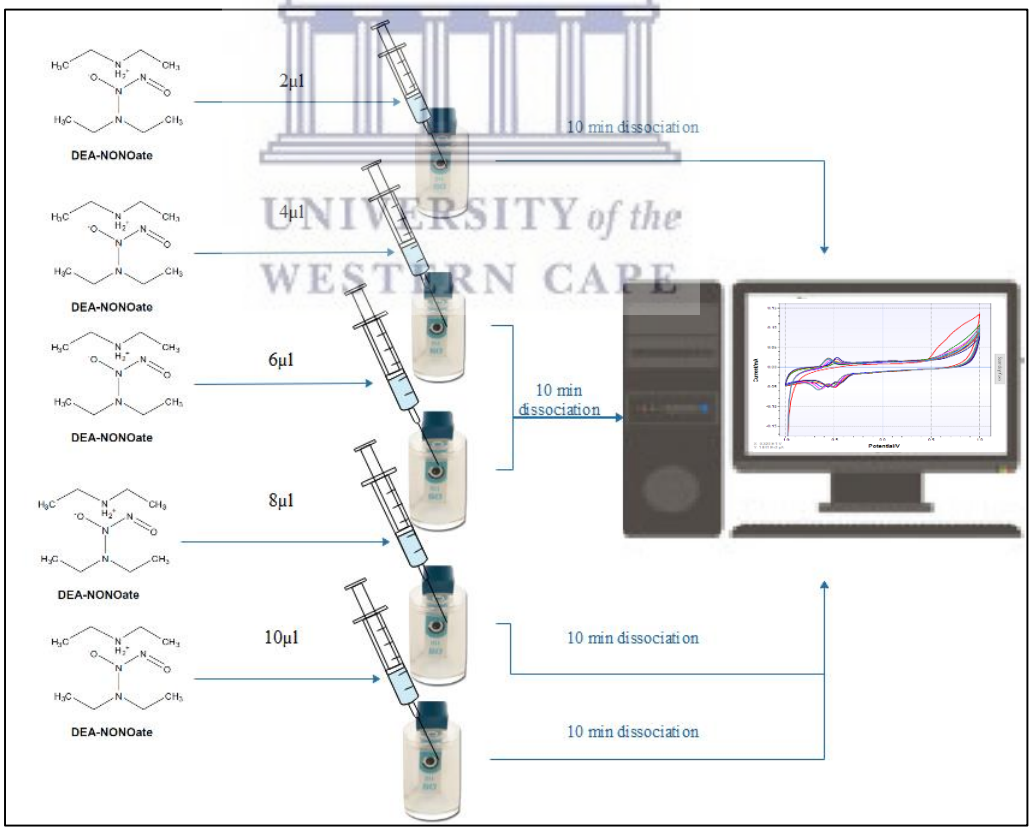

Figure 52: Cyclic voltammetric study of DEANONOate dissociation in 0.1M in PBS

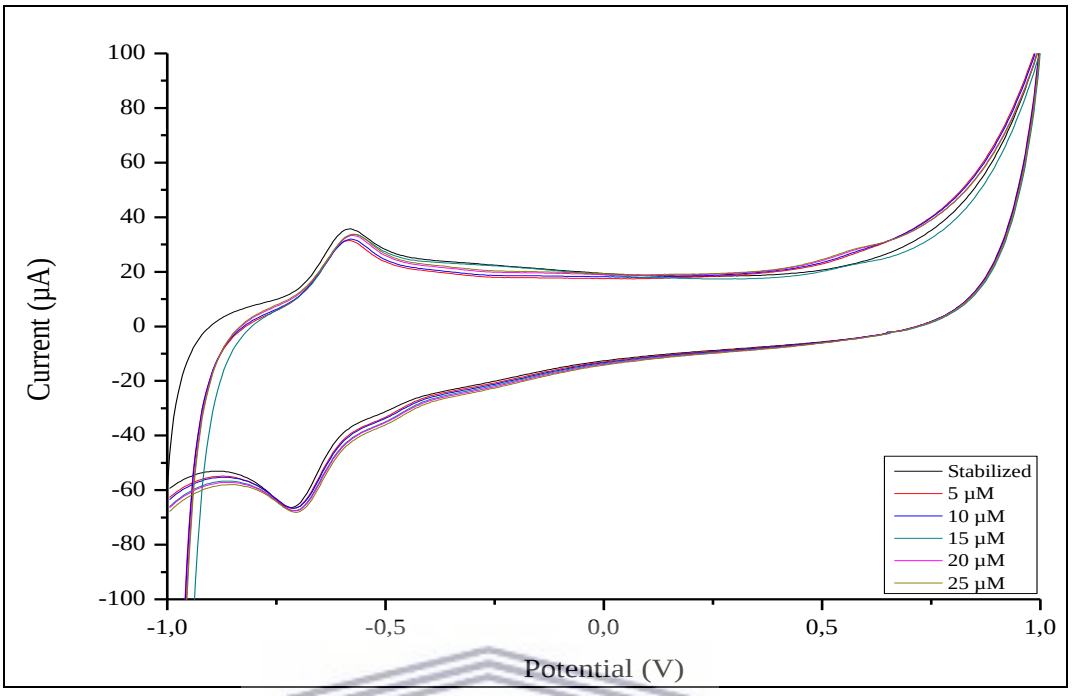

Figure 53: Cyclic voltammograms illustrating the electrochemical response of denatured cytochrome, sensor strategy B, ligand modified SPCE vs Ag/AgCl, to DEANONOate in 0.1M PBS (pH=7.1) at a scan rate 50 mV/s at different concentrations

Figure 53 illustrates the current response of sensor strategy B to nitric oxide in PBS. DEANONOate upon exposure to PBS spontaneously decomposed to produce NO and the parent amine. NO has been reported to coordinate strongly with the iron heme of cytochrome-c to form linear nitrosyls with the Fe^{2+} metal centres. Coordination of nitric oxide to the iron centres were expected to alter the redox behaviour of the system. However analysis of the data revealed negligible to no effects to the redox behaviour. Nitric oxide has been reported to exhibit trans-effects which would inhibit coordination to the iron centre[164]. The poor electrochemical response of the iron heme metal centre to nitric oxide was thus attributed to steric crowding surrounding the heme.

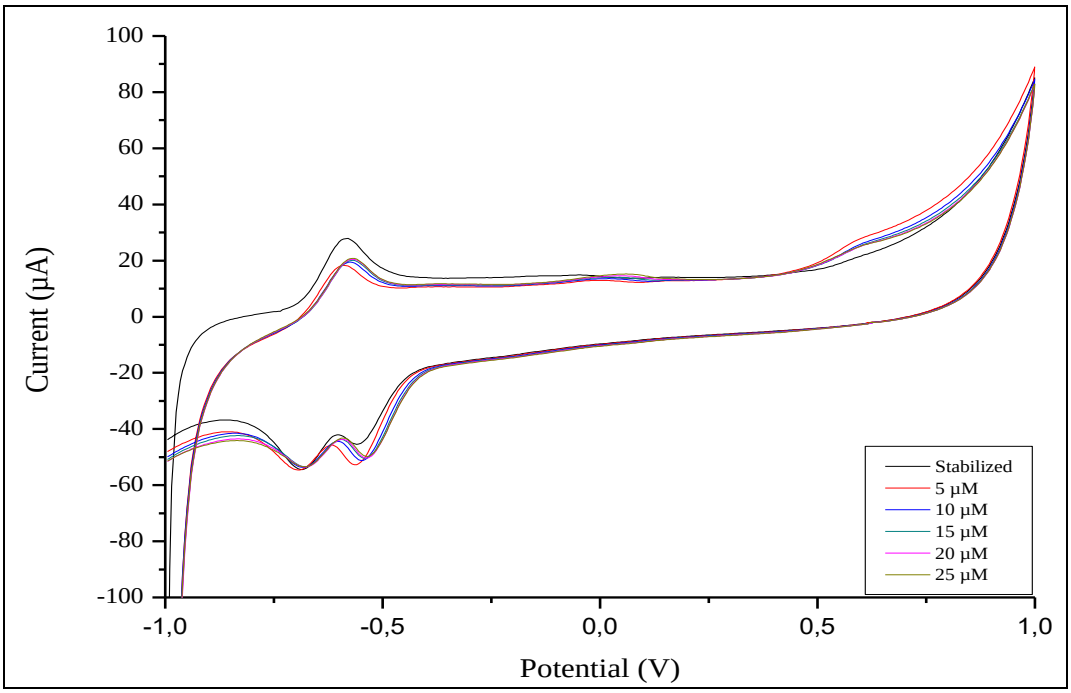

Figure 54: Cyclic voltammograms illustrating the electrochemical response of iron chelated ligand, sensor strategy C, modified SPCE vs Ag/AgCl, to DEANONOate in 0.1M PBS (pH=7.1) at a scan rate 50 mV/s at different concentrations

Nitric oxide was found to have inhibitory effects on the anodic peak currents of sensor strategy C, see figure 54. Nitric oxide coordinate to iron metal centres as powerful ligands which was observed in the results. NO had inhibitory effects on the redox chemistry of sensor strategy C.

Alam et al., (2018) fabricated a rhodamine based Schiff base composite fluorescent chemosensor for NO detection. Method of detection proceeded via the formation of a nitrosohydroxylamine that altered adsorption and fluorescent properties of the sensors[165].

In order to establish the effect of DEANONOate dissociation in PBS a series of cyclic voltammetric studies were performed at different concentrations. The expected outcome was for a linear relationship between the concentration of nitric oxide and the inhibitory effect elicited to be reflected. In preliminary studies the response of the sensor to nitric oxide correlated to initial injection of the analyte only. Therefore the concentration effect was limited to single dose analysis.

A 0.1 M PBS solution (8 ml) was injected with a single dose of DEANONOate and analysed following a dissociation period of ten minutes. Each experiment was conducted in triplicate.

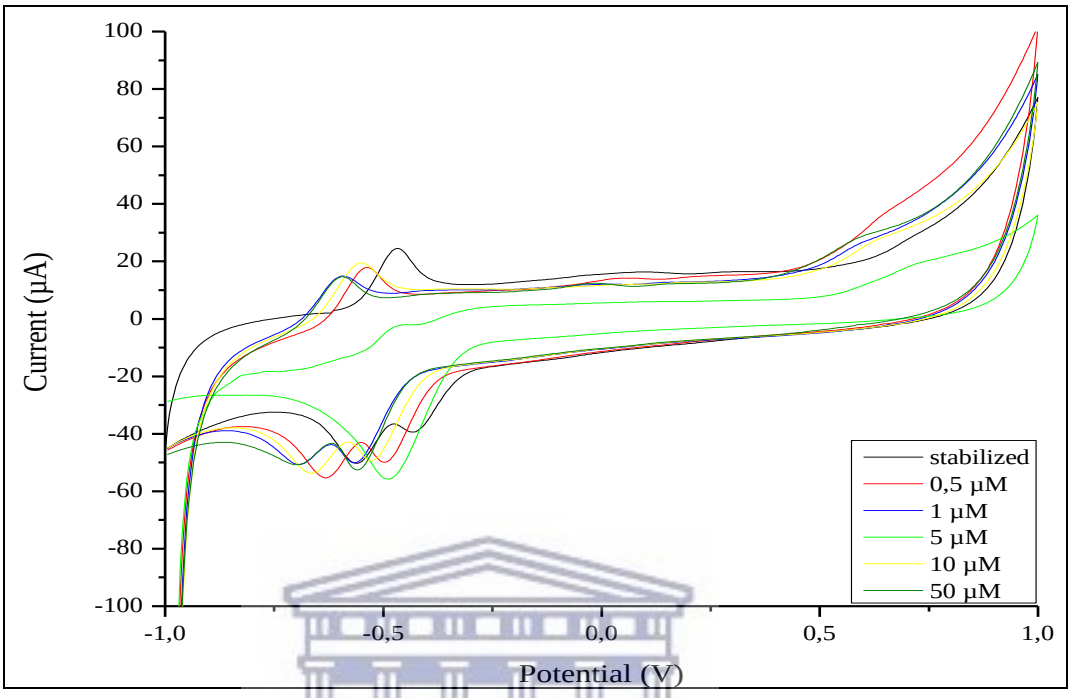

Figure 55: Cyclic voltammograms illustrating the current response of the iron ligand, sensor strategy C, modified SPCE vs Ag/AgCl, to DEANONOate dissociation in 0.1 M PBS (pH=7.1) at a scan rate of 50 mV/s at different concentrations

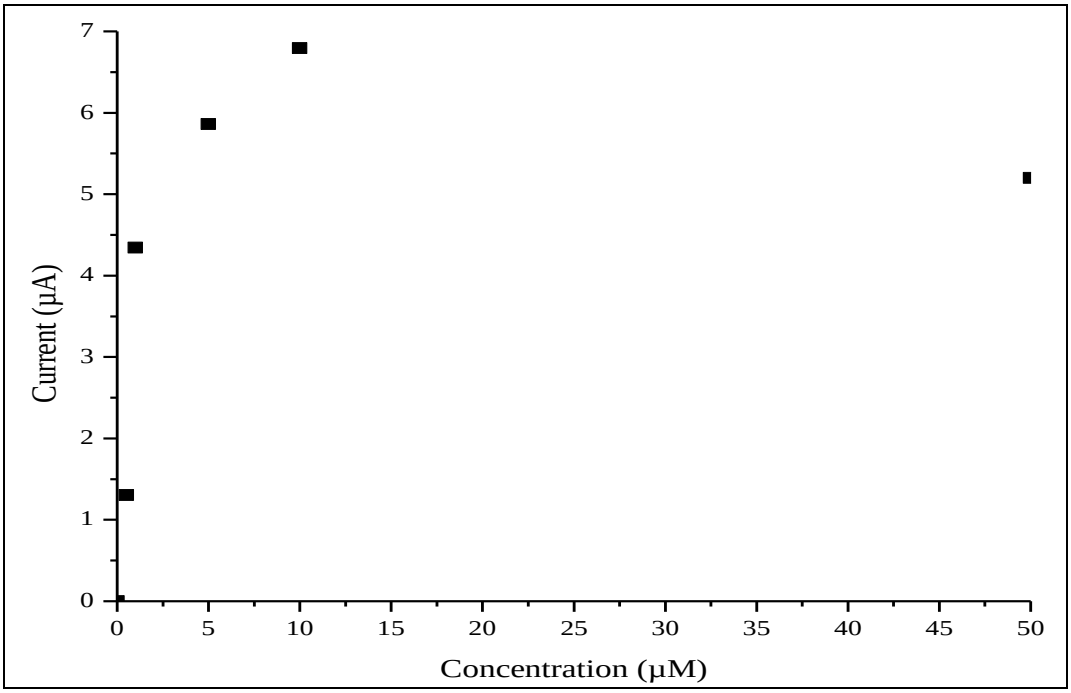

Figure 56: Linear plot of current response to DEANONOate dissociation as a function of concentration

Figure 55 illustrates the inhibitory effect of DEANONOate on the anodic peak current at NONOate concentrations 0.5 µM to 50 µM. The recorded inhibitory effects were a function of NO concentration. In figure 56 the effect of DEANONOate dissociation, producing nitric oxide, on the electrochemical activity of sensor strategy C is plotted linearly against initial concentration. Alterations to the Fe(II)/Fe(III) redox chemistry of sensor strategy C was associated with NO coordination to the iron metal centres. The greatest inhibitory effect was recorded at 10 µM. NONOate also appeared to alter the redox chemistry of the iron ligand system. A negative shift in the standard redox potentials were recorded. The changes in the electron transfer processes were associated with NO coordination to the metal centre.

The current response of the iron ligand complex was assessed against a series of aliquots of the nitric oxide donor. The experiments were conducted by measuring the current response to one time injections of DEANONOate. The experiments were performed in triplicate to establish a calibration curve for DEANONOate in solution as well as the percentage error.

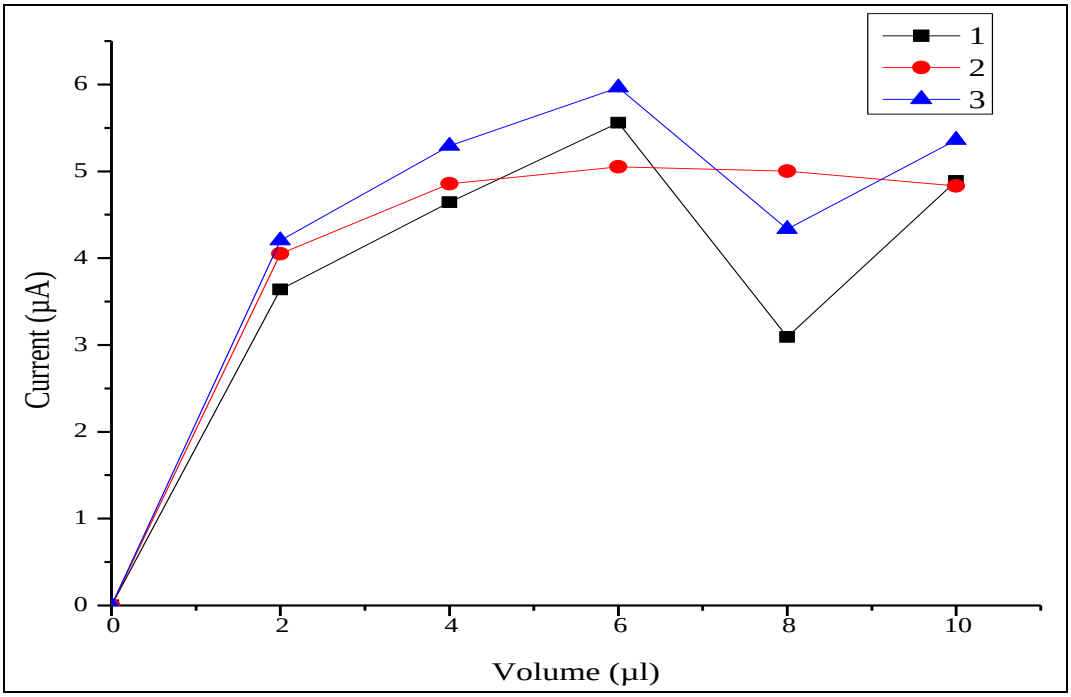

Figure 57: Triplicate studies illustrating the current response of sensor strategy C, deposited on SPCE, in 0.1 M PBS vs Ag/AgCl to 2, 4, 6, 8, 10 µl aliquots (125, 250, 375, 500 and 625 nM molar equivalent) DEANONOate

Table 14: DEANONOate current inhibition statistical data

[NONOate] (nM)	Current inhibition(µA)			mean	SD	UL	LL	STD error
0,000	0,000	0,000	0,000	0,000	0,000	0,000	0,000	0,000
125	3,640	4,050	4,202	3,657	0,291	3,948	3,366	7,949
250	4,644	4,858	5,292	4,497	0,330	4,827	4,167	7,342
375	5,560	5,053	5,964	5,525	0,456	5,981	5,069	8,262
500	3,093	5,002	4,334	4,131	0,969	5,100	3,162	23,450
625	4,889	4,833	5,361	5,474	0,290	5,764	5,184	5,298

Standard deviation (SD), upper limit (UL), lower limit (LL), standard error (STD)

Table 15: Nitric oxide concentration at 10 minute mark

[DEANONOate] (nM)	[NO] (nM)
0	0
125	64.5
250	129
375	194
500	258
625	323

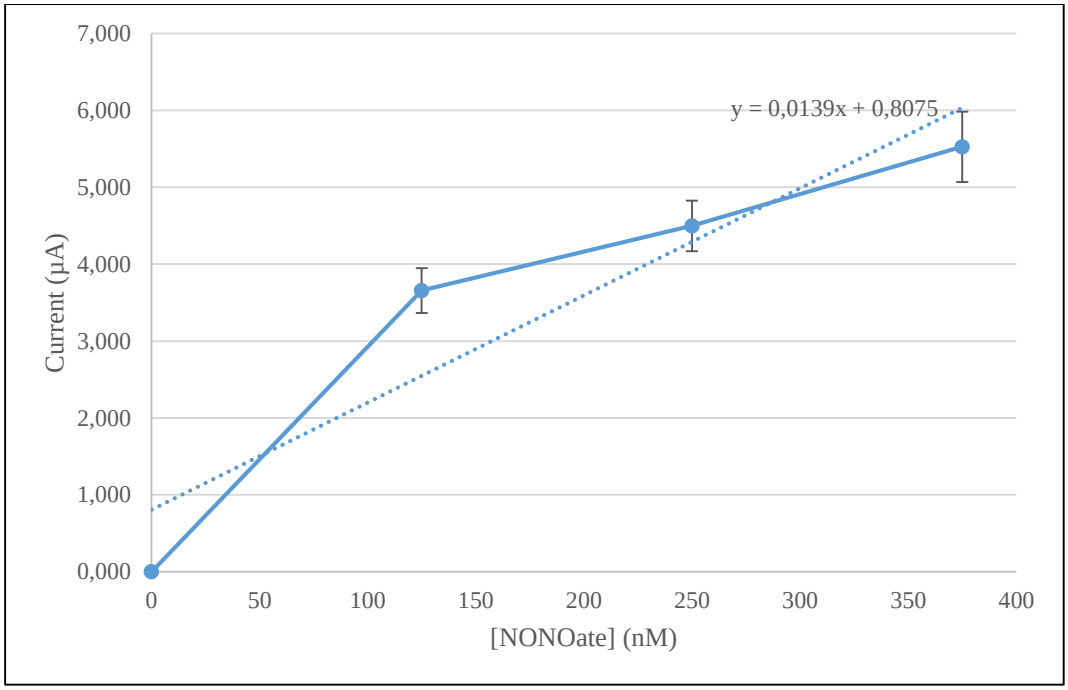

Figure 58: Mean standard error of nitric oxide detection in PBS

Figure 57 depicts the current response of sensor strategy C to of 0, 125, 250, 375, 500 and 625 nM DEANONOate in 0.1M PBS. For each experiment the current response was measured 10 minutes after injection of the analyte. On average the concentration of DEANONOate where the greatest inhibitory effect was recorded was at 375 nM. At higher DEANONOate concentrations the current response was inconsistent. This was believed to be a result of surface fowling blocking the metal centre. In figure 58 the mean range for sensor strategy C, SPCE electrode coated with the iron ligand complex, with current response to DEANONOate dissociation after 10 minutes in 0.1 M PBS is illustrated. The sensor displayed a linear dynamic range for DEANONOate from 125 to 375 nM. It managed a lower limit of detection of 62.742 nM for DEANONOate with a sensitivity of 0.0139 µA/nM. Table 15 shows NO concentrations which was calculated based on DEANONOate reaction rate, 1.29×10^{-3} s^{-1}, at room temperature. Based on the calculations it was extrapolated that the sensor could detect NO in the range of 30 to 40 nM. The standard error of detection for n=3, up till 375 nM DEANONOate, was relatively low ranging between 5 and 8. Based on standard error the sensing performance of sensor strategy C was found to be repeatable for nitric oxide detection in solution.

Chapter 6

6. Application of sensor strategy c in recovery studies

This chapter investigates the analytical performance of the sensor strategy C in the recovery of nitric oxide within a complex matrix. Synthetic urine simulated a complex biological matrix which provided a platform to assess the selectivity of sensor strategy c to nitric oxide. Sensor strategy A and B were excluded from this study based on the performance of the sensors in preliminary experiments.

6.1 Preparation of synthetic urine

To prepare a 500 ml synthetic urine sample 3.8 g Potassium chloride, 8.5 g sodium chloride, 24.5 g or urea. 1.03 g of citric acid, 0.34 g of ascorbic acid, 1.18 g potassium phosphate, 1.4 g of creatinine, 0.64 g sodium hydroxide, 0.47 g of sodium bicarbonate, and 0.28 ml of sulphuric acid were dissolved in 500 ml deionized Millipore water. The solution was stirred for one hour to facilitate adequate dissolution of the salts and refrigerated.

6.2 Nitric oxide recovery

Experiments were performed to investigate the selectivity of sensor strategy C. Binding of nitric oxide to iron was previously illustrated, see chapter 5, to proceed via a reduction in the anodic peak current for iron. The study was conducted in phosphate buffer pH 7.2. DEANONOate was used as a nitric oxide donor. A parent 50 mM solution of DEANONOate was prepared by diluting the commercial salt with 995 µl of a 0.01 M NaOH solution. The standard was divided into 10 vials each containing 100 µl aliquots, and frozen. On the day a vial was selected and allowed to thaw. This was followed by serial dilution to yield a 1 ml NONOate solution with a 0.5 mM concentration. The diluted samples were only valid for 1 day as per manufacturer

recommendation. The nature of the binding between nitric oxide and iron was non-reversible and each experiment had to be conducted separately. All solutions were degassed with Ar for 10 minutes before commencing studies.

For nitric oxide recovery studies similar a methodology was applied as per section 5.4, see figure 59. Studies were conducted using 8 ml aliquots of synthetic urine that were degassed with Ar for 10 minutes. At the beginning of each experiment cyclic voltammetry was performed to establish a baseline. A potential window of -1 V to 1V was used with a scan rate of 50 mVs^{-1} for three cycles until the current stabilised. Once the baseline was established synthetic urine was injected with a specific quantity of stock DEANONOate 0.5 mM and stirred for ten minutes to facilitate adequate dissociation of DEANONOate into nitric oxide. The DEANONOate quantities used for detection were 2, 4 and 6 µl only with molar equivalents 125, 250 and 375 nM. Each experiment was performed in triplicate.

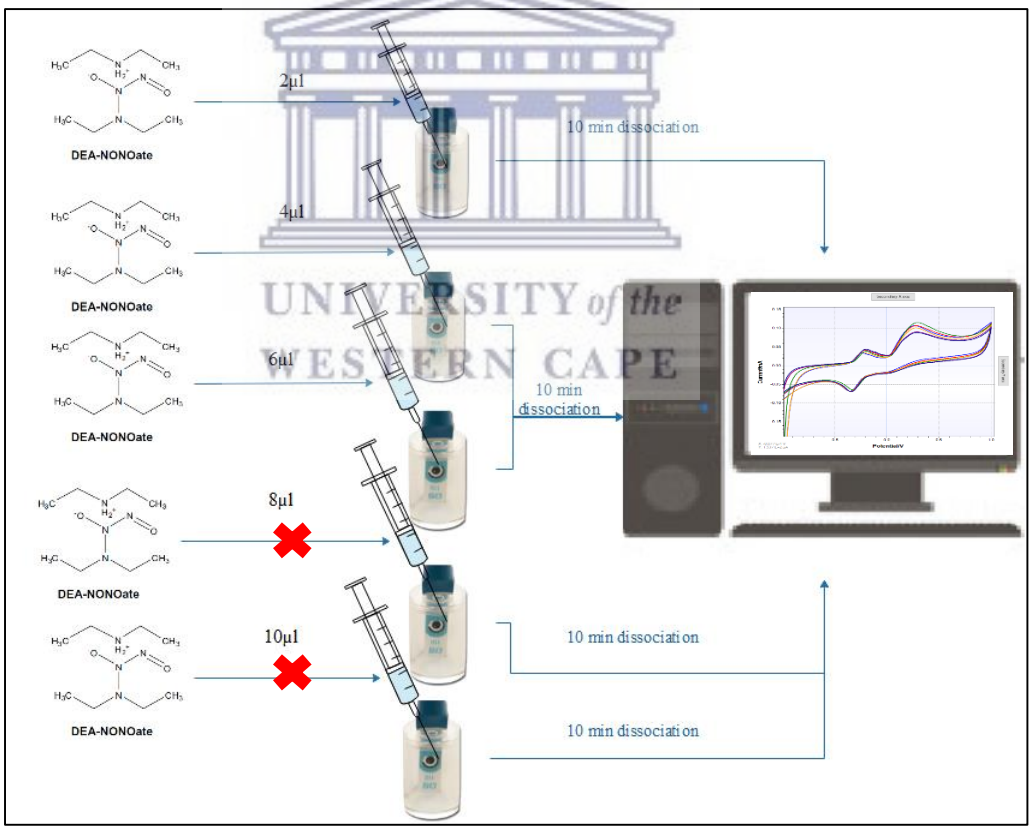

Figure 59: Nitric oxide recovery studies in synthetic urine with cyclic voltammetry

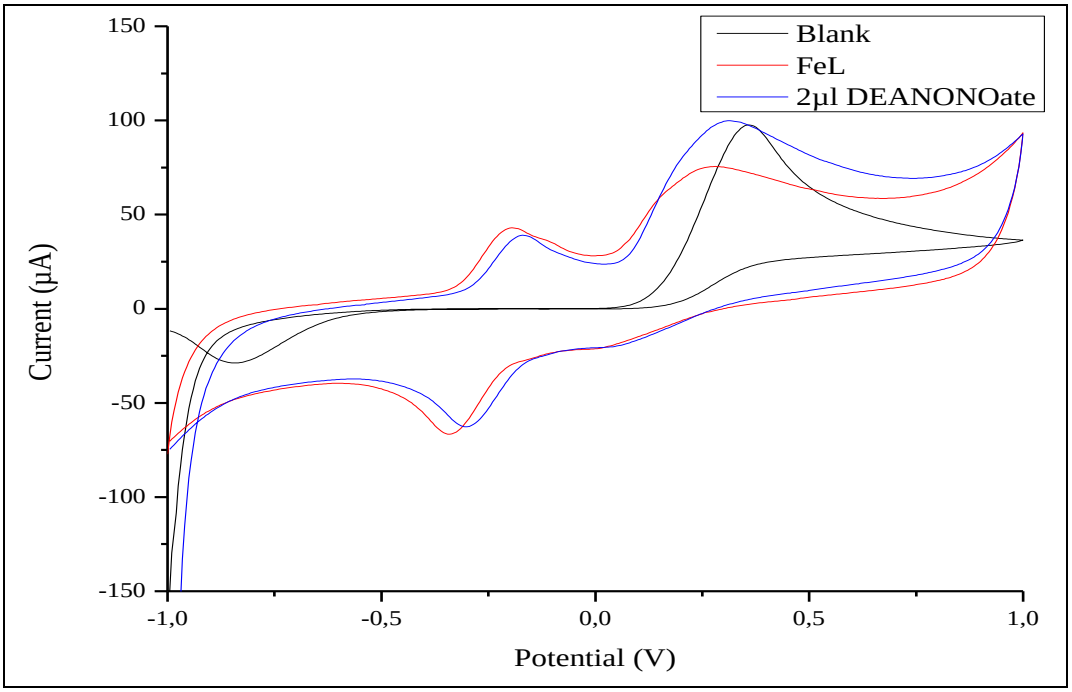

Figure 60: Cyclic voltammetry illustrating the redox response of sensor strategy C, deposited on SPCE, to the dissociation of 2µl DEANONOate in synthetic urine at 50 mVs^{-1} over the potential window -1 V to 1V

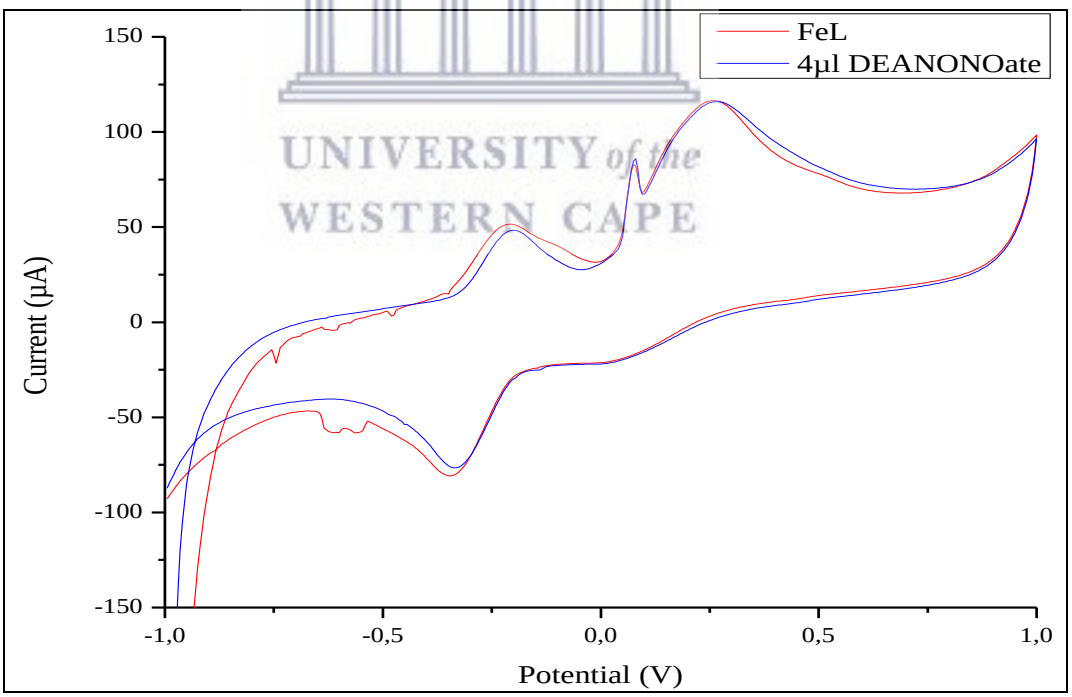

Figure 61: Cyclic voltammetry illustrating the redox response of sensor strategy C, deposited on SPCE, to the dissociation of 4µl DEANONOate in synthetic urine at 50 mVs^{-1} over the potential window -1 V to 1V

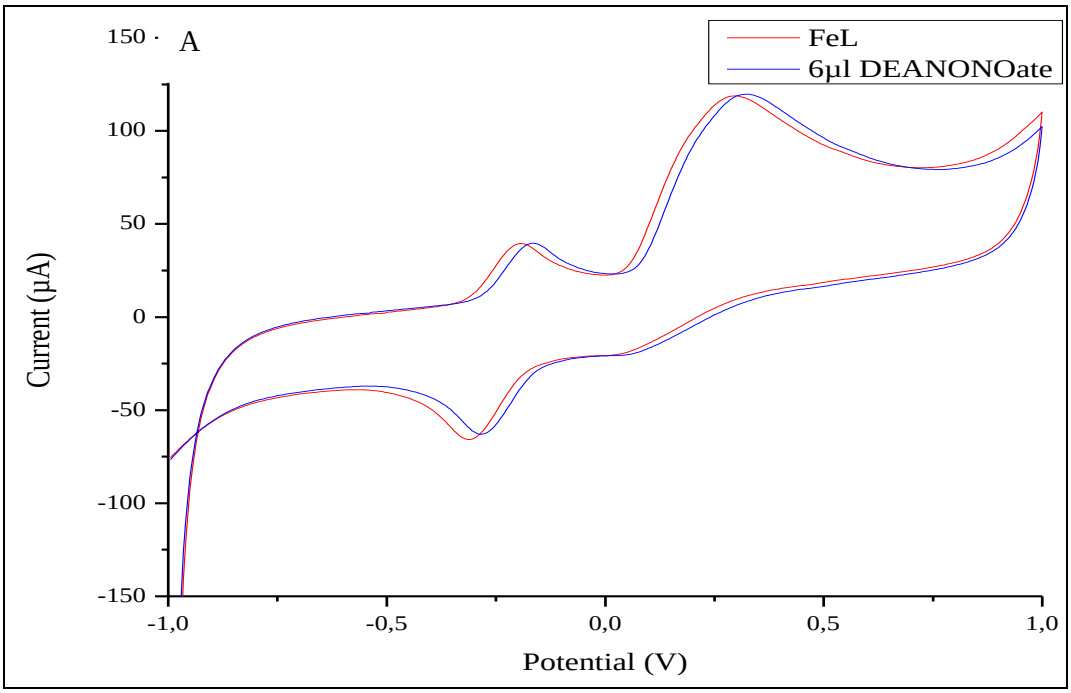

Figure 62: Cyclic voltammetry illustrating the redox response of sensor strategy C, deposited on SPCE, to the dissociation of 6µl DEANONOate in synthetic urine at 50 mVs^{-1} over the potential window -1 V to 1V

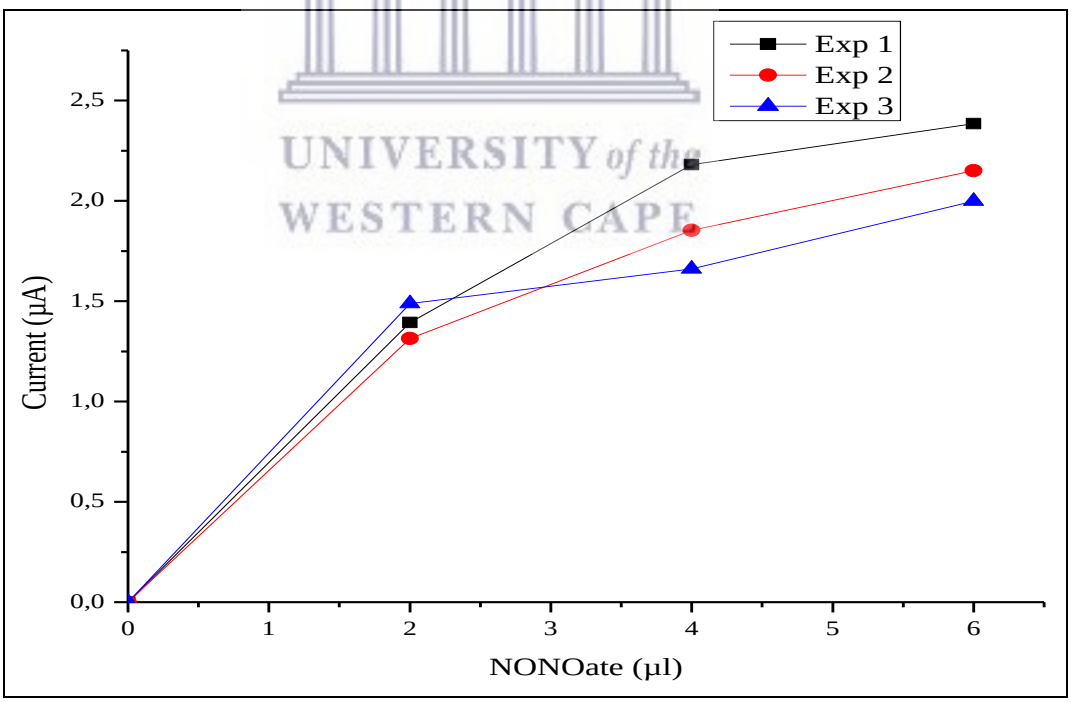

Figure 63: Triplicate studies illustrating the current response of sensor strategy C, deposited on SPCE, in synthetic urine vs Ag/AgCl to 2, 4, and 6 µl aliquots of DEANONOate

Figures 60, 61 and 62 illustrates the analytical detection of nitric oxide in synthetic urine with sensor strategy C. Detection was performed using three volumetric profiles of 0.5 mM DEANONOate, 2 µl (figure 60), 4 µl (figure 61) and 6 µl (figure 62). The experiments were conducted in triplicate. In figure 60 the "blank" cyclic voltammogram showed the background current of synthetic urine using a blank SPCE. At first sight it is evident that the iron ligand system is electroactive in synthetic urine and unaffected by competing analytes within the complex matrix represented by synthetic urine. In figure 60 two anodic peaks were recorded in the forward scan. The first peak at -0.192 V and a second peak at 0.265 V. The first peak was ascribed to oxidation behaviour of the iron ligand complex. The complimentary reduction peak was recorded at -0.344 V in the reverse scan. The redox chemistry of the iron ligand complex displayed redox chemistry characteristic of quasi-reversible systems. The second anodic peak observed in the forward scan was assigned to sulphuric acid, a component of synthetic urine.

Table 16: Statistical data for NO recovery in synthetic urine

NONOate (µl)	Current inhibition(µA)			mean	SD	UL	LL	STD error
0,000	0,000	0,000	0,000	0,000	0,000	0,000	0,000	0,000
2,000	1,394	1,314	1,488	1,399	0,087	1,486	1,312	6,227
4,000	2,181	1,853	1,661	1,898	0,263	2,161	1,635	13,851
6,000	2,385	2,150	1,999	2,178	0,195	2,373	1,983	8,931

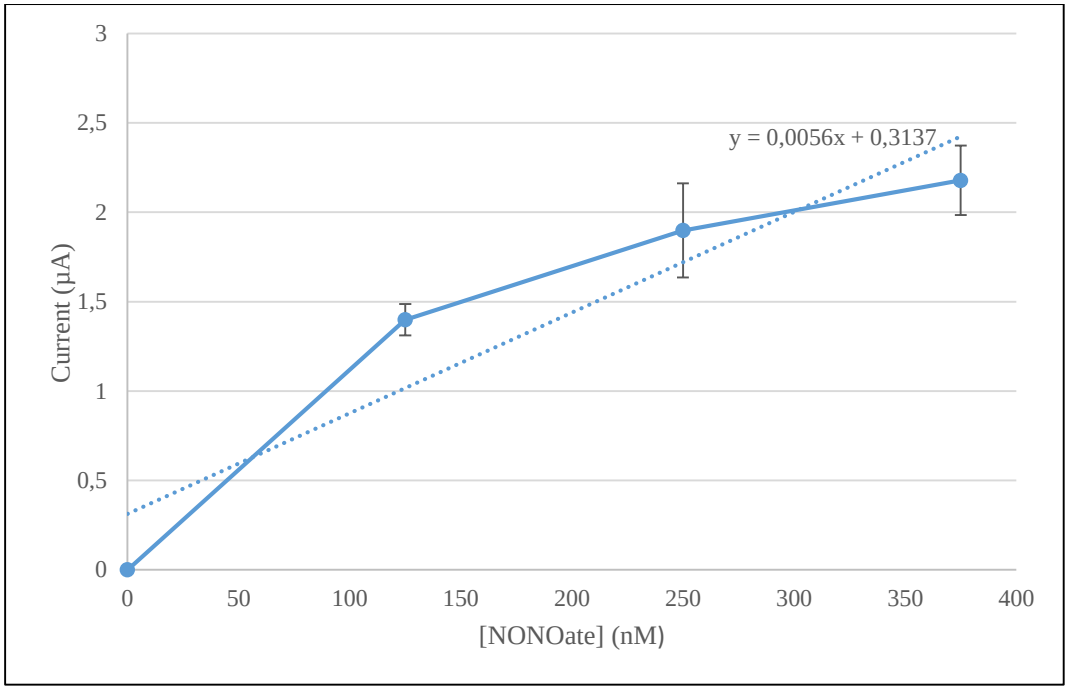

Figure 64: Mean standard error for nitric oxide detection in synthetic urine using sensor strategy C

The analytical results for the detection of nitric oxide in synthetic urine is presented in figure 64. In figure 64 the mean range for sensor strategy C, iron ligand modified SPCE, with current response to DEANONOate dissociation after 10 minutes in synthetic urine is illustrated. The sensor displayed a linear dynamic range for NONOate from 125 to 375 nM. Sensor strategy C was able to successfully facilitate selectivity towards nitric oxide. Standard error values 6.277, 13.851 and 8.931 were recorded and was found to be higher than that of PBS. The recorded variance in the standard error was attributed to a restriction in analyte transport to the sensor surface. In spite thereof, a lower detection limit of 46.657 nM for DEANONOate was achieved with a sensitivity of 0.0056 µA/nM in synthetic urine.

Chapter 7

7. Introduction

This chapter provides an outline of the work performed in the study on "Synthesis strategies for denatured cytochrome-c analogues towards analytical reporting of NOx species". The objectives as outlined in chapter one are concluded by highlighting the findings and achievements. The chapter begins by providing a brief background of the focal points of this work but goes on to discuss the significance of the outcomes of the study, as well as recommendations for future work.

7.1 Electrochemical sensors

Conductive organic polymers have been subject to scrutiny for their application as electroactive materials. Organic polymers that have been extensively researched are poly(acetylene), poly(thiophene) and poly(pyrrole). Poly(pyrrole) showed great potential and found diverse application in research [166]. Synthesis of poly(pyrrole) is not very complicated, oxidative anodic coupling of the monomer is one such method where the monomeric units link α-α with 180^{o} dihedral angles between the units to form highly conjugated linear chains. Fundamentally macromolecules all follow similar reaction pathway, monomer + monomer to yield hybrid monomer, by means of dehydration. Dehydration reactions form a subset of condensation reactions. Schiff-bases, systems consisting of conjugated -C=C- and -C=N- bonds, have received substantial interest. These systems are generally produced by the condensation of amines and carbonyl compounds and have good thermal stability, semi-conductivity, electrochemical and nonlinear optic properties[112]. The characteristic thermal stability, mechanical strength and opto-electronic properties of Schiff bases have been reported to be resultant of aromaticity and conjugation. Based on literature, which explored

naphthalene incorporation into Schiff bases and pyrrole's diverse properties, pyrrole was cross-linked with naphthalene[113].

Monomer precursors pyrrole-2-carboxaldehyde and 2, 3-diaminonaphthalene were cross-linked through a Schiff base reaction to yield a hybrid monomer *N, N-bis((1H-pyrrol-2-yl)methylene)naphthalene-2,3-diamine).* The synthesis of the hybrid monomer was a slow process. The reaction was allowed to run for 48 hours to completion at 70 ^{o}C under nitrogen gas. Spectroscopic analysis of the monomer *N, N-bis((1H-pyrrol-2-yl)methylene)naphthalene-2,3-diamine)* confirmed successful formation. UV-Vis analysis confirmed a system with extended conjugation that was absent in the monomer precursors. FTIR analysis identified the formation of a new bond at 1595 cm^{-1} which corresponded to literature reports on successful imine bond formation. Microscopy results identified changes to the morphology of the monomer. H-NMR spectroscopy identified variations in the molecular configuration of *N, N-bis((1H-pyrrol-2-yl)methylene)naphthalene-2,3-diamine.* New symmetrical peaks were recorded at 8.1 and 7.7 ppm associated to imine formation. Electrochemical analysis of the electrodeposited monomer reported a redox system at -0.522 V and -0.676 V. The redox system was preceded by a heterogeneous chemical reaction that was expressed as an irreversible one electron transfer process at 0.687 V. The Randle-Sevcik equation, which described the effect of scan rate on the peak currents, identified non-diffusion controlled electron transfer behaviour.

Three sensor synthetic strategies were developed with commercial screen-printed carbon electrodes. Sensor strategy A modelled the electrochemical behaviour of denatured cytochrome-c with disposable SPCEs. Electrochemical analysis of the denatured enzyme identified irreversible electrochemistry and was excluded from further experiments.

For sensor strategy B the monomer N, N-bis((1H-pyrrol-2-yl)methylene)naphthalene-2,3-diamine) was electrodeposited onto disposable SPCEs to form the ligand. The ligand was modified with denatured cytochrome-c by cross-linking the two layers to form a stacked system. The electrochemistry of sensor strategy B compared to the ligand, electrodeposited monomer N, N-bis((1H-pyrrol-2-yl)methylene)naphthalene-2,3-diamine), displayed improved electron transfer behaviour. Sensor strategy B also showed improved electrochemistry in comparison to sensor strategy A, which

displayed non-reversible electron transfer behaviour. Randles-Sevcik plot identified a linear relationship between the peak currents and square root of scan rates. Anodic De values of 1.31 x 10^{-6} cm^2/s were recorded indicating rapid electron transfer between SPCE and denatured cytochrome-c. Electron transfer was established to be reversible under diffusion controlled conditions. The results suggested the ligand formed a conducting layer on the SPCE surface enabling electron transfer between the electrode and redox centre of denatured cytochrome-c.

An analogue of cytochrome-c was synthesized by doping the monomer, N, N-bis((1H-pyrrol-2-yl)methylene)naphthalene-2,3-diamine), with iron. The doping processes was facilitated by refluxing the monomer, N, N-bis((1H-pyrrol-2-yl)methylene)naphthalene-2,3-diamine), in a methanolic solution of $FeCl_2.4H_2O$ for 3 hours. Microscopy, spectroscopy and electrochemistry confirmed successful formation of the macromolecule, iron ligand complex. UV spectroscopy identified narrowing of the absorption bands which was associated with coordination of iron to the ligand. FTIR spectroscopic analysis suggested coordination to iron at the pyrrole ring and not over the imine bond. EDS analysis confirmed the presence of iron in the macromolecule. TEM analysis confirmed changes to the morphology of the macromolecule. In order to confirm successful coordination of the iron EELS analysis was performed with a Zeiss Auriga EMU unit. EELS analysis recorded changes in the L3/L2 peak intensity ratios. Changes to these ratios have been reported in literature to indicate changes to the electronic environment surrounding the metal. Analysis of the data confirmed coordination of iron to the ligand.

The synthesized iron ligand complex, macromolecule, was incorporated into sensor strategy C. The iron ligand complex was electrodeposited onto disposable SPCEs. Electrochemical analysis of sensor strategy C demonstrated electron transfer behaviour analogues to sensor strategy B although higher diffusion coefficient values were established for sensor strategy B. Diffusion coefficient values for sensor strategy C were 8.86 x 10^{-7} cm^2s^{-1} oxidation, and 9.38 x 10^{-7} cm^2s^{-1} reduction. When compared to phenazine-2,3-diimino(pyrrole-2-yl) (PPDP), a similar type hinge system, doped with 1,4-naphtaquinone sulphonic acid (NQSA) and polyvinylsulfonic acid (PVSA) the diffusion rates were competitive. The following diffusion rate values for PPDP doped with NQSA were reported; D_e – 4.62 x 10^{-7} (anodic) and D_e – 4.39 x 10^{-7} (cathodic). PDDP doped with PVSA on the other hand reported superior diffusion

rates, D_e – 9.28 x 10^{-3} (anodic) and D_e – 1.60 x 10^{-2} (cathodic). Reversible electron transfer was identified for sensor strategy C coupled with diffusion controlled electron transfer characteristics. No leaching of the iron ligand complex into solution was recorded. The iron ligand complex was found to be stable once electrodeposited.

7.2 Challenges in NOx detection

Advancements in improving sensitivity and selectivity with these sensors have been established in literacy to evolve around the development of suitable membranes for these electrodes[52]. Badea et al, 2001 designed a sensor that could effectively discriminate against nitrites and nitrates based on nitrite oxidation in acetate buffer using a Pt electrode. The electrode was polarised at +900 mV against AgCl reference electrode. In order to make Pt electrodes selective to nitrite oxidation the electrodes were modified with cellulose acetate membranes. The membrane was applied in the design of an amperometric sensor for the detection of H_2O_2. Although the sensors were never tested for nitrite permeability in its application the sensor displayed good mechanical stability and selectivity towards nitrite, though low. But by modifying the electrodes with an electropolymerized film using 1, 8-diaminonaphthalene the sensitivity of the systems were enhanced five times. It was found that these sensors were quite effective for rapid detection of nitrites and nitrates in water. The electropolymerized membranes however required one night of stabilization in pH 4 acetate buffer at 900 mV[50].

Out of the three sensor strategies that were analysed two sensor strategies were applied in NOx studies. Electrochemical analysis revealed analogues redox chemistry for sensor strategies B and C. These systems were applied in NO_x electroanalytical studies of nitric oxide and nitrogen dioxide in phosphate buffer solution. Further applications saw sensor strategy C applied in the recovery of nitric oxide from a complex matrix, synthetic urine.

The detection of nitric oxide has been a contentious issue. Specificity and sensitivity are of the major problems. Nitric oxide has a short half-life and is oxidized rapidly. The reactions below illustrates the electrochemical reactions of nitric oxide at electrode surfaces over the +600 to 900 mV potential range.

$$NO \longrightarrow NO^+ + e^- \quad (7.1)$$

$NO^+ OH^-$ ⟶ HNO_2 (7.2)

$HNO_2 + H_2O$ ⟶ $NO_3^- + 2e^- + 3H^+$ (7.3)

It's these reactions which impede the detection of nitric oxide and the formation of NO-derivatives. In the third reaction nitrite is electrochemically oxidized to nitrate. Endogenous nitrites therefore ran direct interference[167]. Materials selective towards nitric oxide for electrode modification have been an effective strategy to improve specificity[168169].

The response of sensor synthesis strategies B and C were evaluated using nitric oxide donor diazeniumdiolates (Z)-1-(N,N-diethylamino)-diazen-1-ium-1,2-diolate (DEANONOate) over the potential window -1 V to 1 V. Nitric oxide, donated by the decomposition of the nitric oxide donor, displayed inhibitory effects on the anodic peak currents for sensor strategy C. Sensory strategy B on the other hand experienced less interference by NO and displayed minor changes to the redox couple. This was ascribed to unfolding of the heme that provided insufficient access to the iron centre due to steric crowding.

Strategies in literature which allow for real time detection of NO are based on chemically modified ultramicroelectrodes with good selectivity, sensitivity and stability etc. Sensor strategy C successfully detected nitric oxide in solution. The alteration in the Fe(II)/Fe(III) redox activity for sensor strategy C was attributed to the affinity of iron for NO. The mechanism for nitric oxide detection by sensor strategy C was described as the complexation of NO with iron. This was illustrated by a suppression in the anodic peak current recorded in potential range of –500 mV. Metal complexes with catalytic activity towards NO oxidation have been extensively studied. There exists a need for molecular materials capable of shifting NO oxidation to less positive values. Most negative shifts in nitric oxide oxidation potential has been reported at approximately 0.150 V. Values for nitric oxide oxidation by platinized carbon-fibre microelectrodes has been reported at 0.650 V. The focus for advancements in sensors selective to NO are based on membranes selective towards NO with long-term stability over 1 to 2 hour. Selectivity in sensor strategy C was found to be associated with nitric oxide coordination to the iron metal centres. The iron ligand complex, used in sensor strategy C, following electrochemical deposition onto SPCE showed stability exceeding the 1 to 2 hour reported range for electrodes

used in real time NO detection. The sensor displayed a linear dynamic range for NONOate from 125 to 375 nM. It managed a lower limit of detection with an extrapolated value of 62.742 nM for NONOate with a sensitivity of 0.0139 µA/nM. The sensor was capable of detecting NO. It was speculated that the sensor could detect NO at concentrations as low as 64.5 nM. Based on the standard error, the sensing performance of sensor strategy C was found to be repeatable. In synthetic urine a lower detection limit of 46.657 nM for NONOate was achieved with a sensitivity of 0.0056 µA/nM. NO detection in synthetic urine, plotting concentration vs. anodic current, displayed a linear relationship with a low standard error margin. Nitric oxide adsorption to the iron ligand complex, sensor strategy C, was found to be irreversible.

Concurrent NO_2^- studies were also performed in PBS with sensor strategies C to analyse possible cross interference by NO_2^-. Electro-analytical results revealed no interference by the nitrite ions on the redox system of the iron ligand complex.

7.3 Recommendations for further studies

The following aspects of synthesis strategies for denatured cytochrome-c analogues presented herewith requires further investigation. In this study a sensor synthesis strategy was developed that produced a biosensor which replicated the electrochemical behaviour of the denatured metalloprotein cytochrome-c;

A novel monomer, which formed the supporting layer for the denatured enzyme, was successfully synthesized through a Schiff base reaction. The monomer, N, N-bis((1H-pyrrol-2-yl)methylene)naphthalene-2,3-diamine), once electrodeposited to form the ligand could harness the electron transfer capability of denatured cytochrome-c. The monomer also facilitated the coordination of Fe (II) to produce a macromolecule that could replicate the electron transfer capabilities of the iron heme of cytochrome-c. More work needs to be done on the long term stability of the iron ligand complex and to establish the half-life of the macromolecule.

The FeL_4 iron ligand complex successfully coordinated to the monomer but further in-depth analysis is required to physically identify the binding interaction.

The synthesis strategy of the Schiff base metal ligand complex, FeL_4, can be extended to other metal centres such as Cu and Ni. The motivation for this is to develop ligands with the ability of enzymes with metal centres to catalyse chemical pathways.

Further nitric oxide studies is required to refine the calibration curves and establish lower concentration ranges.

References

1. Tyson, P., Preston, R. The Composition and structure of the atmosphere. in *The Weather and climate of Southern Africa* (ed. Attwell, A.) 3–10 (Oxford University Press Southern Africa, 2000).

2. Fueglistaler, S., Dessler A. E., Dunkerton T. J., Folkins I., Fu Q., Mote P. W. Tropical Tropopause Layer. *Reviews of Geophysics* **47**, 1–31 (2009).

3. Drake, F. Stratospheric ozone depletion-an overview of the scientific debate. *Progress in Physical Geography* **19**, 1–17 (1998).

4. Atkinson, R., Arey, J. Gas-phase tropospheric chemistry of biogenic volatile organic compounds: a review. *Atmospheric Environment* **37**, 197–219 (2003).

5. Knelson, J. H., Lee, R. E. Oxides of nitrogen in the atmosphere: Origin, Fate and public health implications. *Ambio* **6**, 126–130 (1977).

6. Wang, W. C., Mohnen, V. A. Tropospheric ozone and climate change. *Air and Waste* **43**, 1332–1334 (1993).

7. Schlager, H., Grewe, V. Roiger, A. Chemical Composition of the Atmosphere. in *Atmospheric Physics* (ed. Schumann, U.) 17–35 (Springer-Verlag Berlin Heidelberg, 2012). doi:10.1007/978-3-642-30183-4_2

8. Piketh, S. J., Walton, N. M. Characteristics of Atmospheric Transport of Air Pollution for Africa. in *Air Pollution. Handbook of Environmental Chemistry* **4**, 173–195 (Springer Berlin Heidelberg, 2004).

9. Schwela, D. Air Quality Management. in *Sustainable Transport: A Sourcebook for Policy-makers in Developing Cities* (eds. Breithhupt, M. & Obermeyer, A.) 64 (GTZ, 2009).

10. Hunter, D., Salzman, J. Zaelke, D. *International Environmental Law and Policy*. (Foundation Press/Thomson Reuters, 2011).

11. Koenig, J. Q. *Health Effects of Ambient Air Pollution*. (Springer US, 2000). doi:10.1007/978-1-4615-4569-9

12. Walton, N. M. Characterisation of Cape Town Brown Haze. (University of the

Witwatersrand, Johannesburg, 2005).

13. Department of Environmental Affairs(2015). *EIA guideline for renewable energy projects*. (2015).

14. Kox, M. A. R., Jetten, M. S. The nitrogen cycle. in *Principles of Plant-Microbe Interactions: Microbes for Sustainable Agriculture* 205–214 (Springer, Cham, 2015). doi:10.1007/978-3-319-08575-3_22

15. Gilchrist, M., Benjamin, N. Nitrite and Nitrate in Human Health and Disease. in *Nutrition and Health* (eds. Bryan, N. S. & Loscalzo, J.) 11–20 (Hunana Press, 2017). doi:10.1007/978-3-319-46189-2

16. Arneth, A., Sitch, S., Bondeau, A., Butterbach-Bahl K., Foster, P., Gedney, N., de Noblet-Ducoudré, Prentice, I. C., Sanderson, M., Thonicke K., Wania, R., Zaehle, S. *From biota to chemistry and climate: towards a comprehensive description of trace gas exchange between the biosphere and atmosphere*. *Biogeosciences* 7, (2010).

17. Delon, C. Reeves, C. E., Stewart, D. J., Serça, D., Dupont, R., Mari, C., Chaboureau, J. P., Tulet, P. *Biogenic nitrogen oxide emissions from soils-impact on NO x and ozone over West Africa during AMMA (African Monsoon Multidisciplinary Experiment): modelling study. Atmos. Chem. Phys* **8**, (2008).

18. Steinkamp, J., Ganzeveld, L. N., Wilcke, W. Lawrence, M. G. Influence of modelled soil biogenic NO emissions on related trace gases and the atmospheric oxidizing efficiency. *Atmospheric Chemistry and Physics discussions* **8**, 10227–10255 (2008).

19. Portmann, R. W., Daniel, J. S. Ravishankara, A. R. Stratospheric ozone depletion due to nitrous oxide: influences of other gases. *Philosophical Transactions of the Royal Society B: Biological Sciences* **367**, 1256–1264 (2012).

20. Ludwig, J., Meixner, F. X., Vogel, B. Förstner, J. Soil-air exchange of nitric oxide: An overview of processes, environmental factors, and modeling studies. *Biogeochemistry* **52**, 225–257 (2001).

21. Pilegaard, K. Processes regulating nitric oxide emissions from soils.

Philosophical Transactions of the Royal Society B: Biological Sciences B **368**, 1–8 (2013).

22. Davidson, E., Keller, M., Erickson, H., Verchot, L. Veldkamp, E. Testing a conceptual model of soil emissions of nitrous and nitric oxides. *BioScience* **50**, 667–680 (2000).

23. Davidson, E. A., Keller, M., Erickson, H. E., Verchot, L. V Veldkamp, E. Testing a Conceptual Model of Soil Emissions of Nitrous and Nitric Oxides. *BioScience* **50**, 667–680 (2000).

24. Caranto, J. D. Lancaster, K. M. Nitric oxide is an obligate bacterial nitrification intermediate produced by hydroxylamine oxidoreductase. *PNAS* **114**, 8217–8222 (2017).

25. Oluwoye, I., Dlugogorski, B. Z., Gore, J., Oskierski, H. C., Altarawneh, M. Atmospheric emission of NO x from mining explosives: A critical review. *Atmospheric Environment* **167**, 81–96 (2017).

26. Astier, J., Jeandroz, S., Wendehenne, D. Nitric oxide synthase in plants: The surprise from algae. *Plant Science* **268**, 64–66 (2018).

27. Sasaki, Y., Oguchi, H., Kobayashi, T., Kusama, S., Sugiura, R. Nitrogen oxide cycle regulates nitric oxide levels and bacterial cell signaling. *Scientific Reports* **6**, 1–11 (2016).

28. Scheler, C., Durner, J., Astier, J. Nitric oxide and reactive oxygen species in plant biotic interactions. *Current Opinion in Plant Biology* **16**, 534–539 (2013).

29. del Giudice, J., Cam, Y., Damiani, I., Fung-Chat, F., Meilhoc, E., Bruand, C., Brouquisse, R., Puppo, A., Boscari, A. Nitric oxide is required for an optimal establishment of the medicago truncatula-sinorhizobium meliloti symbiosis. *New Phytologist* **191**, 405–417 (2011).

30. D'Autreaux, B., Touati, D., Bersch, B., Latour, J.-M., Michaud-Soret, I. Direct inhibition by nitric oxide of the transcriptional ferric uptake regulation protein via nitrosylation of the iron. *PNAS* **99**, 16619–16624 (2002).

31. Sansbury, B. E., Hill, B. G. Regulation of obesity and insulin resistance by nitric oxide. *Free Radic Biol Med* **0**, 383–399 (2014).

32. Lundberg, J. O., Weitzberg, E. NO generation from nitrite and its role in vascular control. *Arteriosclerosis, Thrombosis, and Vascular Biology* **25**, 915–922 (2005).

33. Stanek, A., Gadowska-Cicha, A., Gawron, K., Wielkoszyński, T., Adamek, B., Cieślar, G., Wiczkowski, A., Sieroń, A. Role of nitric oxide in physiology and pathology of the gastrointestinal tract. *Mini reviews in medicinal chemistry* **8**, 1549–1560 (2008).

34. Choudhari, S. K., Chaudhary, M., Bagde, S., Gadbail, A. R., Joshi, V. Nitric oxide and cancer: A review. *World Journal of Surgical Oncology* **11**, 1 (2013).

35. Oess, S., Icking, A., Fulton, D., Govers, R., Müller-esterl, W. M. Subcellular targeting and trafficking of nitric oxide synthases. *Biochemical Journal* **396**, 401–409 (2006).

36. Luiking, Y. C., Engelen, M. P. K. J., Deutz, N. E. P. Regulation of nitric oxide production in health and disease. *Current Opinion in Clinical Nutr Metab Care* **13**, 97–104 (2010).

37. Marlettaz, M. A. Nitric Oxide Synthase Structure and Mechanism. *The journal of biological chemistry* **268**, 12231–12234 (1993).

38. Knowles, R. G., Moncada, S. Nitric oxide synthases in mammals. *Biochemical Journal* **298**, 249–258 (1994).

39. Xu, W., Liu, L. Z., Loizidou, M., Ahmed, M., Charles, I. G. The role of nitric oxide in cancer. *Cell Research* **12**, 311–320 (2002).

40. Hill, B. G., Dranka, B. P., Bailey, S. M., Lancaster, J. R. J., Darley-Usmar, V. M. What part of no don't you understand? Some answers to the cardinal questions in nitric oxide biology. *Journal of biological chemistry* **285**, 19699–19704 (2010).

41. Luiking, Y. C., Poeze, M., Ramsay, G., Deutz, N. E. P. The role of arginine in infection and sepsis. *Journal of parenteral and enteral nutrition* **29**, S70–S74 (2015).

42. Luiking, Y. C., Poeze, M., Ramsay, G., Deutz, N. E. P. Reduced citrulline production in sepsis is related to diminished de novo arginine and nitric oxide

production. *American Journal of Clinical Nutrition* **89**, 142–152 (2009).

43. Georgescu, A., Popov, D., Constantin, A., Nemecz, M., Alexandru, N., Cochior, D., Tudor, A. Dysfunction of human subcutaneous fat arterioles in obesity associated or not with Type 2 diabeties. *Clinical Science* **120**, 463–472 (2011).
44. Kraus, R. M., Houmard, J. A., Kraus, W. E., Tanner, C. J., Pierce, J. R., Choi, M. D., Hickner, R. C. Obesity, insulin resistance, and skeletal muscle nitric oxide synthase. *Journal of applied physiology* **113**, 758–765 (2012).
45. deRojas-Walker, T., Tamir, S., Ji, H., Wishnok, J. S., Tannenbaum, S. R. Nitric oxide induces oxidative damage in addition to deamination in macrophage DNA. *Chemical Research in Toxicology* **8**, 473–477 (1995).
46. Kaise, M., Miwa, J., Iihara, K., Suzuki, N. Helicobacter pylori stimulates inducible nitric oxide synthase in diverse topographical patterns in various gastroduodenal disorders. *Digestive Diseases* **48**, 636–643 (2003).
47. Gal, A., Wogan, G. N. Mutagenesis associated with nitric oxide production in transgenic SJL mice. *Proceedings of the National Academy of Sciences of the United States of America* **93**, 15102–15107 (1996).
48. Thomsen, L., Miles D. W., Happerfield L., Bobrow L. G., Knowles, R. G., Moncada S.. Nitric oxide synthase activity in human breast cancer. *British Journal of Cancer* **72**, 41–44 (1995).
49. Ambs, S., Merriam, W. G., Ogunfusika, M, O., Bennett, W. P., Ishibe, N., Hussain, S. P., Tzeng, E. E., Geller, D. A., Billiar, T. R., Harris, C. C. p53 and vascular endothelial growth factor regulate tumor growth of NOS2-expressing human carcinoma cells. *Nature Medicine* **4**, 1371–1376 (1998).
50. Badea, M., Amine, A., Palleschi, G., Moscone, D., Volpe, G., Curulli, A. New electrochemical sensors for detection of nitrites and nitrates. *Journal of Electroanalytical Chemistry* **509**, 66–72 (2001).
51. Ciszewski, A., Milczarek, G. Electrochemical detection of nitric oxide using polymer modified electrodes. *Talanta* **61**, 11–26 (2003).
52. Bedioui, F., Villeneuve, N. Electrochemical nitric oxide sensors for biological samples–Principle, selected examples and applications. *Electroanalysis* **15**, 5–18 (2003).

53. Fisher, W. R., Taniuchi, H., Anfinsen, C. B. On the Role of Heme in the Formation of the Structure of Cytochrome c. *The journal of biological chemistry* **248**, 3188–3195 (1973).

54. Manickam, P., Kaushik, A., Karunakaran, C. Bhansali, S. Recent advances in cytochrome c biosensing technologies. *Biosensors and Bioelectronics* **87**, 654–668 (2017).

55. López-Bernabeu, S., Huerta, F., Morallón, E., Montilla, F. Direct electron transfer to cytochrome *c* induced by a conducting polymer. *The Journal of Physical Chemistry C* **121**, 15870–15879 (2017).

56. Millar, H., Day, D. Nitric oxide inhibits the cytochrome oxidase but not the alternative oxidase of plant mitochondria. *FEBS letters* **398**, 155–158 (1996).

57. Bedioui, F., Quinton, D., Griveau, S., Nyokong, T. Designing molecular materials and strategies for the electrochemical detection of nitric oxide, superoxide and peroxynitrite in biological systems. *Physical Chemistry Chemical Physics* **12**, 9976–9988 (2010).

58. Zhang, Y., Hogg, N. The mechanism of transmembrane S-nitrosothiol transport. *PNAS* **101**, 7891–7896 (2004).

59. Palmerini, C. A., Arienti, G., Palombari, R. Electrochemical determination of nitric oxide and of its derivatives. *Talanta* **61**, 37–41 (2003).

60. Bedioui, F., Ismail, A., Griveau, S. Electrochemical detection of nitric oxide and S-nitrosothiols in biological systems: Past, present & future. *Current Opinion in Electrochemistry* **12**, 42–50 (2018).

61. Brown, M. D., Schoenfisch, M. H. Catalytic selectivity of metallophthalocyanines for electrochemical nitric oxide sensing. *Electrochimica Acta* **273**, 98–104 (2018).

62. Gupta, N., Sharma, S., Mir, I. A., Kumar, D. Advances in sensors based on conducting polymers. *Journal of Scientific and Industrial Research* **65**, 549–557 (2006).

63. Freire, R. S., Pessoa, C. A., Mello, L. D., Kubota, L. T. Direct Electron Transfer : An Approach for Electrochemical Biosensors with Higher Selectivity

and Sensitivity. *Journal of Brazilian Chemical Society* **14**, 230–243 (2003).

64. Umaña, M., Waller, J. Protein-Modified Electrodes. The Glucose Oxidase/Polypyrrole System. *Analytical Chemistry* **58**, 2979–2983 (1986).

65. Gaihre, B., Ashraf, S., Spinks, G. M., Innis, P. C. Wallace, G. G. Comparative displacement study of bilayer actuators comprising of conducting polymers, fabricated from polypyrrole, poly(3,4-ethylenedioxythiophene) or poly(3,4-propylenedioxythiophene). *Sensors and Actuators A: Physical* **193**, 48–53 (2013).

66. Tsakova, V., Seeber, R. Conducting polymers in electrochemical sensing: factors influencing the electroanalytical signal. *Analytical and Bioanalytical Chemistry* **408**, 7231–7241 (2016).

67. Potje-kamloth, K. Gas Sensing with Conducting Polymers. in *Electropolymerization: Concepts, Materials and Applications* (eds. Cosnier Serge & Arkady, K.) 153–171 (2010). doi:10.1002/9783527630592

68. Fraind, A. M., Tovar, J. D. Comparative Survey of Conducting Polymers Containing Benzene, Naphthalene, and Anthracene Cores: Interplay of Localized Aromaticity and Polymer Electronic Structures. *Journal of Physical Chemistry B* **114**, 3104–3116 (2010).

69. Park, D.S. Degradation Kinetics of Polypyrrole Films. *Journal of The Electrochemical Society* **140**, 2749 (1993).

70. Rahman, M. A., Kumar, P., Park, D.S., Shim, Y. B. Electrochemical Sensors Based on Organic Conjugated Polymers. *Sensors* **8**, 118–141 (2008).

71. Heeger, A. J. Charge storage in conducting polymers: Solitons, polarons, and bipolarons. *Polymer Journal* **17**, 201–208 (1985).

72. Swann, M. J., Bloor, D., Haruyama, T., Aizawa, M. The role of polypyrrole as charge transfer mediator and immobilization matrix for D-fructose dehydrogenase in a fructose sensor. *Biosensors and Bioelectronics* **12**, 1169–1182 (1997).

73. Ryder, K. S., Schweiger, L. F., Glidle, A., Cooper, J. M. Strategies towards functionalised electronically conducting organic copolymers: Part 2.

Copolymerisation. *Journal of Materials Chemistry* **10**, 1785–1793 (2000).

74. Swann, M. J., Glidle, A., Gadegaard, N., Cui, L., Barker, J. R., Cooper, J. M. Distribution of adsorbed molecules in electronic nose sensors. *Physica B: Condensed Matter* **276**–**278**, 357–358 (2000).

75. Nero, J., Galvão, D., Laks, B. Electronic structure investigation of biosensor polymer. *Optical Materials* **21**, 461–466 (2003).

76. Chah, S., Kumar, C. V, Hammond, M. R., Zare, R. N. Denaturation and Renaturation of Self-Assembled Yeast Iso-1-cytochrome c on Au. *Analytical Chemistry* **76**, 2112–2117 (2004).

77. Caban, K., Offenhäusser, A., Mayer, D. Electrochemical characterization of the effect of gold nanoparticles on the electron transfer of cytochrome c. *Physica Status Solidi (a)* **206**, 489–500 (2009).

78. Tanimura, R., Hill, M., Margoliash, E., Niki, K., Ohno, H., Gray, H. Active Carboxylic Acid-Terminated Alkanethiol Self-Assembled Monolayers on Gold Bead Electrodes for Immobilization of Cytochromes c. *Electrochemical and Solid-State Letters* **5**, E67–E70 (2002).

79. Suá Rez, G., Santschi, C., Martin, O. J. F., Slaveykova, V. I. Biosensor based on chemically-designed anchorable cytochrome c for the detection of H2O2 released by aquatic cells. *Biosensors and Bioelectronic* **42**, 385–390 (2013).

80. Zhang, L. Direct electrochemistry of cytochrome c at ordered macroporous active carbon electrode. *Biosensors and Bioelectronics* **23**, 1610–1615 (2008).

81. Rhoten, M. C., Burgess, J. D., Hawkridge, F. M. The reaction of cytochrome c from different species with cytochrome c oxidase immobilized in an electrode supported lipid bilayer membrane. *Journal of Electroanalytical Chemistry* **534**, 143–150 (2002).

82. Wang, L., Waldeck, D. H. Denaturation of Cytochrome c and Its Peroxidase Activity When Immobilized on SAM Films. *Journal of Physical Chemistry C* **112**, 1351–1356 (2008).

83. Lötzbeyer Thomas, Schuhmann Wolfgang, Schmidt Hanns-Ludwig. Electron transfer principles in amperometric biosensors: direct electron transfer between

enzymes and electrode surface. *Sensors and Actuators B: Chemical* **33**, 50–54 (1996).

84. Szücs, A., Novàk, M. Stable and Reversible Electrochemistry of cytochrome-c on Bare Electrodes. Part 1: Effect of ionic strength. *Journal of Electroanalytical Chemistry* **383**, 75–84 (1995).

85. Szücs, A., Novàk, M. Stable and reversible electrochemistry of cytochrome-c on bare electrodes Part II: Effects of experimental conditions. *Journal of Electroanalytical Chemistry* **384**, 47–55 (1995).

86. Bonanni, B., Alliata, D., Bizzarri, A. R., Cannistraro, S. Topological and Electron-Transfer Properties of Yeast Cytochrome c Adsorbed on Bare Gold Electrodes. *ChemPhysChem* **4**, 1183–1188 (2003).

87. Chen, X., Ferrigno, R., Yang, J., Whitesides, G. M. Redox properties of cytochrome c adsorbed on self-assembled monlayers: a probe for protein confrmation and orientation. *Langmuir* **18**, 7009–7015 (2002).

88. Rhoten, M. C., Burgess, J. D., Hawkridge, F. M. Temperature and pH effects on cytochrome c oxidase immobilized in an electrode-supported lipid bilayer membrane. *Electrochimica Acta* **45**, 2855–2860 (2000).

89. Hanrahan, K.-L., Macdonald, S. M., Roscoe, S. G. An electrochemical study of the interfacial and conformational behaviour of cytochrome c and other heme proteins. *Elecrrochimica Acta* **41**, 2469–2419 (1996).

90. Stamler, J. S., Singel, D. J., Loscalzo, J. Biochemistry of Nitric Oxide and Its Redox-Activated Forms. *Science* **258**, 1898–1902 (1992).

91. Lyons, M. E. G. Mediated Electron Transfer at Redox Active Monolayers Part 2 : Analysis of the Chronoamperometric Response to a Potential Step Perturbation. *Sensors* **2**, 314–330 (2002).

92. Frew, J. E., Hill, H. A. Direct and indirect electron transfer between electrodes and redox proteins. *European Journal of Biochemistry* **172**, 261–269 (1988).

93. Daido, T., Akaike, T. Electrochemistry of cytochrome-c: Influence of coulombic attraction with indium tin oxide electrode. *Journal of Electroanalytical Chemistry* **344**, 91–106 (1993).

94. Wei, J., Liu, H., Khoshtariya, D. E., Yamamoto, H., Dick, A., Waldeck, D. H. Electron-transfer dynamics of cytochrome C: A change in the reaction mechanism with distance. *Angewandte Chemie - International Edition* **41**, 4700–4703 (2002).

95. Bianco, P. Lattuca, C. Membrane-assembly of carbon microelectrodes for the electrochemical study of redox proteins. *Analytica Chimica Acta* **353**, 53–59 (1997).

96. Bond, A. M. Hill, H. A.O., Komorsky-Lovrić, Š., Lovric, M., McCartby, M., Psalti, I., Walton, N. J. Investigation of the mass transport process in the voltammetry of cytochrome c at 4,4'-Bipyridyl Disulfide modified stationary and rotated macro-and microdisk gold electrodes. *Journal of Physical Chemistry* **96**, 8100–8105 (1992).

97. Eguílaz, M., Agüí, L., Yáñez-Sedeño, P., Pingarrón, J. M. A biosensor based on cytochrome c immobilization on a poly-3-methylthiophene/multi-walled carbon nanotubes hybrid-modified electrode. Application to the electrochemical determination of nitrite. *Journal of Electroanalytical Chemistry* **644**, 30–35 (2010).

98. Geng, R., Zhao, G., Liu, M., Li, M. A sandwich structured SiO_2/cytochrome c/SiO_2 on a boron-doped diamond film electrode as an electrochemical nitrite biosensor. *Biomaterials* **29**, 2794–2801 (2008).

99. Haruyama, T., Shiino, S., Yanagida, Y., Kobatake, E., Aizawa, M. Two types of electrochemical nitric oxide (NO) sensing systems with heat-denatured Cyt C and radical scavenger PTIO. *Biosensors & Bioelectronics* **13**, 763–769 (1998).

100. Ho, C., Ikawa, T., Nisizawa, K. Nitrite-reducing activity of modified cytochrome c-553 from the red alga Porphyra yezoensis Ueda. *Plant & Cell physiology* **17**, 431–438 (1976).

101. Yamada, S., Suruga, K., Ogawa, M., Hama, T., Satoh, T., Kawachi, R., Nishio, T., Oku, T. Appearance of Nitrite Reducing Activity of Cytochrome c upon Heat Denaturation. *Bioscience, Biotechnology, and Biochemistry* **66**, 2044–2051 (2002).

102. Csonka, C., Páli, T., Bencsik, P., Görbe, A., Ferdinandy, P., Csont, T.

Measurement of NO in biological samples. *British Journal of Pharmacology* **172**, 1620–1632 (2015).

103. Bedioui, F., Griveau, S. Electrochemical Detection of Nitric Oxide : Assessement of Twenty Years of Strategies. *Electroanalysis* **25**, 587–600 (2013).

104. Borgmann, S. Electrochemical quantification of reactive oxygen and nitrogen: challenges and opportunities. *Anal Bioanal Chem* **394**, 95–105 (2009).

105. Shibuki, K. An electrochemical microprobe for detecting nitric oxide release in brain tissue. *Neuroscience Research* **9**, 69–76 (1990).

106. Zhou, J., Lu, X., Hu, J., Li, J. Reversible immobilization and direct electron transfer of cytochrome c on a pH-sensitive polymer interface. *Chemistry - A European Journal* **13**, 2847–2853 (2007).

107. Pashai, E., Najafpour, G. D., Jahanshahi, M., Rahimnejad, M. Highly Sensitive Amperometric Sensor Based on Gold Nanoparticles Polyaniline Electrochemically Reduced Graphene Oxide Nanocomposite for Detection of Nitric Oxide. *International Journal of Engineering* **31**, 188–195 (2018).

108. Musameh, M. M., Dunn, C. J., Uddin, H., Sutherland, T. D., Rapson, T. D. Silk provides a new avenue for third generation biosensors: Sensitive, selective and stable electrochemical detection of nitric oxide. *Biosensors and Bioelectronics* **103**, 26–31 (2018).

109. López-Bernabeu, S., Gamero-Quijano, A., Huerta, F., Morallón, E., Montilla, F. Enhancement of the direct electron transfer to encapsulated cytochrome c by electrochemical functionalization with a conducting polymer. *Journal of Electroanalytical Chemistry* **793**, 34–40 (2017).

110. Tümer, M., Akgün, E., Toroğlu, S., Kayraldiz, A., Dönbak, L. Synthesis and characterization of Schiff base metal complexes: Their antimicrobial, genotoxicity and electrochemical properties. *Journal of Coordination Chemistry* **61**, 2935–2949 (2008).

111. Tümer, M. Polydentate Schiff-base ligands and their Cd(II) and Cu(II) metal complexes: Synthesis, characterization, biological activity and electrochemical

properties. *Journal of Coordination Chemistry* **60**, 2051–2065 (2007).

112. Yılmaz Baran, N., Saçak, M. Preparation of highly thermally stable and conductive Schiff base polymer: Molecular weight monitoring and investigation of antimicrobial properties. *Journal of Molecular Structure* **1163**, 22–32 (2018).

113. Simionescu, C. I., Grigoras, M., Cianga, I., Olaru, N. Synthesis of new conjugated polymers with Schiff base structure containing pyrrolyl and naphthalene moieties and HMO study of the monomers reactivity. *European Polymer Journal* **34**, 891–898 (1998).

114. Ansari, R. Polypyrrole Conducting Electroactive Polymers: Synthesis and Stability Studies. *E-Journal of Chemistry* **3**, 186–201 (2006).

115. Machida, S., Miyata, S., Techagumpuch, A. Chemical synthesis of highly electrically conductive polypyrrole. *Synthetic Metals* **31**, 311–318 (1989).

116. Rapi, S., Bocchi, V., Gardini, G. P. Conducting polypyrrole by chemical synthesis in water. *Synthetic Metals* **24**, 217–221 (1988).

117. Xin, Y., Yuan, J. Schiff's base as a stimuli-responsive linker in polymer chemistry. *Polymer Chemistry* **3**, 3045 (2012).

118. Xavier, A., Srividhya, N. Synthesis and Study of Schiff base Ligands. *Journal of applied chemistry* **7**, 6–15 (2014).

119. Ward, M., Botha, S., Iwuoha, E., Baker, P. Actuation Behaviour of a Derivatized Pyrrole Accordion Type Polymer. *International Journal of Electrochemical Science* **9**, 4776–4792 (2014).

120. Muzammil, K., Trivedi P., Khetani, D. Synthesis and Characterization of Schiff base m-nitro aniline and their complexes. *Research Journal of Chemical Sciences* **5**, 52–55 (2015).

121. Faizul, A., Satendra, S., Lal, K. S., Om, P. Synthesis of Schiff bases of naphtha[1,2-d]thiazol-2-amine and metal complexes of 2-(2'-hydroxy)benzylideneaminonaphthothiazole as potential antimicrobial agents. *Journal of Zhejiang University Science B* **8**, 446–452 (2007).

122. Barbon, S. M., Staroverov, V. N., Gilroy, J. B. Effect of extended π conjugation on the spectroscopic and electrochemical properties of boron difluoride formazanate complexes. *Journal of Organic Chemistry* **80**, 5226–5235 (2015).

123. Adejoro I. A., Ibeji C. U. A theoretical study on the effect of substituents on the properties of pyrrole and thiophene. *New York Science Journal* **6**, 99–105 (2013).

124. Sek, D., Siwy, M., Bijak, K., Filapek, M., Malecki, G., Nowak, E. M., Sanetra, J., Jarczyk-jedryka, A., Laba, K., Lapkowski, M. Optical and electrochemical properties of novel thermally stable Schiff bases bearing naphthalene unit. *Journal of electroanalytical chemistry* **751**, 128–136 (2015).

125. Elgrishi, N., Rountree, K. J., McCarthy, B. D., Rountree, E. S., Eisenhart, T. T., Dempsey, J. L. A Practical Beginner's Guide to Cyclic Voltammetry. *Journal of Chemical Education* **95**, 197–206 (2018).

126. Deletioglu, D., Hasdemir, E., Solak, A. O., Sari, N. Electrochemical behaviour of acrylamide polymers functionalized with some schiff bases. *Gazi University Journal of Science* **24**, 715–722 (2011).

127. Zhan, S., Hawley, D. Electrochemical properties of benzophenone imine and the use of the corresponding anion radical as a strong electrogenerated base. *Journal of Electroanalytical Chemistry* **319**, 275–290 (1991).

128. Al-salih, T. E., Al-taha, R. W. Cyclic voltammerty study of schiff-base ligand and the effect of groups substitutes on potential and electroactivity. *Der Pharma Chemica* **6**, 42–50 (2014).

129. Bott, A. W. Characterization of Chemical Reactions Coupled to Electron Transfer Reactions Using Cyclic Voltammetry. *Current Separations* **18**, 9–16 (1999).

130. Van Benschoten, J. Y., Lewis, J. J., Heineman, W. R. Cyclic Voltammetry Experiment. *Journal of Chemical Education* **60**, 772–776 (1983).

131. Ameur, Z. O., Husein, M. M. Electrochemical Behavior of Potassium Ferricyanide in Aqueous and (w/o) Microemulsion Systems in the Presence of Dispersed Nickel Nanoparticles. *Separation Science and Technology* **48**, 681–689 (2013).

132. Murgida, D. H., Hildebrandt, P. Redox and redox-coupled processes of heme proteins and enzymes at electrochemical interfaces. *Physical Chemistry Chemical Physics* **7**, 3773–3784 (2005).

133. Sagara, T., Niwa, K., Sone, A., Niki, K., Hinnen, C. Redox Reaction Mechanism of Cytochrome c at Modified Gold Electrodes. *Langmuir* **6**, 254–262 (1990).

134. Clark, R., Bowden, E. F. Voltammetric Peak Broadening for Cytochrome c /Alkanethiolate Monolayer Structures: Dispersion of Formal Potentials. *Langmuir* **13**, 559–565 (1997).

135. Eddowes, M. J., Hill, H. A. O. Electrochemistry of Horse Heart Cytochrome c. *Journal of the American Chemical Society* **101**, 4461–4464 (1979).

136. O'Dea, J. J., Osteryoung, J., Osteryoung, R. A. Theory of Square Wave Voltammetry for Kinetic Systems. *Analytical Chemistry* **53**, 695–701 (1981).

137. De Groot, M. T., Evers, T. H., Merkx, M., Koper, M. T. M. Electron transfer and ligand binding to cytochrome c′ immobilized on self-assembled monolayers. *Langmuir* **23**, 729–736 (2007).

138. Clark, R. A., Bowden, E. F. Voltammetric Peak Broadening for Cytochrome c /Alkanethiolate Monolayer Structures: Dispersion of Formal Potentials. *Langmuir* **13**, 559–565 (1997).

139. Chidsey, C., Bertozzi, C., Putvinski, T. M., Mujsce A. M. Coadsorption of ferrocene-terminated and unsubstituted alkanethiols on Gold: Electroactive self-assembled monolayers. *J. Chem. Phys. In press* **112**, 546–558 (1990).

140. Abass, A. K., Hart, J. P. Direct electrochemistry of cytochrome c at plain and membrane modified screen-printed carbon electrodes. *Electrochimica Acta* **46**, 829–836 (2001).

141. Hinnen, C., Parsons, R., Niki, K. Electrochemical and spectroreflectance studies of the adsorbed horse heart cytochrome c and cytochrome c3 from D. Vulgaris, miyazaki strain, at gold electrode. *Journal of Electroanalytical Chemistry* **147**, 329–337 (1983).

142. Berdiell, I., Kulmaczewski, R., Halcrow, M. A. Iron(II) Complexes of 2,4-

Dipyrazolyl-1,3,5-triazine Derivatives - The Influence of Ligand Geometry on Metal Ion Spin State. *Inorganic Chemistry* **56**, 8817–8828 (2017).

143. Doddi, G., Illuminati, G., Mencarelli, P., Stegel, F. Nucleophilic Substitution at the Pyrrole Ring. Comparison with Furan, Thiophene, and Benzene Rings in Piperidinodenitration. *Journal of Organic Chemistry* **41**, 2824–2826 (1976).

144. Hawrelak, E. J., Bernskoetter, W. H., Lobkovsky, E., Yee, G. T., Bill, E., Chirik, P. J. Square Planar vs Tetrahedral Geometry in Four Coordinate Iron (II) Complexes. *Inorganic Chemistry* **44**, 3103–3111 (2005).

145. Chaudhary, N. K., Mishra, P. Metal Complexes of a Novel Schiff Base Based on Penicillin : Characterization , Molecular Modeling , and Antibacterial Activity Study. *Bioinorganic Chemistry and Applications* **2017**, 1–13 (2017).

146. Beyazit, N., Çobanoğlu, S., Demetgül, C. Metal complexes of perimidine and Schiff base ligands bearing both naphthalene and chromone moieties : synthesis and catalytic activity. *Bulgarian Chemical Communications* **49**, 115–121 (2017).

147. Khalil, M. M. H., Ismail, E. H., Mohamed, G. G., Zayed, E. M., Badr, A. Synthesis and characterization of a novel schiff base metal complexes and their application in determination of iron in different types of natural water. *Open Journal of Inorganic Chemistry* **2**, 13–21 (2012).

148. Blyth, D. J., Aylott, J. W., Moir, J. W. B., Richardson, D. J., Russell, D. A. Optical biosensing of nitric oxide using the metalloprotein cytochrome c'. *Analyst* **124**, 129–134 (1999).

149. Grosvenor, A. P., Kobe, B. A., Biesinger, M. C., Mcintyre, N. S. Investigation of multiplet splitting of Fe 2p XPS spectra and bonding in iron compounds. *Surface and Interface Analysis* **36**, 1564–1574 (2004).

150. Sparrow, T. G., Williams, B. G., RAO, C. N. R., Thomas, J, M. L_3/L_2 white-line intensity ratios in the electron energy-loss spectra of 3d transition-metal oxides. *Chemical Physical Letter* **108**, 547–550 (1984).

151. Zaheer, M., Shah, A., Akhter, Z., Qureshi, R., Mirza, B., Tauseef, M., Bolte, M. Synthesis, characterization, electrochemistry and evaluation of biological

activities of some ferrocenyl Schiff bases. *Applied Organometallic Chemistry* **25**, 61–69 (2011).

152. Latimer, W. M., Hildebrand, J. H. Iron. in *Reference book of Inorganic chemistry* 380–399 (The Macmillan Company, 1944). doi:10.15713/ins.mmj.3

153. Mostany, J., Scharifker, B. R. Impedance spectroscopy of undoped, doped and overoxidized polypyrrole films. *Synthetic Metals* **87**, 179–185 (1997).

154. Wang, J., Wang, J., Kong, Z., Lv, K., Teng, C., Zhu, Y. Conducting-Polymer-Based Materials for Electrochemical Energy Conversion and Storage. *Advanced Materials* **29**, 1–11 (2017).

155. Cysewska, K., Virtanen, S., Jasiński, P. Electrochemical Activity and Electrical Properties of Optimized Polypyrrole Coatings on Iron. *Journal of The Electrochemical Society* **162**, E307–E313 (2015).

156. Feelisch, M. The use of nitric oxide donors in pharmacological studies. *Naunyn-Schmiedeberg's Arch Pharmacol* **358**, 113:122 (1998).

157. Hrabie, J. A., Keefer, L. K. Chemistry of the Nitric Oxide-Releasing Diazeniumdiolate (Nitrosohydroxylamine) Functional Group and Its Oxygen-Substituted Derivatives. *Chem. Rev.* **102**, 1135–1154 (2002).

158. Griveau, S., Dumézy, C., Goldner, P., Bedioui, F. Electrochemical analysis of the kinetics of nitric oxide release from two diazeniumdiolates in buffered aqueous solutions. *Electrochemistry Communications* **9**, 2551–2556 (2007).

159. Hasan, N., Cao, J., Choi, M., Lee, B. L., Jung, Y., Yoo, J. Nitric oxide-releasing poly(lactic-co-glycolic acid)-polyethylenimine nanoparticles for prolonged nitric oxide release, antibacterial efficacy, and in vivo wound healing activity. *International Journal of Nanomedicine* **10**, 3065–3080 (2015).

160. Broder, T. L., Silvester, D. S., Aldous, L., Hardacre, C., Compton, R. G. Electrochemical oxidation of nitrite and the oxidation and reduction of NO2 in the room temperature ionic liquid [C2mim][NTf 2]. *Journal of Physical Chemistry B* **111**, 7778–7785 (2007).

161. Broder, T. L., Silvester, D. S., Aldous, L., Hardacre, C., Compton, R. G. Electrochemical oxidation of nitrite and the oxidation and reduction of NO2 in the room temperature Ionic Liquid [C 2 mim][NTf 2]. *Journal of Physical*

Chemistry B **111**, 7778–7785 (2007).

162. Almeida, G., Serra, A., Silveira, C. M., Moura, J. J. G. Nitrite Biosensing via Selective Enzymes - A Long but Promising Route. *Sensors* **10**, 11530–11555 (2010).

163. Griveau, S., Bedioui, F. Overview of significant examples of electrochemical sensor arrays designed for detection of nitric oxide and relevant species in a biological environment. *Anal Bioanal Chem* **405**, 3475–3488 (2013).

164. Wang, P. G., Xian, M., Tang, X,. Wu, X., Wen, Z., Cai, T., Janczuk, A. J. Nitric Oxide Donors: Chemical Activities and Biological Applications. *Chemical Reviews.* **102**, 1091–1134 (2002).

165. Alam, R., Saleh, A., Islam, M., Sasmal, M., Katarkar, A., Ali, M. A rhodamine-based turn-on nitric oxide sensor in aqueous medium with endogenous cell imaging: an unusual formation of nitrosohydroxylamine †. *Organic Biomolecular Chemistry* **16**, 3910–3920 (2018).

166. Jangid, N., Chauhan, S., Meghwal, K., Ameta, R., Pinki, P. Research Journal of Pharmaceutical , Biological and Chemical Sciences A Review : Conducting Polymers and Their Applications . *Research Journal of Pharmaceutical, Biological and Chemical Science* **5**, 383–413 (2014).

167. Privett, B., Ho, S. J., Schoenfisch, M. H. Tutorial review: Electrochemical nitric oxide sensors for physiological measurements. *Chemical Society Reviews* **39**, 1925–1935 (2010).

168. Bedioui, F., Quinton, D., Griveau, S., Nyokong, T. Designing molecular materials and strategies for the electrochemical detection of nitric oxide, superoxide and peroxynitrite in biological systems. *Physical Chemistry Chemical Physics.* **12**, 9976–9988 (2010).

169. Bedioui, F., Griveau, S. Electrochemical Detection of Nitric Oxide: Assessement of Twenty Years of Strategies. *Electroanalysis* **25**, 587–600 (2013).

Acronyms and abbreviations

µ	Micro
CV	Cyclic voltammetry
DEANONOate	Diethylamine NONOate
EDS	Electron dispersive x-ray spectroscopy
EELS	Electron energy loss spectroscopy
Epa	Peak oxidation potential
Epc	Peak reduction potential
HRSEM	High resolution scanning electron microscopy
mM	millimolar
N_2O	Nitrous oxide
nM	nanomolar
NO	Nitric oxide
NO_2^-	Nitrite
NO_3^-	Nitrate
O_3	Ozone
PBS	Phosphate buffer solution
POPs	Persistent organic pollutants
SPCE	Screen print carbon electrodes
TEM	Transition electron microscopy
UV-Vis	Ultraviolet-visible spectroscopy
VOC	Volatile organic contaminants